Numerical analysis of bubble nucleation processes for first-order phase transitions within quantum fields

by David Adrian Samuel

A thesis submitted in partial fulfillment of the requirements for the degree of Doctor of Philosophy in Physics
Montana State University

Abstract:
The well established links between statistical mechanics and quantum field theory have resulted in the extension of the theory of phase transitions to quantum fields. Within this framework first-order phase transition rates for quantum fields have traditionally been calculated via the Coleman "thin-wall" approximation. This approximation scheme is claimed to have validity in the situation where a first-order phase transition takes place between two nearly degenerate vacuum (ground) states.

It is the purpose of this dissertation to make a comprehensive study of the range of validity of the "thin-wall" approximation via a comparison of its results with exact results obtained numerically. It is found that both in the absence of gravity and the presence of gravity the "thin-wall" approximation has a very restricted range of validity, and that it characteristically overestimates the phase transition rate. A new approximation scheme is presented which considerably improves upon the original "thin-wall" approximation, yet requires roughly the same degree of calculation effort as the original "thin-wall". approximation.

The numerical analysis of first-order phase transitions within quantum fields is also extended to regimes not applicable to the "thin-wall" approximation in a search for new physical effects. An evolution from the "thin-wall" tunneling mode to the Hawking-Moss tunneling mode is observed for the decay from a de Sitter spacetime to a Minkowski spacetime. For the decay from Minkowski spacetime to an anti-de Sitter spacetime, the "thin-wall" approximation is seen to over-estimate the size of the "forbidden region" (predicted within the "thin-wall" approximation) in which the transition is not allowed.

The effect of gravitationally compact objects upon vacuum phase transitions is considered within a perturbative analysis. It is found that they may act as nucleation sites for first-order phase transitions. The nucleation rate is. maximized when the size of the gravitationally compact object is comparable to the size of the nucleating bubble associated with the phase transition.

Some astrophysical applications of first-order vacuum phase transitions are analyzed. In particular, the post-nucleation evolution of a bubble of "new" phase; together with a relationship between the number density of possible astrophysical nucleation sites within the Universe (e.g., microscopic black-holes) and the mass of fermions within the Standard Model.

NUMERICAL ANALYSIS OF BUBBLE NUCLEATION PROCESSES FOR FIRST-ORDER PHASE TRANSITIONS WITHIN QUANTUM FIELDS

by

David Adrian Samuel

A thesis submitted in partial fulfillment
of the requirements for the degree

of

Doctor of Philosophy

in

Physics

MONTANA STATE UNIVERSITY
Bozeman, Montana

December 1991

APPROVAL

of a thesis submitted by

David Adrian Samuel

This thesis has been read by each member of the thesis committee and has been found to be satisfactory regarding content, English usage, format, citations, bibliographic style, and consistency, and is ready for submission to the College of Graduate Studies.

18 December 1991
Date

Chairperson, Graduate Committee

Approved for the Major Department

18 December 1991
Date

Head, Major Department

Approved for the College of Graduate Studies

19 December 1991
Date

Graduate Dean

STATEMENT OF PERMISSION TO USE

In presenting this thesis in partial fulfillment of the requirements for a doctoral degree at Montana State University, I agree that the Library shall make it available to borrowers under rules of the Library. I further agree that copying of this thesis is allowable only for scholarly purposes, consistent with "fair use" as prescribed in the U. S. Copyright Law. Requests for extensive copying or reproduction of this thesis should be referred to University Microfilms International, 300 North Zeeb Road, Ann Arbor, Michigan 48106, to whom I have granted "the exclusive right to reproduce and distribute copies of the dissertation in and from microfilm and the right to reproduce and distribute by abstract in any format. "

Signature D A. Samuel

Date 18 December 1991

ACKNOWLEDGMENTS

I wish to express my appreciation to Dr. William Hiscock, my advisor. His helpfulness during my graduate studies at Montana State University has been unending. It is a position of privilege to have an advisor who allows one to have intellectual freedom but who can also provide direction when needed. I would also like to thank Dr. Hiscock for his financial support, through a research assistantship from his National Science Foundation grant.

My studies in relativity and quantum field theory, at the Physics Department of Montana State University, have also benefited from discussions with Dr. Lee Lindblom, Dr. John Mc.Laughlin, and Dr. Paul Anderson.

I am indebted to Dr. Lane Hughston for initially introducing me to quantum field theory and relativity, at Lincoln College, Oxford, and for his continued guidance and stimulating conversations over the past several years.

Finally, I would like to express gratitude to my wife, Julia, for enduring an increasingly absent husband during my writing of this dissertation !

TABLE OF CONTENTS

TABLE OF CONTENTS-Continued

LIST OF FIGURES

LIST OF FIGURES-Continued

Figure Page

LIST OF FIGURES-Continued

LIST OF FIGURE-Continued

ABSTRACT

The well established links between statistical mechanics and quantum field theory have resulted in the extension of the theory of phase transitions to quantum fields. Within this framework first-order phase transition rates for quantum fields have traditionally been calculated via the Coleman "thin-wall" approximation. This approximation scheme is claimed to have validity in the situation where a first-order phase transition takes place between two nearly degenerate vacuum (ground) states.

It is the purpose of this dissertation to make a comprehensive study of the range of validity of the "thin-wall" approximation via a comparison of its results with exact results obtained numerically. It is found that both in the absence of gravity and the presence of gravity the "thin-wall" approximation has a very restricted range of validity, and that it characteristically overestimates the phase transition rate. A new approximation scheme is presented which considerably improves upon the original "thin-wall" approximation, yet requires roughly the same degree of calculation effort as the original "thin-wall" approximation.

The numerical analysis of first-order phase transitions within quantum fields is also extended to regimes not applicable to the "thin-wall" approximation in a search for new physical effects. An evolution from the "thin-wall" tunneling mode to the Hawking-Moss tunneling mode is observed for the decay from a de Sitter spacetime to a Minkowski spacetime. For the decay from Minkowski spacetime to an anti-de Sitter spacetime, the "thin-wall" approximation is seen to over-estimate the size of the "forbidden region" (predicted within the "thin-wall" approximation) in which the transition is not allowed.

The effect of gravitationally compact objects upon vacuum phase transitions is considered within a perturbative analysis. It is found that they may act as nucleation sites for first-order phase transitions. The nucleation rate is maximized when the size of the gravitationally compact object is comparable to the size of the nucleating bubble associated with the phase transition.

Some astrophysical applications of first-order vacuum phase transitions are analyzed. In particular, the post-nucleation evolution of a bubble of "new" phase; together with a relationship between the number density of possible astrophysical nucleation sites within the Universe (e.g., microscopic black-holes) and the mass of fermions within the Standard Model.

CHAPTER 1

INTRODUCTION

VACUUM - empty space; specifically, an enclosed space devoid of matter...

" The Encyclopedia Britannica"

How arid the vacuum used to be! Fortunately, the arrival of quantum field theory has brought with it a dynamic life for the vacuum. No longer do we think of the vacuum as empty space but rather as a sea of virtual particles, a medium capable of transition, and the stage for particle physics and cosmology. In some ways we may think of it as the long sought after "aether" of the nineteenth century.

Under the classical definition of the vacuum the question of stability was not an issue. How may one question the stability of emptiness? Perhaps this may be the subject for some esoteric philosophical argument but it is certainly not a physical issue. However, such a question has been thrown into the physicists' arena with the introduction of quantum field theory. Though the vacuum may be classically stable it is possible that it may undergo some form of quantum decay. The emission of an alpha particle from a radioactive nucleus provides us with a loose analogy here. Classically, the nucleus should be stable and the alpha particle bound to it by a potential barrier; however, quantum theory allows for tunneling through the barrier and the resultant escape of the alpha particle. Quantum field theory allows for the association of potentials with the various quantum fields in nature. Such potentials may also have

"barriers" similar to those which bind alpha particles to nuclei, and quantum tunneling of the field through the potential barrier may then be a possibility.

Within the framework of quantum field theory, a vacuum is defined as being the ground state for the quantum fields, where the ground state is defined to be a local minimum of the associated field potential. Within this picture the "sea of virtual particles" may be thought of as the quantum fluctuations of the field about the ground state. If a potential has more than one local minimum then there are multiple ground states available to the field. Multiple ground states would mean, by definition, multiple vacuum states. Thus it is necessary for us to make some form of distinction between these possible multiple vacuum states. We shall refer to the vacuum state with the lowest potential energy as the "true vacuum". Under the assumption that the potential is bounded from below, the true vacuum will have absolute stability, i.e., stability against quantum decay as well as classical stability. The remaining vacuum states shall be referred to as "false vacua"; such vacua enjoy only classical stability. Figure 1 illustrates these ideas.

The picture of false vacuum states separated from the true vacuum by potential barriers, with the resultant decay of the false vacua, has a very close analogy in another branch of physics, notably the theory of first order phase transitions in thermodynamic systems. A first order phase transition may be associated with the presence of a potential barrier separating the two ground (vacuum) states within the transition. When this barrier is absent then the phase transition becomes second (or higher) order.

The condensation of gases to form liquids, the onset of ferromagnetism and even the everyday appearance of bubbles of carbon dioxide in a newly opened bottle of soda are examples of first order phase transitions. The important common

characteristic here is that the transition occurs via nucleation of bubbles of the new phase within the medium of the old phase.

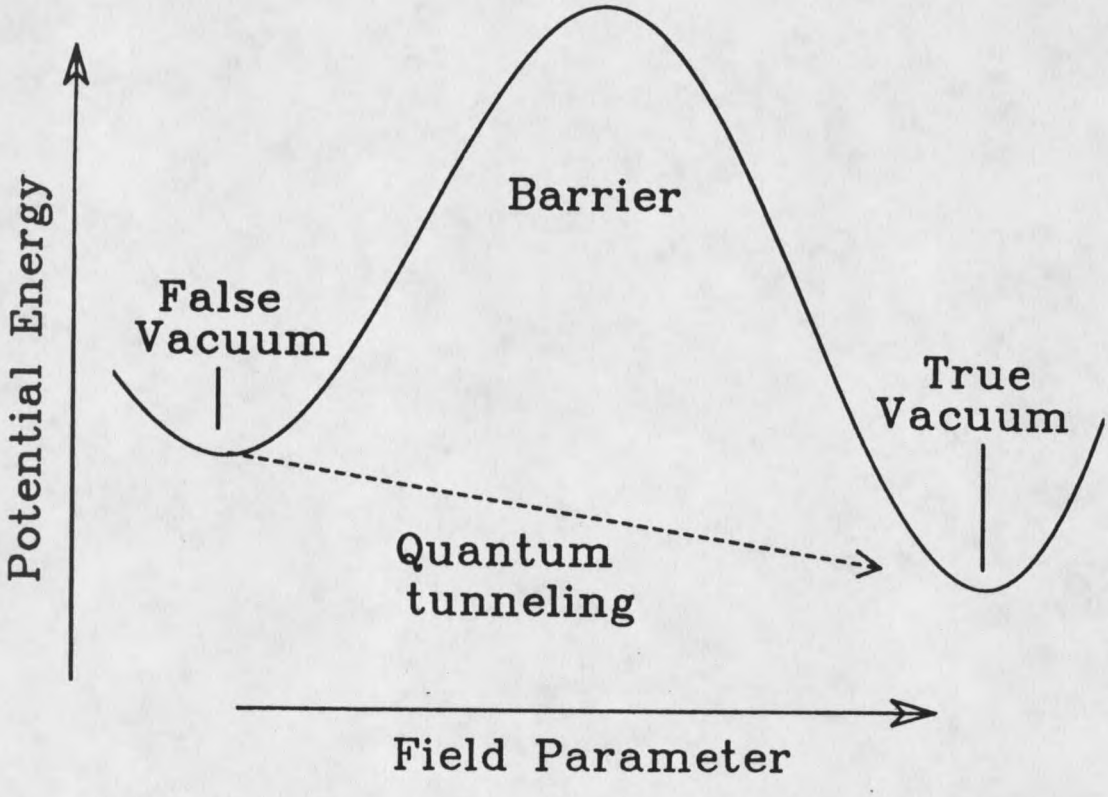

Figure 1 Decay from a false vacuum state to the true vacuum state. The potential barrier separating the false vacuum from the true vacuum allows for classical stability of the false vacuum, but quantum barrier penetration results in its eventual decay to the true vacuum state.

The links between quantum field theory and statistical mechanics are well established (see, for example, Allen (1986)). As a result, first order phase transitions for the decay of false vacua associated with quantum fields will proceed in a similar manner to first order phase transitions in everyday matter. Bubbles of new phase will

be nucleated via quantum fluctuations rather than statistical fluctuations, but there will otherwise be very little difference.

When considering phase transitions in everyday matter we usually do not consider the effects of gravity. In the absence of gravity we are free to choose the zero level of our energy; the physics being sensitive only to energy differences and not to the absolute values of the energy. However, when considering phase transitions in quantum fields we are often faced with a cosmological setting. As gravity plays a fundamental role in most cosmological settings we are forced to consider its possible effects upon such phase transitions.

If gravity is included in the analysis then we no longer have the freedom of arbitrarily choosing a zero-level for the energy of the quantum fields. The energy density associated with the quantum fields will be a source for the gravitational field via the stress-energy tensor for the quantum fields. Thus, arbitrarily fixing zero levels for the energy of the quantum fields could have a drastic effect upon the evolution of a spacetime. General relativity predicts that if the energy density of the vacuum state for the quantum fields is positive, zero or negative then an otherwise empty universe will be described by a de Sitter, Minkowski or anti-de Sitter spacetime, respectively. As the properties of these are vastly different it is necessary to conclude that quantum fields may have an essential role to play in cosmology.

Today we find ourselves living in a universe described by a Robertson-Walker spacetime with zero vacuum energy density. The smallness of the present vacuum energy density is, in fact, the most accurately known quantity in the physical sciences at this time: The observational bound on the mass density of the universe is 10^{-28} g cm^{-3} ; while, for example, the characteristic mass density associated with the electroweak

theory is 10^{26} g cm^{-3}. Thus, in dimensionless units the maximum vacuum energy density of the Universe is of the order of 10^{-54}, which for all practical purposes is zero!

If we are currently living in a false vacuum state then its decay would result in an anti-de Sitter spacetime, i.e., a spacetime corresponding to a negative vacuum energy density. Similarly, any first-order phase transition, with supercooling (i.e., where thermal excitations are insufficient to push the field over the potential barrier), which may have taken place in the past would have placed us into our current state from an initial de Sitter spacetime (i.e., a spacetime corresponding to a positive vacuum energy density). Such a scenario is commonly accepted because the inflation of the Universe during its de Sitter phase would solve many of the problems of present day cosmology; for example, the lack of magnetic monopoles, the flatness problem and the isotropy of the Universe.

Another interesting phenomenon associated with first order phase transitions is their ability to be nucleated by an inhomogeneity or some other form of nucleation site. An example of this is the preferential formation of rain drops around dust particles in the atmosphere. The presence of nucleation sites can considerably enhance the nucleation rate for a phase transition, and their absence can often result in the phenomenon of supercooling. One is therefore led to ask whether there are analogous nucleation sites for vacuum phase transitions. In particular, can inhomogeneities in the gravitational field act as nucleation sites for vacuum phase transitions? Such inhomogeneities may find their origin with black holes, boson stars or other gravitationally compact objects. Even density perturbations in the background metric associated with a hot early universe might act as nucleation sites.

The Higgs fields of the electroweak theory of Glashow (1961), Weinberg (1964), and Salam (1968) (hereafter referred to as GWS theory) provide the motivation

for most of the study of vacuum phase transitions with quantum fields. The Higgs field provides an example of a quantum field in which vacuum phase transitions are believed to occur; there are also very compelling reasons to believe in the existence of the Higgs fields.

The "weak interaction" proved to be problematic for most of the early days of particle physics (non-renormalizable in a point-like interaction model, for example). The interaction is short ranged and must therefore be transmitted via a heavy (vector) boson. Fortunately, massive bosons may be generated quite naturally within gauge theories via the process of spontaneous symmetry breaking (SSB) of a continuous symmetry within the Lagrangian of the field theory. There is an added bonus in that such theories are also renormalizable. Within the GWS theory, the SSB is generated via the Higgs field (i.e., the broken symmetry vacuum state of the Higgs field does not respect the full symmetry of the Lagrangian for the theory). The required vector gauge-bosons, together with their masses and couplings, are predicted quite naturally within the theory; this is a compelling reason to believe in the theory.

The creation of the electroweak theory provided a unification of the electromagnetic and weak forces. This unification has been extended in various theories to include the strong interaction (Grand Unified Theories, or GUTs); and even grander unification schemes have been proposed. The motivation for these "unifications" are the numerous problems in particle physics and cosmology that they may solve (together, of course, with their aesthetic appeal). A characteristic of many of these grand unification schemes are the presence of Higgs fields.

An initial study of false vacuum decay, in the absence of gravity, was made by Coleman (1977) in which he formulated the "thin-wall" approximation scheme. Coleman showed that the "nucleating bubble profile" should be given by the solution to

the Euclideanized field equations with appropriate boundary conditions. The number of nucleating bubbles per unit four volume within this analysis may be expressed by $\Gamma = A \exp(-B)$, where B is the difference between the Euclidean action for the spacetime with and without the bubble. The coefficient 'A' is a functional determinant associated with the field equation, and is typically of the order of the mass scale of the field to the fourth power.

The terminology "nucleating bubble profile" should be read with caution as it is misleading to think of the bubble field profile *at the moment of nucleation* to be given by the solution to the Euclideanized field equations. The reason for this is that at the moment of nucleation the quantum fluctuations in the field are comparable in "size" to the field profile of the nucleating bubble. Thus the notion of a "classical field profile" is misleading in this situation. However, the "classical field profile", to the exterior of the lightcone centered on the nucleation site, is at late times (i.e., at times much greater than m^{-1}, where m is the characteristic mass scale of the quantum field undergoing the phase transition) well represented by the solution to the Euclideanized field equations "rotated" into the Lorentzian sector. Thus, whenever the terminology "nucleating bubble profile" shall be used then the above qualifications will be understood to apply. We also note that the solutions to the Euclideanized scalar field equations are also used in the evaluation of the Euclidean action of the nucleating bubble.

The "thin-wall" model assumes that the bubble created as a result of quantum fluctuations has a well defined core of new phase, a very thin wall and an exterior of old phase. Such a bubble profile is an approximate solution to the Euclideanized field equations when there is a small vacuum energy density difference between the two vacuum states. This approximation scheme provides a straight forward and often an analytic way of determining bubble nucleation rates in a field theoretic context.

In a later paper Coleman and De Luccia (1980) extended the "thin-wall" approximation with the inclusion of gravity. Their analysis was specialized to the formation of O(4)-symmetric bubbles in the decay from de Sitter to Minkowski space and from Minkowski to anti-de Sitter space. Coleman, et. al. (1978), have shown that in the absence of gravity, O(4)-symmetric bubbles always have the least action and are therefore the dominant decay mode for first order vacuum phase transitions. Several proofs extending this result to the situation where gravity is present have been offered, but all have been shown to be flawed. Though no proof exists at this time to demonstrate that O(4)-symmetric bubbles will always have the lowest action when gravity is included, it is widely believed to be true.

Quantum fields have associated with them a stress-energy tensor and are therefore a source for the gravitational field, as given by the Einstein field equations. Thus the Coleman-De Luccia analysis required the approximate solution of the coupled Euclideanized field and Einstein equations in order to incorporate the effects of the self-gravity of the bubble. Their results showed an enhanced rate for vacuum decay from de Sitter to Minkowski space and a decreased rate for decay from Minkowski to anti-de Sitter space. This was associated with a decrease in the nucleating bubble size for the decay from de Sitter to Minkowski space and an increase in the nucleating bubble size for the decay from Minkowski to anti-de Sitter space as compared with the nucleating bubble in the absence of gravity. There was also a predicted forbidden region for the decay from Minkowski to anti-de Sitter space in which false vacuum decay was prohibited. This region corresponded to a small vacuum energy density difference between the two vacuum states.

As might be expected, the effect of self-gravity on the false vacuum decay rate is negligible unless the mass of the field concerned is close to the Planck mass. Thus

for phase transitions at the electroweak energy scale (10^2 GeV), and even the GUT energy scale (of the order of 10^{16} GeV), the effect of self gravity is usually neglected (n.b., the Planck scale is of the order 10^{19} GeV). In such situations gravity would play a more dominant role in the later evolution of the bubble (i.e., on a cosmological scale) rather than in its formation. However, it is conceivable that either in the very early Universe, or even today, a phase transition could occur which is associated with a highly massive field.

The effect of gravitational nucleation sites upon false vacuum decay has been studied within the "thin-wall" approximation by Hiscock (1987), who considered the effect of black holes, and Mendell and Hiscock (1989) who considered the effect of gravitationally compact objects such as neutron stars. Their analysis proceeded via the solution of the Israel (1966) equations corresponding to the "patching" together of two spacetimes (and is therefore a "thin-wall" analysis). For example, in the analysis of the effect of a black hole upon false vacuum decay from a Schwarzschild spacetime to a Schwarzschild - anti - de Sitter spacetime, the solution of the Israel equations corresponding to the patching together of a bubble core of Schwarzschild-anti-de Sitter spacetime to an exterior of Schwarzschild spacetime is required. Their analysis showed that the gravitationally compact objects under consideration have the effect of reducing B, the difference between the Euclidean action for the spacetime with and without the bubble, and that these objects may therefore play the role of nucleation sites.

It is the purpose of this dissertation to make a study of bubble nucleation processes for first-order phase transitions in quantum scalar fields. This is to be achieved via the exact numerical solution of the relevant field equations, or in some instances where exact solutions are intractable, a perturbative numerical approach is adopted. The field of study is specialized to: O(4)-symmetric bubble nucleation

without gravity, O(4)-symmetric bubble nucleation with gravity (for the decays from de Sitter to Minkowski space and Minkowski to anti-de Sitter space), and O(3)-symmetric bubble nucleation around gravitationally compact objects. In all of these instances a comparison is made of exact numerical results with those of the "thin-wall" approximation; this will allow us to estimate the range of validity of the "thin-wall" approximation in the various scenarios. A search is also made for new physical effects which may not be apparent from the "thin-wall" analysis.

Finally, some astrophysical aspects of the bubble nucleation processes are addressed in light of the exact numerical results. In particular, the evolution of the interior of the nucleating bubble is considered together with a model for placing bounds upon the number density of astrophysical nucleation sites. This bound shall be based upon the GWS electroweak theory in which a sufficiently massive top-quark may render our current vacuum state a false-vacuum (Politzer and Wolfram (1976), Flores and Sher (1983), Duncan et. al. (1985)).

The convention, $c = G = h = 1$, shall be used throughout this dissertation, except for Chapter 3 which will use $c=h=1$, and $G=1/m_p^2$, where m_p is the Planck mass.

CHAPTER 2

FIRST - ORDER VACUUM PHASE TRANSITIONS IN THE ABSENCE OF GRAVITY

Motivation and Background

The theory of the decay of an apparent ground state to a deeper lying or absolute ground state of a physical system via some quantum process or statistical fluctuation has its roots in many branches of the physical sciences. It has recently found a stage for its action in the "marriage" of high energy and elementary particle physics with cosmology.

The advent of the electroweak theory of Glashow, Weinberg and Salam showed that the fundamental quantum fields of nature may play an important role in the evolution of the Universe. This is a result of a possible non-zero vacuum energy density associated with some of the quantum fields of the theory (the Higgs fields). A non-zero vacuum energy density has quite a dramatic effect on the evolution of a spacetime; a positive vacuum energy density may result in the exponential expansion of a spacetime, whereas a negative vacuum energy density may result in a spacetime in which the "Cauchy Problem" is not even well defined. Verification of the GWS electroweak theory, through the discovery of neutral currents and the W and Z particles, gave credibility to other unified models, for example the "Grand Unified Theories". Such theories also predict states for the quantum fields in which the vacuum energy density would be non-zero.

A characteristic of unified field theories is the presence of a temperature dependent (Higgs) field potential. The vacuum state corresponding to the Higgs field potential respects the symmetry of the Lagrangian at high temperatures. However, at low temperatures spontaneous symmetry breaking occurs, and the true vacuum state no longer has the symmetry of the Lagrangian. The true vacuum will lie at some non-zero value of the Higgs field, and may be separated from the false (symmetric) vacuum by a potential barrier. Figure 2 illustrates these ideas.

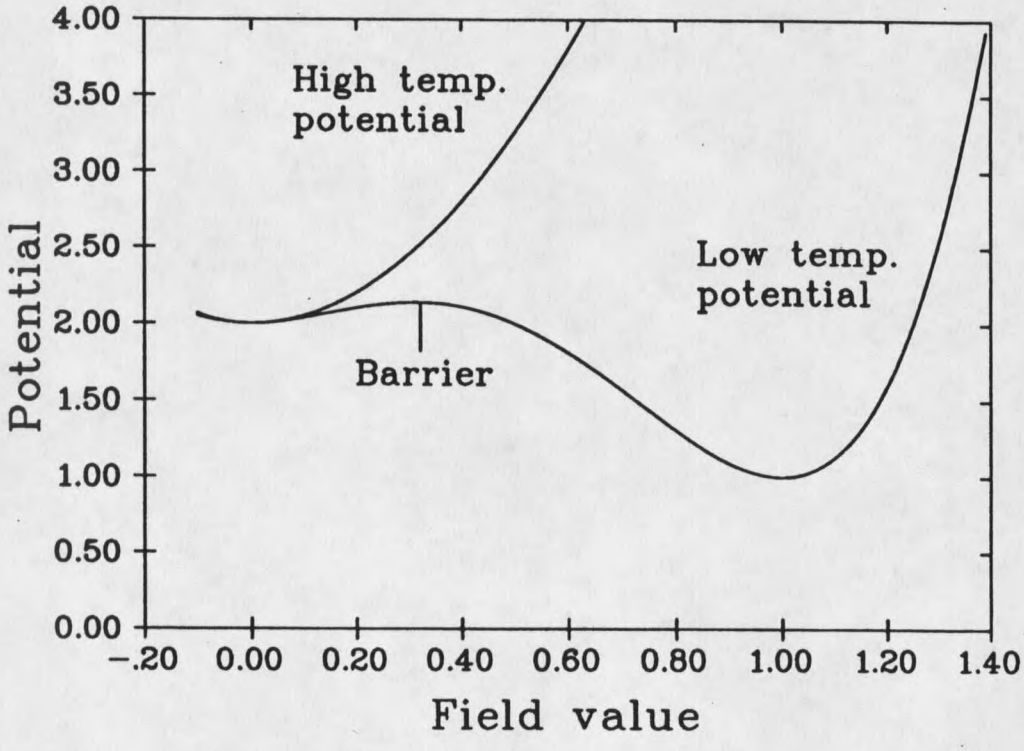

Figure 2 The temperature dependent field potential which is a characteristic of many unified field models.

In a cosmological setting, a "Hot Big Bang" would initially place the Higgs potential into its symmetric state due to the very high temperatures shortly after the Big Bang. Such a state would have a positive vacuum energy density as shown in Figure 2. The energy density of the Universe would initially be dominated by a "hot gas" of relativistic particles, and the evolution would be described by a Friedman-Robertson-Walker cosmological model. However, as the Universe expanded the energy density of the hot gas of particles would decrease and the temperature would fall. Eventually, some point would be reached where the vacuum energy density would dominate over that of the hot gas.

Within many of the grand unified models the quantum field that is driving the exponential expansion of the Universe will now find itself in a trapped false vacuum state. The evolution of the Universe would then be well modeled by a de Sitter spacetime in which the Universe undergoes an exponential expansion. Such an expansion will in a very short time, drop the temperature of the initially hot gas of particles to some value very close to zero. If the field behaved in a classical manner then this would be the end of the story (i.e., an exponentially expanding Universe). However, quantum fluctuations in the field allow it to escape from its trapped state, tunneling through the barrier and thus enabling it to reach the true vacuum state.

The quantum tunneling of a field through a barrier in the effective field potential is analogous to an order parameter of a thermodynamic system tunneling through a barrier in the free energy of the system as a result of statistical fluctuations. These processes are characteristic of first order phase transitions; such transitions being accomplished via the nucleation of bubbles of the new phase within the medium of the old phase.

Coleman (1977) has provided us with an analysis which shows that the field

profile of the nucleating bubble, for a first order phase transition, is given by the solution of the Euclideanized field equations with appropriate boundary conditions. Additionally, the "bubble nucleation rate" is determined by the Euclidean action of the nucleating bubble.

The Coleman analysis goes further by providing us with an analytical approximation scheme, the "thin-wall" approximation, for the calculation of the Euclidean action of a nucleating bubble for a given field theory. This approximation scheme is valid in the situation where the energy density difference between the false vacuum (ground) state and the true vacuum (ground) state is small. When this is the case then the approximate solution to the Euclideanized field equations results in a nucleating bubble which has a well defined core of "new" phase, a thin-wall, in which there is a rapid transition from the "new" to the "old" phase, and an exterior of "old" phase. An example of a "thin-wall" nucleating bubble profile is shown in Figure 3.

In this chapter we shall review the "thin-wall" approximation for a particular "toy model" field theory (without the effects of gravity). We shall also obtain exact nucleating bubble profiles and Euclidean actions via the numerical solution of the Euclideanized field equations; this will allow us to critically analyze the "thin-wall" approximation and determine its range of validity. This analysis will eventually lead us to a new approximation scheme, which considerably improves upon the results of the original "thin-wall" approximation (these results have been reported in Samuel and Hiscock (1991[a])).

We shall consider first-order phase transitions for the decay of false vacua with quantum scalar fields, i.e., fields of zero intrinsic spin. It is conceivable that phase transitions processes may differ somewhat for fields of higher spin (e.g., possible

Fermi-Dirac and Bose-Einstein statistical effects); however, the scalar field analysis should provide the appropriate analysis for phase transitions within Higgs fields.

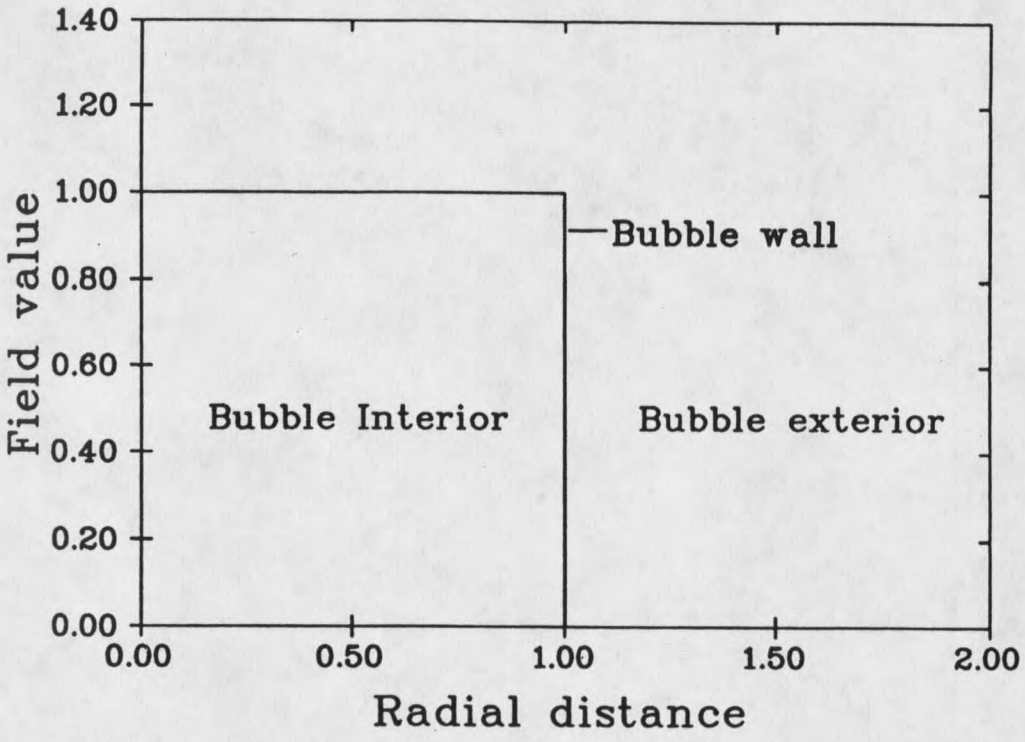

Figure 3 Nucleating bubble profile for the "thin-wall" approximation.

In order to analyze first-order phase transitions during false vacuum decay it will be necessary to consider a potential function, say $U(\phi)$, which has at least two local minima separated by a potential barrier. In the context of field theory these local minima represent vacuum states. On the assumption that we do not have degenerate vacua then there will be just one true vacuum state which is both classically stable and also stable to quantum decay. All other vacua will only have classical stability and will eventually decay to lower lying vacuum states.

"Thin-wall" Approximation and a "Toy" Model

We shall consider a "toy" model of vacuum decay for a potential of the form $U(\phi)=m^2\phi^2-\eta\phi^3+\lambda\phi^4$, which we shall refer to from now on as a $\phi^{2\text{-}3\text{-}4}$ potential. Such a potential has, for a suitable choice of parameters, two vacuum states. In fact it is the simplest polynomial potential which contains two vacuum states where we are able to independently vary the relative depth and the field distance between the vacuum states, it also enjoys the privilege of being the most arbitrary renormalizable potential.

Thus, we start our analysis with the self interacting, scalar field potential,

$$U = m^2\phi^2 - \eta\phi^3 + \lambda\phi^4 \quad , \qquad \text{with } m^2, \eta, \lambda \geq 0 . \tag{2.1}$$

As we shall be making a numerical study of phase transitions within this potential, it shall be convenient to convert the potential to a dimensionless form via the introduction of the dimensionless variables,

$$\psi = \phi / m \quad , \quad \tilde{\eta} = \eta / m , \quad \text{and} \quad \tilde{U} = U / m^4 \quad .$$

Expressing our potential in terms of these variables gives,

$$\tilde{U} = \psi^2 - \tilde{\eta}\psi^3 + \lambda\psi^4 . \tag{2.2}$$

The polynomial coefficients η and λ give a simple algebraic form for the potential. However, it will suit us to use parameters which have a more physical basis. Thus we re-express the potential in terms of the parameters ψ_+, the value of the field at the true vacuum (the false vacuum will always be located at $\psi = 0$ with our choices of

parameters), and $\tilde{\varepsilon}$, minus the (dimensionless) energy density of the true vacuum, $\tilde{\varepsilon} = -\tilde{U}(\psi_+)$. With this parameterization the potential takes the form,

$$\tilde{U} = \psi^2 - 2(2\tilde{\varepsilon} + \psi_+^2)\frac{\psi^3}{\psi_+^3} + (3\tilde{\varepsilon} + \psi_+^2)\frac{\psi^4}{\psi_+^4} \quad . \qquad (2.3)$$

We finally define a dimensionless scale parameter ω which will later be found to be a suitable parameter for defining the range of validity of the "thin-wall" approximation,

$$\omega = \frac{\tilde{\varepsilon}}{\psi_+^2} \quad ; \qquad (2.4)$$

and re-scale the field one last time by defining $\sigma = \psi/\psi_+$ (so that the false and true vacua are located at $\sigma = 0$ and $\sigma = 1$, respectively). Figure 4 shows this potential for the choice of dimensionless parameter ω=0.1. The conversion of our field variable, ϕ, first to a dimensionless quantity ψ, and then to a scaled variable σ is done simply to aid in the comparison of vacuum decay for different values of ω; there is no physical basis behind this transformation.

The nucleating bubble profile (i.e., σ as a function of the spacetime coordinates) at the moment of creation is given by the solution of the Euclideanized field equation with the appropriate boundary conditions. The Euclideanized field equation in this case is simply the Klein-Gordon equation with the substitution $t \rightarrow i\tau$. The solution of this second order differential equation requires two boundary conditions. One of the boundary conditions is provided by the requirement that far away from the bubble the field should be in the false vacuum state, i.e., σ=0. The second boundary condition will become evident from the form of the Euclideanized field equation and the necessity that

the field, σ, not experience singular behavior. This results in the field having zero derivative with respect to the O(4) radial Euclideanized spacetime coordinate at the center of the bubble.

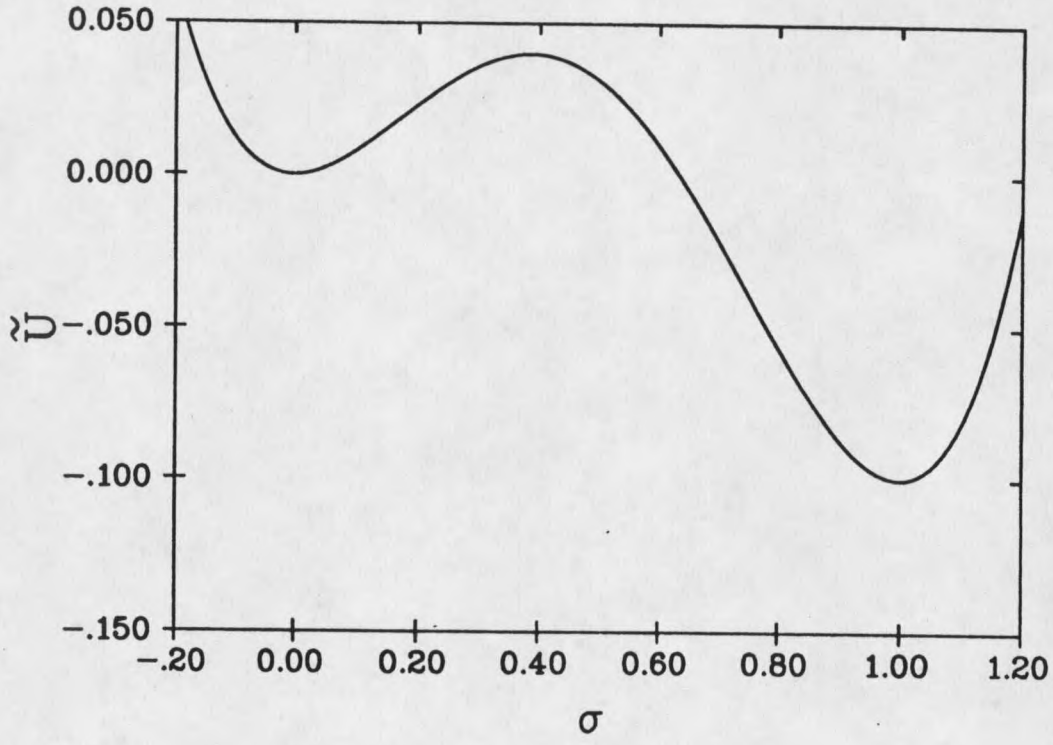

Figure 4 The dimensionless $\phi^{2\text{-}3\text{-}4}$ potential with ω=0.1.

As we are not considering the effect of gravity in this "toy" model then the appropriate spacetime metric is Minkowskian. The line element for such a spacetime is

$$ds^2 = - dt^2 + dr^2 + r^2 d\Omega^2 \quad . \qquad (2.5)$$

Upon Euclideanization we are left with an O(4)-symmetric spacetime and it is appropriate to define an O(4) radial variable $\zeta^2 = \tau^2 + r^2$. We shall consider

O(4) symmetric bubble nucleation as such bubbles have been shown by Coleman, et. al. (1978), to have the least action in the absence of gravity, and hence are dominant in the decay process. With O(4) symmetry the bubble profile will be a function of ζ only, i.e., $\sigma=\sigma(\zeta)$.

The scalar field equation may be represented quite simply, and generally, in terms of the metric by,

$$g^{-\frac{1}{2}}\partial_\mu\left(g^{\frac{1}{2}}\,g^{\mu\nu}\,\partial_\nu\right)\phi=\frac{dU}{d\phi}, \qquad \text{where} \quad g=\det(g_{\mu\nu})\ . \tag{2.6}$$

The resulting Euclideanized scalar field equation, in terms of our metric and coordinate system is:

$$\frac{d^2\sigma}{d\zeta^2}+\frac{3}{\zeta}\frac{d\sigma}{d\zeta}=\frac{m^2}{\psi_+^2}\frac{d\tilde{U}}{d\sigma} \tag{2.7}$$

To conform with our dimensionless potential we may re-express equation (2.7) in terms of the dimensionless radial variable $\xi = m\zeta$, and those previously defined;

$$\frac{d^2\sigma}{d\xi^2}+\frac{3}{\xi}\frac{d\sigma}{d\xi}=\frac{1}{\psi_+^2}\frac{d\tilde{U}}{d\sigma}\ , \tag{2.8}$$

with the boundary conditions,

$$\sigma(\xi\to\infty)=0\ , \tag{2.9}$$

and,

$$\frac{d\sigma}{d\xi}(\xi=0)=0\ . \tag{2.10}$$

The second boundary condition is given by the requirement that the scalar field, σ, not experience singular behavior. As there is a $(3/\xi)$ coefficient to the $(d\sigma/d\xi)$ term in the differential equation then we are required to force $(d\sigma/d\xi) = 0$ at the origin of the coordinate system, i.e., at $\xi=0$.

Coleman (1977) draws the analogy between the solution to Eq.(2.8) and the classical motion of a particle of unit mass in the inverted potential, $-\tilde{U}(\sigma)$, where σ represents the position of the particle and ξ corresponds to the time. The motion is also subject to a damping force with a somewhat unusual damping coefficient, $(3/\xi)$, i.e., the damping coefficient is inversely proportional to the time. This analogy will aid us considerably by allowing the formation of intuitive pictures of the solutions via reference to the particle motion.

Consideration of the intuitive picture will also aid in the development of the "thin-wall" approximation. Figure 5 shows the inverted potential for $\omega=0.1$. We know from one of the boundary conditions that as ξ (the 'time' from the start of motion) $\rightarrow\infty$ the particle should come to rest at $\sigma=0$, (i.e., as one moves away from the bubble centered at $\xi=0$ then one should return to the false vacuum state). The second boundary condition requires the particle to start from rest at $\xi=0$, otherwise there would be singular behavior in σ. So we start with the particle at some position close to $\sigma=1$ (but obviously less than 1 so that it roles down the correct side of the hill and eventually reach $\sigma=0$). Now, if the initial position is not "high enough" then there will be an undershoot, i.e., the initial excess energy will not be sufficient to overcome the friction and the particle will not reach $\sigma=0$. If the initial position is too high then there will be an overshoot, i.e., the friction is not sufficient to eliminate the excess energy by the time the particle reaches $\sigma=0$, and so the particle passes $\sigma=0$ and continues to role down the hill on the other side. Between these two scenarios there is a starting position that

will result in a motion satisfying both of the boundary conditions, i.e., the initial excess energy is exactly countered by the friction with the result that the particle comes to rest a $\sigma=0$.

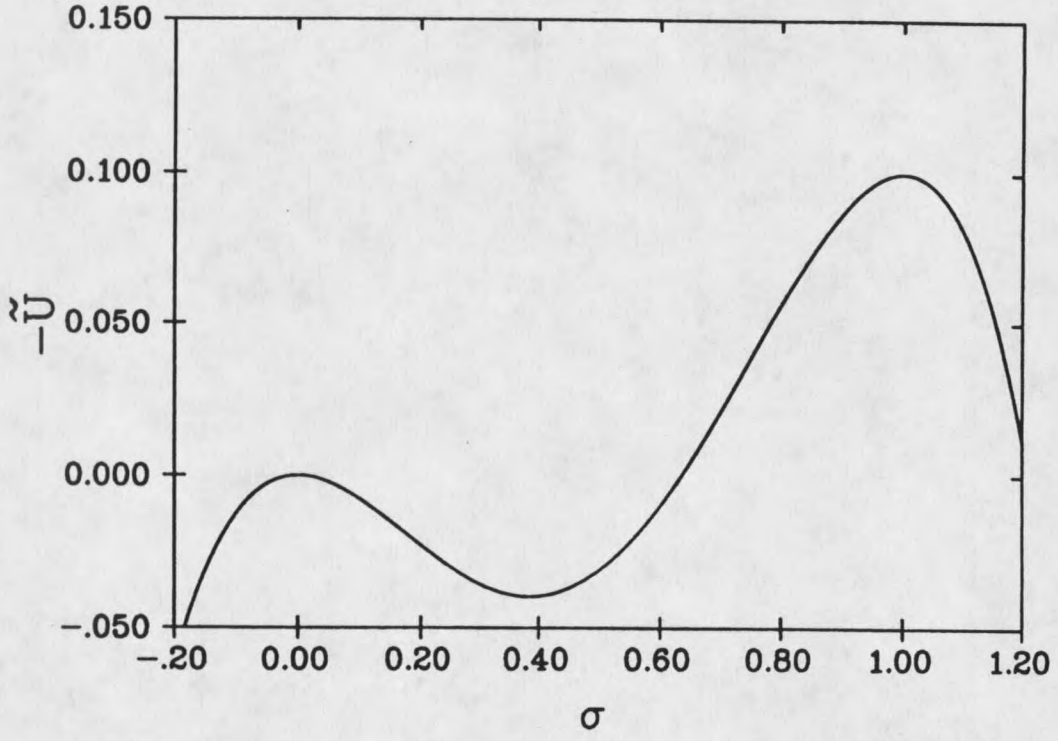

Figure 5 The inverted $\phi^{2\text{-}3\text{-}4}$ potential which provides the stage for the classical particle motion analogy

We now specialize our consideration to the case of nearly degenerate vacua (i.e, where the energy density difference between the two vacuum states is very small), and again consider the particle motion analogy. In this situation it will be possible to put the differential equation into an approximate form, and thus allow approximate solutions and the associated Euclidean actions to be obtained in closed form.

When the energy density difference between the two vacuum states is small then the "excess energy" available to the particle to overcome the friction is "restrictably small". However, the frictional term may also be made arbitrarily small by remaining close to the top of the hill ($\sigma \approx 1$) for a sufficiently long time, as the friction coefficient is inversely proportional to this time. Thus we envisage a situation where the particle starts very close to the top of the hill, the driving force is very small here because the derivative of the potential is small, and as a result it takes a long time for the particle to roll off the hill. The energy lost to friction during this phase is minimal as the velocity is small. When the particle eventually rolls off then the hill the frictional term may be neglected as the time is large enough to have rendered it insignificant. The time taken for the particle to roll from $\sigma=1$ to $\sigma=0$ is small in comparison to the time spent near the top of the hill.

Thus we have our model for the "thin-wall" approximation. Translated to the field solution corresponding to the nucleating bubble profile we have a core of true vacuum ($\sigma=1$) and then a rapid transition to the false vacuum ($\sigma=0$) (i.e., a thin wall in comparison to the thickness of the core). The Euclidean action for the nucleating bubble is required in order to determine the false vacuum decay rate. In the "thin-wall" approximation this action now splits into two pieces, (i) the action of the bubble core, and (ii) the action of the bubble wall. There is no contribution to the action from the exterior of the bubble as the field is constant here and the potential energy of the field is zero. In the absence of gravity we may always add a constant to the potential in order to have a zero contribution to the action from the exterior of the bubble. Now of course in order to obtain the decay rate we must have the difference between the Euclidean actions for the spacetimes with and without the bubble, however, in this situation the Euclidean action for the spacetime without the bubble vanishes.

The Euclidean action for a scalar field is given by

$$S = \int d^4 y \, g^{1/2} \left[\tfrac{1}{2} g^{\mu\nu} \partial_\mu \phi \, \partial_\nu \phi - U(\phi) \right], \qquad (2.11)$$

where g is the determinant of the Euclideanized metric. The contribution to the Euclidean action from the interior of the bubble involves only the potential term and is given by

$$S_{\text{interior}} = -\frac{\pi^2}{2} \xi_w^4 \, \tilde{\varepsilon} \quad , \qquad (2.12)$$

where ξ_w is the dimensionless radius of the bubble.

We next require an expression for the action of the bubble wall. To obtain this we transform the Euclideanized field equation into an approximate form suitable for the "thin-wall" model. Thus we have (upon dropping the frictional term)

$$\frac{d^2 \sigma}{d \xi^2} = \frac{1}{\psi_+^2} \frac{d \tilde{U}_0}{d \sigma} \qquad (2.13)$$

We have discarded the frictional term as this is negligible during the motion from σ=1 to σ=0. The new potential function $\tilde{U}_0$ is a degenerate potential function formed from $\tilde{U}$, satisfying,

$$\tilde{U}_0(0)=\tilde{U}_0(1)=0 \quad , \qquad (2.14)$$

and,

$$\frac{d\tilde{U}_0}{dx}(0) = \frac{d\tilde{U}_0}{dx}(1) = 0 \quad . \qquad (2.15)$$

There is in general no unique way to construct this degenerate potential from the original potential. However, for the polynomial potential under consideration we may uniquely define $\tilde{U}_0$, by demanding that it also be a polynomial of no greater than fourth order. Thus with the original potential given by,

$$\tilde{U}(\sigma) = \psi_+^2\{\sigma^2 - 2(1+2\omega)\sigma^3 + (1+3\omega)\sigma^4\} \quad , \qquad (2.16)$$

we obtain the degenerate potential by setting $\omega=0$, as shown in Figure 6. Motion in this degenerate potential is now assumed to go from $\sigma=1$ to $\sigma=0$.

The approximate differential equation of motion is integrable and may be expressed as

$$\frac{d}{d\xi}\left[\frac{\psi_+^2}{2}\left(\frac{d\sigma}{d\xi}\right)^2 - \tilde{U}_0\right] = 0 \ ; \qquad (2.17)$$

and thus with the boundary condition $\sigma(\xi\rightarrow\infty)=0$ (i.e., the potential and derivative terms in Eq.(2.17) go to zero as $\xi\rightarrow\infty$) we have,

$$\frac{\psi_+^2}{2}\left(\frac{d\sigma}{d\xi}\right)^2 - \tilde{U}_0 = 0 \quad . \qquad (2.18)$$

It is now possible to write an explicit expression for the action of the bubble wall.

$$S_{wall} = 2\pi^2\,\xi_w^3 \int_{wall} dx \left[\frac{\psi_+^2}{2}\left(\frac{d\sigma}{d\xi}\right)^2 + \tilde{U}_0\right] \quad , \qquad (2.19)$$

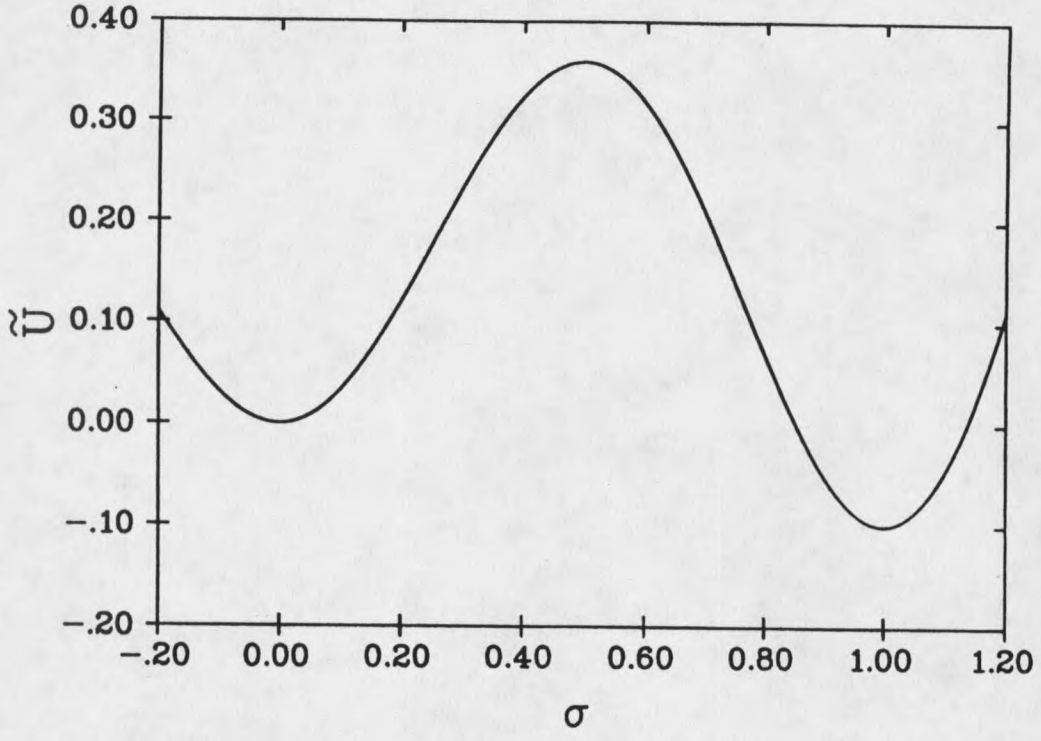

Figure 6 The degenerate potential obtained from the $\phi^{2\text{-}3\text{-}4}$ potential by setting ω=0.

$$= 2\pi^2 \psi_+ \xi_w^3 \int_0^1 d\sigma \, (2\tilde{U}_0)^{1/2} \qquad \text{from Eq.(2.18)} \qquad (2.20)$$

$$= 2\pi^2 \xi_w^3 S_1 \quad , \qquad (2.21)$$

with

$$S_1 = \psi_+ \int_0^1 d\sigma \, (2\tilde{U}_0)^{1/2} \quad . \qquad (2.22)$$

Combining the Euclidean action for the bubble core and wall gives,

$$S_{tw} = -\frac{\pi^2}{2} \xi_w^4 \tilde{\varepsilon} + 2\pi^2 \xi_w^3 S_1 \quad . \qquad (2.23)$$

Minimizing S_{tw} with respect to ξ_w gives the bubble radius and Euclidean action in terms of the expressions for S_1 and $\tilde{\varepsilon}$,

$$\xi_m = \frac{3\,S_1}{\tilde{\varepsilon}} \quad , \tag{2.24}$$

and,

$$S_{tw} = \frac{27\,\pi^2\,S_1^4}{2\tilde{\varepsilon}^3} \tag{2.25}$$

For the $\phi^{2\text{-}3\text{-}4}$ potential, the integral for S_1 reduces to,

$$S_1 = \psi_+^2 \int_0^1 [\,2\,\sigma^2\,(1-\sigma)^2\,]^{\frac{1}{2}}\,d\sigma = \frac{\psi_+^2}{3\sqrt{2}} \quad , \tag{2.26}$$

and the Euclidean action in the "thin-wall" approximation is then

$$S_{tw} = \frac{\pi^2\,\psi_+^2}{24\,\omega^3} \tag{2.27}$$

We note that the "thin-wall" approximate action may be written as $\psi_+^{\,2}$ times a function of ω. This is not a result of the approximation scheme but rather due to a convenient symmetry which exists for the $\phi^{2\text{-}3\text{-}4}$ potential. The field equation, Eq.2.8, is dependent only upon ω, and not on some independent combinations of $\tilde{\varepsilon}$ and ψ_+. Thus we may re-scale $\tilde{\varepsilon}$ and ψ_+, and keep the solution $\sigma(\xi)$ invariant, provided the re-scaling in performed in such a way so as to keep $\omega=\tilde{\varepsilon}/\psi_+^2$ constant. Thus the solution $\sigma(\xi)$ remains invariant under the rescaling,

$$\tilde{\varepsilon} \rightarrow a^{-1}\,\tilde{\varepsilon} \quad , \qquad (2.28)$$

and,

$$\psi_{+} \rightarrow a^{-1/2}\psi_{+} \quad . \qquad (2.29)$$

The Euclidean action for the nucleating bubble is also found to scale under these transformations, this scaling being given by,

$$S_E \rightarrow a^{-1}\,S_E \quad . \qquad (2.30)$$

In order to obtain the number of nucleating bubbles per unit four volume it is necessary to calculate the difference between the Euclidean action for the spacetime with and without the bubble. We have obtained an expression for the Euclidean action of the spacetime with the bubble and so all that is required now is the Euclidean action for the empty spacetime. However, this empty spacetime is just Minkowski space as given by the line element in Eq.(2.5) . The scalar field in this "empty" spacetime takes the constant value of ϕ=0 and so there is neither a kinetic nor a potential contribution to the action. Thus we have,

$$B = S\,(\text{bubble}) - S\,(\text{empty}) \qquad (2.31)$$
$$= S\,(\text{bubble})$$

Figure 7 shows a graph of the ratio of B for the "thin-wall" approximation to the value of B determined by the *exact numerical solution* of the Euclideanized field equation (a description of the numerical methods associated with the solution to the Euclideanized field equations and the evaluation of the exact Euclidean action may be

found in the Appendix). We immediately observe that the "thin-wall" approximation is at best a zeroth order approximation, at least for the $\phi^{2\text{-}3\text{-}4}$ potential. The "thin-wall" approximate action is exact for the limiting case of $\omega=0$ and remains within 10% of the exact result only up to $\omega\approx 0.02$. Thus we are led to conclude that the reliability of the "thin-wall" approximation may be questionable.

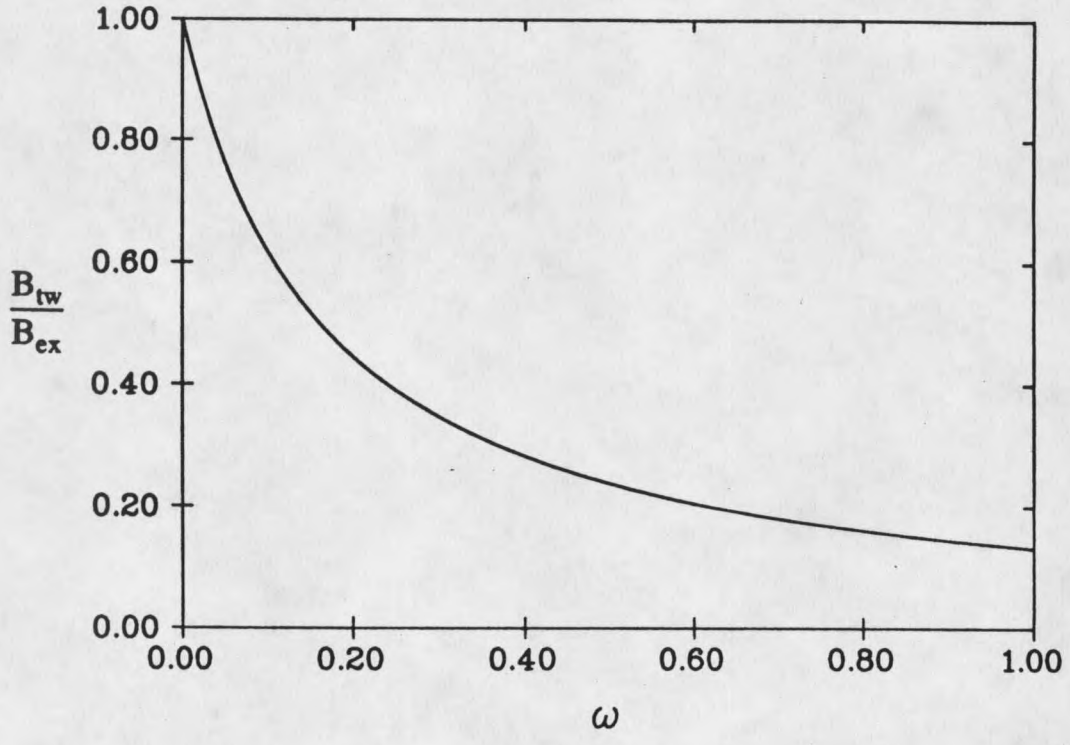

Figure 7 A comparison of the "thin-wall" approximation and exact results for the Euclidean action of nucleating bubbles formed with a $\phi^{2\text{-}3\text{-}4}$ potential. The curve gives the ratio of the approximate to the exact Euclidean action as a function of ω.

A New Approximation Scheme

In the new approximation scheme we obtain a degenerate potential, $\tilde{U}_0^{New}$, from the full potential by adding a term linear in the field, σ, to the original potential such that $[\tilde{U}_0^{New}(\sigma=0)]=[\tilde{U}_0^{New}(\sigma=1)]=0$. However, we note that the derivative of $\tilde{U}_0^{New}$ will not be zero at $\sigma=0$ and $\sigma=1$; in this way the new approximation deviates from Coleman's definition of the "thin-wall" approximation. Thus we have

$$\tilde{U}_0^{New}(\sigma) = \psi_+^2 \left(\sigma^2 - 2(1+2\omega)\sigma^3 + (1+3\omega)\sigma^4 + \sigma\omega \right) \quad ; \qquad (2.32)$$

and the S_1 integral takes the form,

$$S_1^{New} = 2^{1/2} \psi_+^2 \int_0^1 \tilde{U}_0^{New} \{ | \tilde{U}_0^{New} | \}^{-1/2} d\sigma \qquad (2.33)$$

The unusual appearance of the integrand as compared to the previous expression given in Eq.(2.22) is due to the fact that the new degenerate potential is not positive semi-definite; the form of the integrand in Eq.(2.30) is such that the integral will at least be a C^1 function. It may be considered that this expression is too artificial, however, for the purpose of the approximation scheme it does serve as the most convenient definition. An alternative definition may take the limits of integration to go from zero to the point where the argument of the square root becomes negative. However, this is found in general to change the value of S_1 by at most a few percent and is not worth the extra complication. After all, a good approximation scheme should be both well defined and calculationally simple!

The value for S_1^{New} is now substituted into the expressions (Eqs. (2.24) & (2.25)) as for the original "thin-wall" approximation, the results are shown in Figure 8.

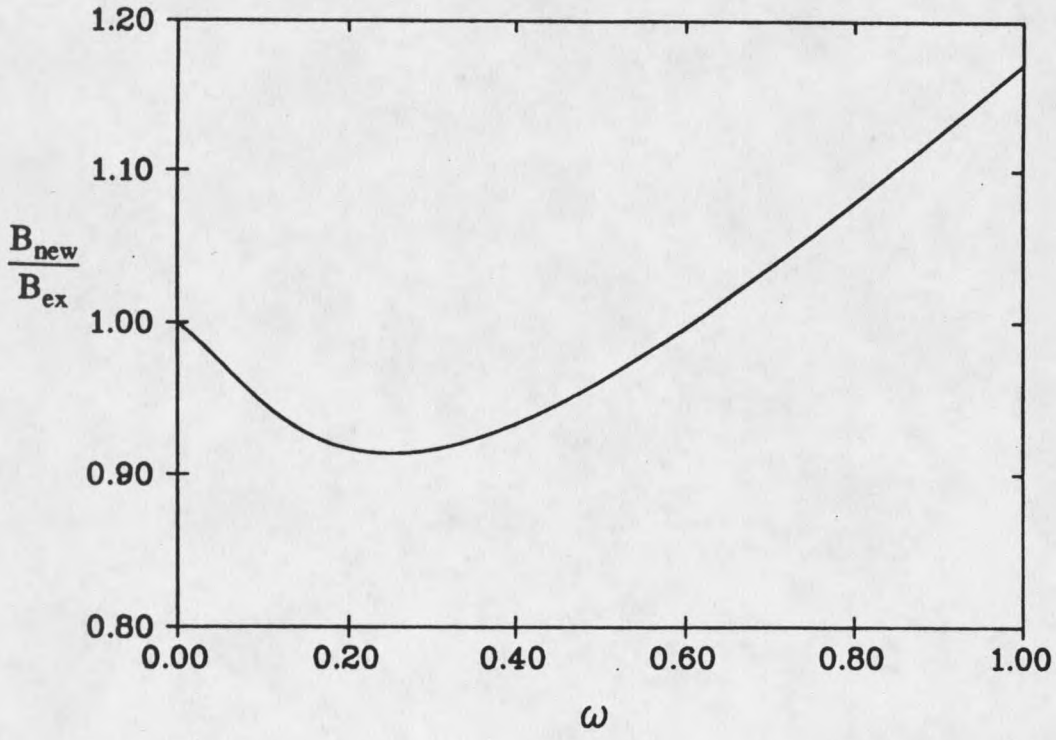

Figure 8 A comparison of the new approximation and the exact numerical results for the Euclidean action of nucleating bubbles formed with a $\phi^{2\text{-}3\text{-}4}$ potential. The curve shows the ratio of the approximate to the exact Euclidean action as a function of ω.

The results for the new approximation scheme obviously fair far better than the original "thin-wall" approximation, at least for the $\phi^{2\text{-}3\text{-}4}$ potential. The approximate value for B is again exact for ω=0 and remains within 10% of the exact results up to about ω=0.85; this is a range of between one and two orders of magnitude greater than for the original "thin-wall" approximation. Figure 9 gives a superposition of Figures 7 and 8, and allows for a better comparison of the two approximation schemes. We note

that the original "thin-wall" approximation always underestimates B and hence overestimates the decay rate. When the new approximation diverges from within 10% of the exact results then it does so in a way so as to overestimate B and hence underestimate the decay rate.

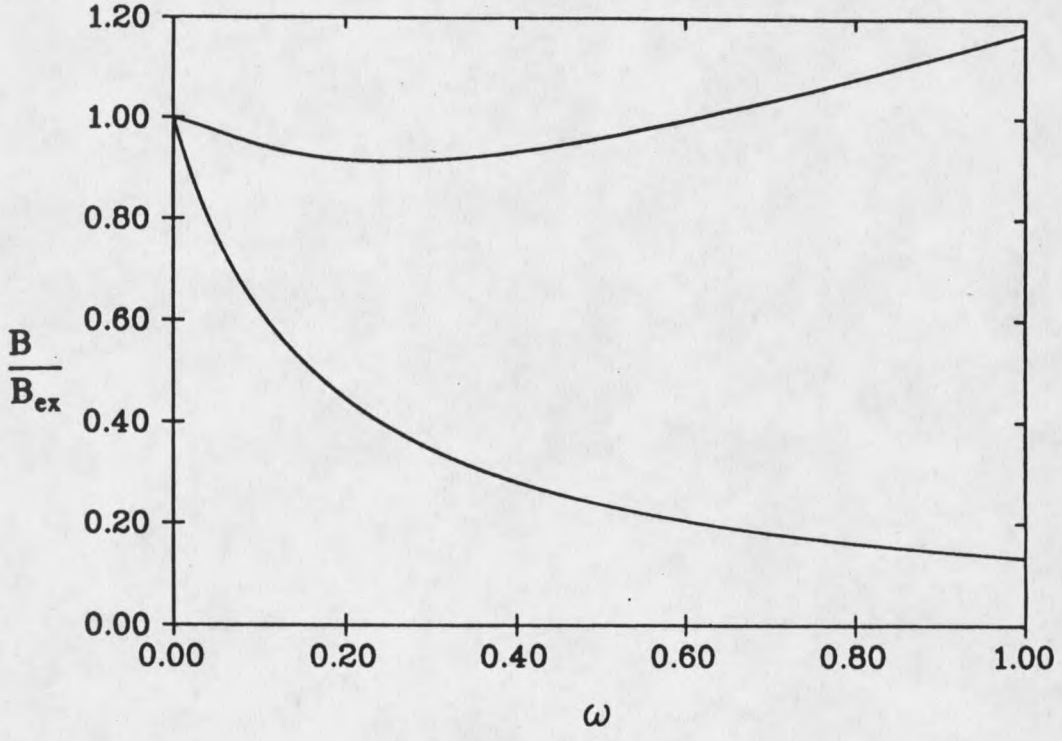

Figure 9 A comparison of the original "thin-wall" approximation and the 'new' approximation scheme for bubble nucleation with a $\phi^{2\text{-}3\text{-}4}$ potential. The upper curve shows the ratio of B(approx)/B(exact) for the new approximation and the lower curve shows the same ratio for the original "thin-wall" approximation.

We noted that the regime in which the approximation methods hold, at least for the $\phi^{2\text{-}3\text{-}4}$ potential, corresponds to a small value of ω. Confusion has arisen here where some of the earlier literature, e.g., Coleman (1977), has suggested that a small value of $\tilde{\varepsilon}$ be the requirement for the "thin-wall" approximation to hold. We may in fact let $\tilde{\varepsilon}$

take any value and still have a valid approximation scheme as long as ψ_+ is sufficiently large so as to let ω lie in the appropriate range. The $\phi^{2\text{-}3\text{-}4}$ potential emphasizes this point rather well. The underlying reason behind this is that the Euclideanized field equation is dependent only upon ω and not some other independent combination of $\tilde{\varepsilon}$ and ψ_+.

Robustness Test for the "New" Approximation Scheme

The "new" approximation scheme would be of little value if it were specialized to the $\phi^{2\text{-}3\text{-}4}$ potential. This approximation method is therefore applied to a highly non-polynomial potential, derived from Bessel functions, in order to test its robustness. The robust potential, in dimensionless form, is given by,

$$\tilde{U}(\sigma) = \frac{\tilde{\varepsilon}\ \{\ J_0[a] - J_0[a(1-\sigma)]\ \}}{1 - J_0[a]} \quad , \qquad (2.34)$$

where $J_0[a]$ is the first maximum of J_0 after $J_0[0]$ (see Figure 10), and the derivative function for use in the Euclideanized field equation is given by,

$$\frac{d\tilde{U}}{d\sigma} = -\frac{a\,\tilde{\varepsilon}\,J_1[a(1-\sigma)]}{1 - J_0[a]} \qquad (2.35)$$

We are now faced with the problem of determining an appropriate degenerate potential for the original "thin-wall" approximation. This problem does not arise with the "new" approximation as the degenerate potential is well defined and obtained simply by adding a linear term to the original potential, thus

$$\tilde{U}_0^{New} = \tilde{U} + \sigma\tilde{\varepsilon} \quad . \qquad (2.36)$$

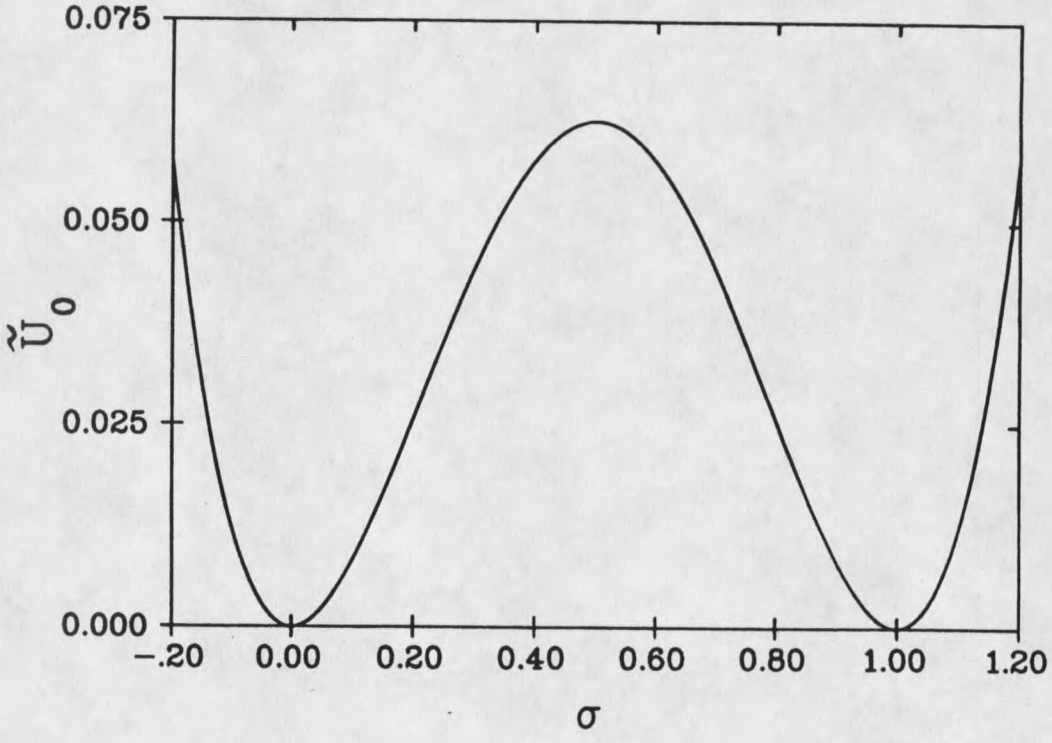

Figure 10 The dimensionless 'robust' potential.

The original "thin-wall" approximation requires a degenerate potential satisfying the conditions $\tilde{U}_0(0)=\tilde{U}_0(1)=0$, and $\frac{d\tilde{U}_0}{dx}(0) = \frac{d\tilde{U}_0}{dx}(1) = 0$. There are obviously an infinite number of potentials satisfying these constraints. With the $\phi^{2\text{-}3\text{-}4}$ potential we were fortunate enough to be presented with an obvious choice for the degenerate potential, this being obtained by setting $\omega=0$ in the original potential, Eq.(2.15). However, with the robust potential we are not so fortunate, there is no parameter which we may set to zero giving the desired result. This will in fact be the

case in general for an arbitrary potential. We shall therefore construct the following degenerate potential, which we may argue is a reasonable choice,

$$\tilde{U}_0 = \frac{\tilde{\varepsilon}}{2}[\,1 - \cos(2\pi\sigma)\,] \qquad (2.37)$$

Unlike the $\phi^{2\text{-}3\text{-}4}$ degenerate potential, the degenerate potential here "scales in height" in accordance with the robust potential. Proceeding with the original "thin-wall" analysis we obtain,

$$B_{tw} = \frac{864}{\pi^2}\frac{1}{\tilde{\varepsilon}} \qquad (2.38)$$

The robust potential has another qualitative difference with respect to the $\phi^{2\text{-}3\text{-}4}$ potential in that it undergoes a simple scaling as we alter the depth of the true vacuum relative to the false vacuum; a change in $\tilde{\varepsilon}$ for the $\phi^{2\text{-}3\text{-}4}$ potential resulted in an associated qualitative change in the shape of the potential. The Euclideanized field equation admits a simple treatment for the scaling of potentials. During the transformation,

$$\tilde{U} \rightarrow \alpha\,\tilde{U} \quad ; \qquad (2.39)$$

we have,

$$\sigma(x) \rightarrow \sigma(\alpha^{1/2}x) \quad ; \qquad (2.40)$$

and,

$$B \rightarrow \alpha^{-2}\,B \quad . \qquad (2.41)$$

Thus it is sufficient to calculate the nucleating bubble profile and Euclidean action for one value of $\tilde{\varepsilon}$, the remainder of the nucleating bubble profiles and Euclidean

actions are then obtained from the above scaling rules. Taking for the initial 'robust' potential $\tilde{\varepsilon}$=0.1, we obtain,

$$B_{tw} = 875.4 \qquad B^{New} = 1776.6 \qquad B_{exact} = 1826.2$$

Alternatively, $\dfrac{B_{tw}}{B_{exact}} = 0.48 \qquad \dfrac{B^{New}}{B_{exact}} = 0.97$.

Thus again with the robust potential, we observe that the new approximation scheme holds up far better than the original "thin-wall" approximation.

Further studies with robust potentials have been presented by Samuel and Hiscock (1991(a)). Their analysis verified the improved values of B obtained via the use of the "new" approximation scheme over the original "thin-wall" approximation. It was also shown that apart from a possible scale change on the ω-axis, the results illustrated in Figure 9 appear to characterize the relative values for B obtained in the two approximation schemes, regardless of the functional form of the potential.

Bubble Profiles

The "thin-wall" approximation inherently assumes that the bubble profile is one of an interior core of true vacuum (σ=1), a very thin-wall where σ evolves rapidly from 1 to 0 and an exterior of false vacuum (σ=0); as shown in Figure 3. We expect the exact bubble profiles to approach the thin-wall profile in the regime of $\omega \rightarrow 0$, however it is instructive to observe the evolution of the bubble profile as the potential moves away from the region applicable to the "thin-wall" model.

Figure 11 shows the bubble profile at the moment of nucleation for a couple of values of ω, with a $\phi^{2\text{-}3\text{-}4}$ potential. We observe that for such a potential the thin-wall profile does not really occur for $\omega>0.2$, and we would have to move to much smaller values of ω in order to obtain such a profile.

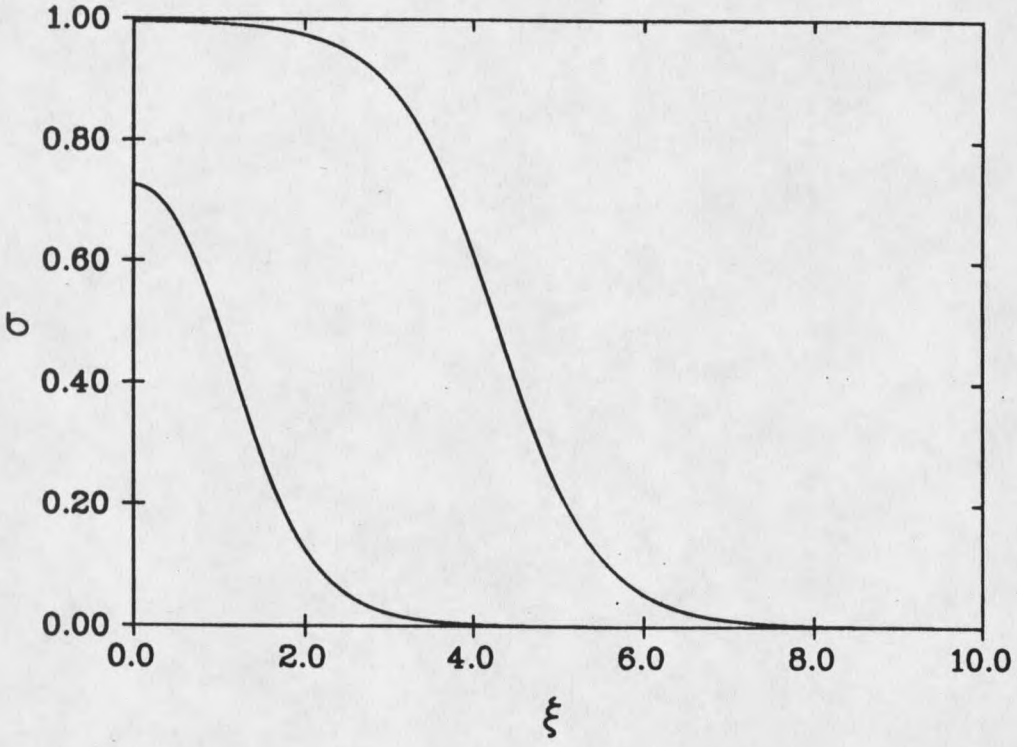

Figure 11 Nucleating bubble field profiles (i.e., solution curves for Eq.(2.8)) for ω=0.2 (upper profile), and ω=1.0 (lower profile).

Figure 12 shows a bubble profile for the robust potential corresponding to $\tilde{\varepsilon}$=1.0, the remaining profiles are obtained from the scaling rule given by Eq.(2.37). This profile fits better into the "thin-wall" model than the corresponding profile for the $\phi^{2\text{-}3\text{-}4}$ potential (with $\tilde{\varepsilon}$=1.0). However, as the results have shown, this does not

necessarily imply that the Euclidean action obtained from the "thin-wall" approximation will be close to the exact Euclidean action.

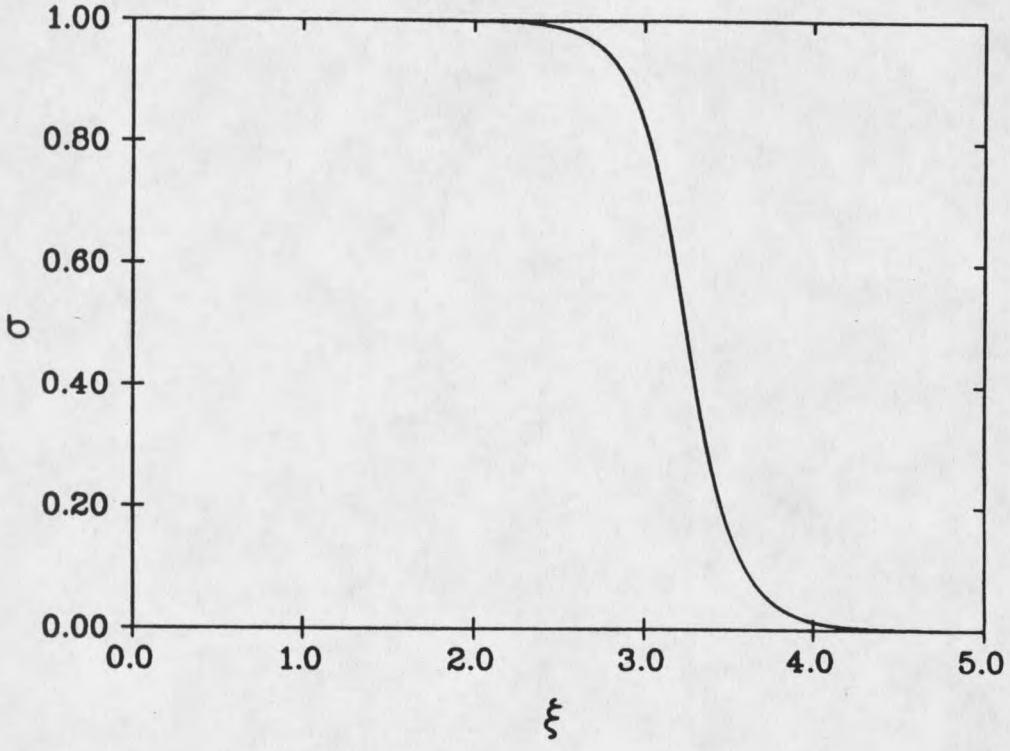

Figure 12 Bubble profile for the robust potential corresponding to $\tilde{\epsilon}$=1.0.

Energy of the Nucleating Bubble

It is a fairly straightforward task to determine the energy of the nucleating bubble. The calculation proceeds as follows: The energy of the nucleating bubble is defined by,

$$E = 4\pi \int_0^{\infty} \rho^2 \left[\frac{1}{2} \left(\frac{d\phi}{d\rho} \right)^2 + U \right] d\rho \qquad (2.42)$$

which may be written as

$$E = 4\pi \int_0^{\infty} \left[\frac{1}{2} \left(\frac{d\phi}{d\rho} \right)^2 + U \right] \frac{d}{d\rho} \left(\frac{1}{3} \rho^3 \right) d\rho \qquad (2.43)$$

Integrating by parts,

$$E = \frac{4\pi}{3} \left[\rho^3 \left\{ \frac{1}{2} \left(\frac{d\phi}{d\rho} \right)^2 + U \right\} \right]_{\rho=0}^{\rho=\infty} - \frac{4\pi}{3} \int_0^{\infty} \rho^3 \frac{d}{d\rho} \left\{ \frac{1}{2} \left(\frac{d\phi}{d\rho} \right)^2 + U \right\} d\rho \qquad (2.44)$$

The first term of this equation vanishes, leaving,

$$E = -\frac{4\pi}{3} \int_0^{\infty} \rho^3 \left(\frac{d\phi}{d\rho} \right) \left\{ \frac{d^2\phi}{d\rho^2} + \frac{dU}{d\rho} \right\} d\rho \qquad (2.45)$$

$$= -\frac{4\pi}{3} \int_0^{\infty} \rho^3 \left(\frac{d\phi}{d\rho} \right) \left\{ \frac{d^2\phi}{d\rho^2} + \frac{1}{\rho^3} \frac{d}{d\rho} \left[\rho^3 \left(\frac{d\phi}{d\rho} \right) \right] \right\} d\rho \qquad (2.46)$$

$$= -\frac{4\pi}{3}\int_0^\infty \rho^3 \left(\frac{d\phi}{d\rho}\right)\left(\frac{d^2\phi}{d\rho^2}\right) d\rho \ \ldots$$

$$\ldots + \frac{4\pi}{3}\int_0^\infty \rho^3 \left(\frac{d\phi}{d\rho}\right)\left(\frac{d^2\phi}{d\rho^2}\right) d\rho - \frac{4\pi}{3}\left[\left(\frac{d\phi}{d\rho}\right)^2 \rho^3\right]_0^\infty \qquad (2.47)$$

$$= 0.$$

Thus we observe, as expected, that the energy of the nucleating bubble is zero, in agreement with the respective conservation laws.

This concludes our review of the "thin-wall" approximation and our analysis of O(4)-symmetric bubble nucleation processes in the absence of gravity. We shall now extend our analysis, in Chapter 3, to the situation where gravity may play a role in the bubble nucleation processes.

CHAPTER 3

FIRST-ORDER VACUUM PHASE TRANSITIONS WITH GRAVITY

Background

One of the more important applications of the theory of false vacuum decay is to cosmology, in particular, the inflationary models of the early universe. These models are of interest because they may provide a solution to many of the contemporary problems of cosmology; for example, the horizon, flatness and monopole problems.

The main characteristic of the inflationary universe models is a de Sitter phase of evolution. The "Higgs fields" provide a driving force for a de Sitter phase of the early Universe via a non-zero vacuum energy density which results in the exponential expansion of the Universe; this expansion being the key to solving many of the cosmological problems. It is obviously necessary for the Universe to evolve out of a de Sitter phase as we find ourselves today living in a Universe with zero vacuum energy density. This evolution is believed to occur within the theories of "old" inflation [Guth (1981)] and "extended" inflation [La and Steinhardt (1989)] via a first-order phase transition within the "Higgs fields".

As the vacuum phase transitions are taking place in a cosmological setting where gravity plays a fundamental role, we may ask whether the self-gravity of the

quantum fields undergoing the phase transition will have an effect on the transition rate. This question has been addressed within the "thin-wall" approximation by Coleman and De Luccia (1980). Their analysis involved the approximate solution of the coupled Euclideanized scalar field and Einstein equations, extending the original "thin-wall" analysis of Coleman (1977), as detailed in Chapter 2, which only required the solution of the Euclideanized scalar field equation.

The analysis of Coleman and De Luccia specifically considered O(4)-symmetric bubble nucleation for the decay from de Sitter to Minkowski space and Minkowski to anti-de Sitter space. They found that gravity enhanced the decay rate for the transition from de Sitter to Minkowski space but impeded the decay rate for the transition from Minkowski to anti-de Sitter space. In fact, there was found to be a forbidden regime in the decay from Minkowski to anti-de Sitter space where no O(4)-symmetric transitions could occur.

The forbidden regime has a simple explanation within the Coleman and De Luccia analysis: There is a gravitational contribution to the energy of the bubble (remembering that the bubble has zero total energy). For the decay from Minkowski to anti-de Sitter space the gravitational contribution to the energy of the bubble results in a bubble of larger radius that in the zero gravity limit. The forbidden regime corresponds to the situation where the bubble cannot be "large enough" to render its energy zero, i.e., the gravitational contribution to the energy of the bubble results in a bubble of infinite radius.

The importance of the self-gravity of a quantum field is governed by the ratio of the mass of the field to the Planck mass. Therefore it may be argued that such effects are negligible as the fields that we are most familiar with have masses well below the Planck mass. For example, the electroweak mass scale of 10^2 GeV is well below the

Planck mass scale of 10^{19} GeV, and thus one would expect gravity to play an insignificant role in the electroweak phase transition. However, it is conceivable that either in the very early Universe (e.g., GUT energy scales may lie between 10^{16} GeV and 10^{18} GeV, and supersymmetric energy scales may also lie close to the Planck scale) or even today a false vacuum phase transition could occur which would be associated with a field of appreciable mass. It is therefore important to obtain a better understanding of the effects of gravity upon such processes.

In Chapter 2 we considered the range of validity of the Coleman "thin-wall" approximation for false vacuum decay in the absence of gravity. In this chapter we shall consider the range of validity of the "thin-wall" approximation with the presence of gravity, via a comparison of the Coleman-De Luccia results with exact numerical results (these results have been reported in Samuel and Hiscock (1991[b])). The analysis shall also be extended beyond those regimes applicable to the "thin-wall" approximation in an attempt to better understand the effect of gravity in these regions.

The analysis shall be based upon bubble nucleation for scalar fields with the polynomial potential, $U(\phi)= U_c + m^2\phi^2 - \eta\phi^3 + \lambda\phi^4$; this is the potential used in the "toy" model analysis of Chapter 2, with the addition of a possible constant term U_c. The constant term will provide the vacuum energy density in the initial false vacuum state, and thus allows us to choose between an initial de Sitter, Minkowski or anti-de Sitter spacetime; these having positive, zero, and negative vacuum energy densities, respectively.

"Thin-Wall" Analysis via a "Toy" Model.

It shall be instructive to review the "thin-wall" approximation for false vacuum decay with the inclusion of gravity, as formulated by Coleman and De Luccia (1980), for the potential under consideration. This will provide us with explicit results with which we may compare the exact numerical results, and hence determine the range of validity of the "thin-wall" approximation. The initial analysis, placing the potential into a suitable form, will proceed in a similar manner to that of Chapter 2.

Consider a self interacting scalar field with a $\phi^{0-2-3-4}$ potential,

$$U=U_c + m^2\phi^2 - \eta\phi^3 + \lambda\phi^4 \quad , \qquad \text{with } m^2 , \eta , \lambda \geq 0. \tag{3.1}$$

U_c shall be the value of the false-vacuum energy density, the false vacuum state being located at $\phi=0$ (with an appropriate choice of parameters). Changing to the dimensionless variables used in Chapter 2;

$$\psi=\phi/m \quad , \quad \tilde{\eta}=\eta/m \quad , \quad \tilde{U}=U/m^4 \quad ,$$

gives,

$$\tilde{U}=\tilde{U}_c + \psi^2 - \tilde{\eta}\psi^3 + \lambda\psi^4 \quad . \tag{3.2}$$

Introduce the parameters ψ_+ , the value of the field at the true vacuum, and $\tilde{\varepsilon}$, the dimensionless energy density difference between the true and false vacuum states. As we shall specifically consider only the decay from de Sitter to Minkowski space, or from Minkowski to anti-de Sitter space, we have placed a constraint upon $\tilde{U}_c$, the dimensionless false vacuum energy density. For the decay from de Sitter to Minkowski

space $\tilde{U}_c=\tilde{\varepsilon}$, and for the decay from Minkowski to anti-de Sitter space $\tilde{U}_c=0$. With this parameterization the potential takes the form,

$$\tilde{U} = [\tilde{\varepsilon}] + \psi^2 - 2(2\tilde{\varepsilon}+\psi_+^2)\frac{\psi^3}{\psi_+^3} + (3\tilde{\varepsilon}+\psi_+^2)\frac{\psi^4}{\psi_+^4} \quad . \qquad (3.3)$$

The first term, in square brackets, is included if we are considering the decay from de Sitter to Minkowski space but excluded for decay from Minkowski to anti-de Sitter space. Finally, we make use of the scaled field variable, $\sigma=\psi/\psi_+$, such that the false vacuum is located at $\sigma=0$ and the true vacuum is located at $\sigma=1$; and again introduce the parameter, $\omega=\tilde{\varepsilon}/\psi_+^2$. Thus ,

$$\tilde{U} = [\tilde{\varepsilon}] + \{\sigma^2 - 2(2\omega+1)\sigma^3 + (3\omega+1)\sigma^4\}\psi_+^2 \quad . \qquad (3.4)$$

Figure 13 shows this potential for the decay from de Sitter to Minkowski space and the decay from Minkowski to anti-de Sitter space. In both cases the potential is illustrated for $\tilde{\varepsilon}=0.1$ and $\psi_+=1.0$. We note that the shape of the potential is the same in both cases, the only difference being a constant energy density shift. In the absence of gravity the solution of the Euclideanized field equation, which gives the nucleating bubble profile and the decay rate, would have been the same for both potentials given here. The reason for this is that the "force term" in the Euclideanized field equation is given by the derivative of the potential and so would not be sensitive to the constant energy shift. The constant term in the vacuum energy density associated with the potential will, however, be a source for the gravitational field and hence have an effect on the nucleating bubble profile and decay rate if the analysis is to include the effects of gravity.

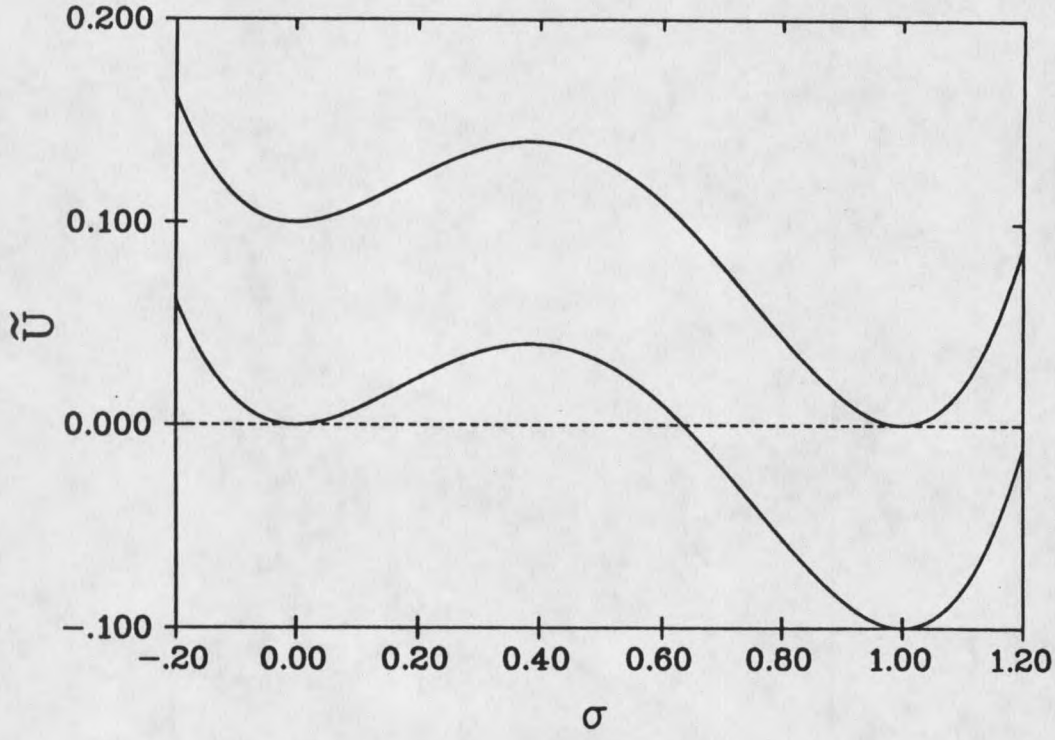

Figure 13 The upper curve shows the form of the potential associated with the decay from de Sitter to Minkowski space, with the false vacuum state having a positive vacuum energy density. The lower curve shows the form of the potential associated with the decay from Minkowski to anti-de Sitter space, with the false vacuum state having zero vacuum energy density. The two curves differ only by a constant energy density shift.

Euclideanized Scalar Field and Einstein Equations

The solution to the coupled Euclideanized scalar field and Einstein equations will provide us with the bubble profile at the moment of nucleation. The associated Euclidean action of this bubble will yield the number of nucleating bubbles per unit four volume via the equation $\Gamma=Ae^{(-B)}$, where B is the difference between the Euclidean action for the spacetime with and without the bubble. The coefficient 'A' is a

functional determinant associated with the Euclideanized scalar field equation and is typically of the order of the field mass to the fourth power.

For the decay from Minkowski to anti-de Sitter space, the initial spacetime without the bubble (i.e., Minkowski space) has a vanishing Euclidean action and hence B is given simply by the Euclidean action for the bubble spacetime. However, for the decay from de Sitter to Minkowski space, the initial empty spacetime (i.e., de Sitter space) does not have a vanishing Euclidean action, and so it is necessary to evaluate a subtraction term in order to obtain B.

In the absence of gravity Coleman, et. al. (1978), have shown that O(4)-symmetric bubbles will always have the least action, and hence be the dominant mode for decay. This result has not at this time been successfully extended to the situation where gravity is present, but it is generally believed to still hold. Thus we shall also consider O(4)-symmetric bubble nucleation in a similar manner to Coleman and De Luccia.

The Euclideanized spacetimes that we are considering (i.e., de Sitter, Minkowski and anti-de Sitter) are all O(4)-symmetric, and so the appropriate line element for the Euclideanized spacetime is given by

$$(ds)^2 = (d\zeta)^2 + \nu(\zeta)^2\,(d\Omega)^2 \quad , \qquad (3.5)$$

where $d\Omega$ is the unit 3-sphere line element. For the Euclideanized de Sitter, Minkowski and anti-de Sitter spaces, the function $\nu(\zeta)$ has the form $\kappa^{-1}\sin(\kappa\zeta)$, ζ, and $\kappa^{-1}\sinh(\kappa\zeta)$, respectively (where κ represents the radius of curvature of the spacetime).

The Euclideanized scalar field equation may be expressed in a generalized form, in terms of the metric and partial derivatives with respect to the coordinate variables, as follows,

$$g^{-1/2}\partial_\mu \left[g^{1/2} g^{\mu\nu} \partial_\nu \right]\phi = \frac{dU}{d\phi} \quad , \qquad (3.6)$$

where g is the determinant of the Euclidean metric. In terms of the coordinates of the line element given in Eq.(3.5), and knowing that for O(4)-symmetric bubbles, $\phi=\phi(\zeta)$, Eq. (3.6) reduces to

$$\frac{d^2\phi}{d\zeta^2} + \frac{3}{\nu}\frac{d\nu}{d\zeta}\frac{d\phi}{d\zeta} = \frac{dU}{d\phi} \qquad (3.7)$$

A scalar field is a source for the gravitational field via the stress-energy tensor for the scalar field. If we assume minimal coupling between the scalar field and the gravitational field then Einstein's equation, $G_{\mu\nu}= 8\pi G T_{\mu\nu}$, gives for the $G_{\zeta\zeta}$ component of the Einstein tensor,

$$\left[\frac{d\nu}{d\zeta}\right]^2 = 1 + \frac{8\pi G}{3}\nu^2\, T_{\zeta\zeta} \quad , \qquad (3.8)$$

where

$$T_{\zeta\zeta} = \frac{1}{2}\left[\frac{d\phi}{d\zeta}\right]^2 - U \quad . \qquad (3.9)$$

We again introduce dimensionless variables,

$\xi=m\zeta$, $\rho=m\nu$,

and make the additional substitution, $G=\frac{1}{m_p^2}$, where m_p is the Planck mass. With these variables the Einstein equation may be written,

$$(\rho')^2 = 1 + \frac{8\pi}{3}\frac{m^2}{m_p^2}\left\{ \tfrac{1}{2}\sigma'^2 - \left([\omega] + \sigma^2 - 2(2\omega+1)\sigma^3 + (3\omega+1)\sigma^4 \right) \right\} \rho^2 \psi_+^2 \quad (3.10)$$

where '=d/dξ , and we have for the Euclideanized scalar field equation ,

$$\sigma'' + \frac{3\rho'}{\rho}\sigma' = 2\sigma - 6(2\omega+1)\sigma^2 + 4(3\omega+1)\sigma^3 \quad . \qquad (3.11)$$

The following boundary conditions are imposed upon Eqs. (3.10) and (3.11) :

$$\rho=0 \text{ at } \xi=0 \quad , \quad , \qquad (3.12)$$

for Eq. (3.10), together with,

$$\sigma'=0 \text{ at } \rho=0 \text{ , and, } \sigma=0 \text{ at } \xi=\infty \quad , \qquad (3.13)$$

for Eq. (3.11).

Euclidean Action for the Nucleating Bubble

The Euclidean action for the nucleating bubble has contributions from both the scalar field potential and kinetic terms together with a gravitational term via the Ricci scalar,

$$S_E = \int d^4x\, g^{1/2}\{ \tfrac{1}{2} g^{\mu\nu} \partial_\mu\phi\, \partial_\nu\phi + U(\phi) + \frac{R}{16\pi G} \} \qquad (3.14)$$

$$= 2\pi^2 \int d\zeta \left[\nu^3 \left[\tfrac{1}{2}\left(\frac{d\phi}{d\zeta}\right)^2 + U \right] + \frac{3}{8\pi G}\left[\nu^2 \frac{d^2\nu}{d\zeta^2} + \nu\left(\frac{d\nu}{d\zeta}\right)^2 - \nu \right] \right] \quad . \qquad (3.15)$$

As the scalar field profile for the nucleating bubble is a solution to the Euclideanized scalar field and Einstein equations we may use these equations to simplify Eq.(3.15). We then have in terms of the dimensionless variables,

$$S_E = -2\pi^2 \int d\xi\, \rho^3 \tilde{U} \quad . \qquad (3.16)$$

Symmetry Transformations within the Theory

In the zero gravity limit, defined by $m_p \to \infty$, the solution to Eq.(3.10) reduces to $\rho = \xi$ and Eq.(3.11) depends only upon ω. We may therefore rescale $\tilde{\varepsilon}$ and ψ_+ , and keep the solution $\sigma(\xi)$ invariant, provided the re-scaling is performed in such a way so as to keep $\omega = \tilde{\varepsilon}/\psi_+^2$ constant. This may be thought of as a consequence of only having one length scale in the theory (i.e., that given by the mass of the field).

When gravity is introduced via a finite Planck mass the above symmetry is broken, because we now have two natural length scales within the theory. However, there is still a similar but weaker symmetry within the theory. The coupled solutions $\sigma(\xi)$ and $\rho(\xi)$ remain invariant under the rescalings,

$$m \to a^{1/2} m \quad , \qquad (3.17)$$

$$\tilde{\varepsilon} \to a^{-1}\, \tilde{\varepsilon} \quad , \qquad (3.18)$$

$$\psi_+ \to a^{-1/2} \psi_+ \quad . \qquad (3.19)$$

Thus, in the zero gravity limit the "m" rescaling was unnecessary. The Euclidean action for the nucleating bubble will also be found to scale under these transformations, this scaling being given by,

$$S_E \to a^{-1}\, S_E \quad . \qquad (3.20)$$

The theory possesses another, more generalized, symmetry that is not dependent upon the form of the $\phi^{0-2-3-4}$ potential. Writing the Euclideanized scalar field and Einstein equations in a model independent form, we have

$$\frac{d^2\psi}{d\xi^2} + \frac{3}{\rho}\frac{d\rho}{d\xi}\frac{d\psi}{d\xi} = \frac{d\tilde{U}}{d\psi} \quad , \tag{3.21}$$

$$\left[\frac{\partial\rho}{\partial\xi}\right]^2 = 1 + \frac{8\pi}{3}\frac{m^2}{m_p{}^2}\rho^2\left[\frac{1}{2}\left[\frac{\partial\psi}{\partial\xi}\right]^2 - \tilde{U}\right] \quad . \tag{3.22}$$

These equations are invariant under the rescalings;

$$\tilde{U} \rightarrow \beta^2\,\tilde{U} \quad , \tag{3.23}$$

$$\xi \rightarrow \beta^{-1}\,\xi \quad , \tag{3.24}$$

$$\rho \rightarrow \beta^{-1}\,\rho \quad . \tag{3.25}$$

We note that no "m" rescaling is necessary within this symmetry transformation, even though we are considering the effects of gravity. The Euclidean action scales under the above transformations according to,

$$S_E \rightarrow \beta^{-2}\,S_E \quad . \tag{3.26}$$

"Frictional" Term in the Presence of Gravity

The "thin-wall" approximation, as presented by Coleman (1978), makes use of the analogy between Eq.(3.11) and the classical motion of a particle of unit mass moving in the inverted potential, $-\tilde{U}$ (as explained in Chapter 2), where σ corresponds to the particle's position and ξ to the time. In the absence of gravity there is a "frictional" term with the unusual "frictional" coefficient given by $(3/\xi)$, i.e., inversely

proportional to the time; when gravity is included this picture still holds, but the "frictional" coefficient is more complicated, now being given by $(3\rho'/\rho)$.

The "thin-wall" approximation assumes that the field remains close to the "top of the hill" of the inverted potential (i.e., close to $\sigma=1$) until ρ becomes very large, thus supposedly allowing the "frictional" coefficient to become arbitrarily small, as this is inversely proportional to ρ. When the field does eventually "roll off the hill" it is assumed that its subsequent motion is unaffected by "friction". In this case the Euclideanized scalar field equation may be written in an approximate form, by dropping the "frictional" term; making the equation more tractable. The validity of this approach is now examined.

The "frictional" term in the presence of gravity may be written as,

$$\frac{3\rho'}{\rho} = 3\left[\frac{1}{\rho^2} + \frac{8\pi}{3}\frac{m^2}{m_p^2}\left\{ \tfrac{1}{2}\sigma'^2 - \left([\omega] + \sigma^2 - 2(2\omega+1)\sigma^3 + (3\omega+1)\sigma^4 \right) \right\} \psi_+^2 \right]^{1/2} \qquad (3.27)$$

Coleman and De Luccia argue that if ρ becomes large before the "field rolls off the hill" the "frictional" coefficient, (Eq.(3.27)), is very small and may be neglected. This is obviously true for the first term in Eq.(3.27), i.e., $1/\rho^2$. However, the second part of the frictional term does not depend upon ρ, its dependence is solely on the shape of the potential and the mass of the scalar field. In the situation where the mass of the scalar field is very small, this second term will also be small and may be neglected in accordance to the analysis of Coleman and De Luccia. We shall see, however, that for the decay from Minkowski to anti-de Sitter space this second term plays a key role in determining the critical mass, above which there are no more allowed decays.

"Thin- Wall" Analysis via the Israel Formalism

The "thin-wall" analysis in the presence of gravity as formulated by Coleman and De Luccia would now proceed with the approximate solution of the coupled Euclideanized scalar field and Einstein equations. This culminates in expressions for B (the difference between the Euclidean action for the bubble-spacetime and the initial spacetime), and ρ (the nucleating bubble radius), for the decays from de Sitter to Minkowski space and Minkowski to anti-de Sitter space. However, we shall present an alternative derivation of the results using the Israel(1966) formalism, which, from the viewpoint of general relativity is somewhat more elegant. This procedure involves the "patching" together of two spacetimes, using the Einstein equations to provide matching or boundary conditions. Thus, for example, with the decay from de Sitter space to Minkowski space we would patch together an interior bubble of Minkowski space to an exterior of de Sitter space. As we will be performing the analysis in the Euclidean sector then we shall patch together Euclideanized spacetimes.

Consider a Riemannian manifold, M, with metric function g_{ab}. The manifold M shall be divided into two pieces, M^- and M^+, by a smooth, closed surface Σ. The metric function in M^- and M^+ shall be given by g_{ab}^- and g_{ab}^+, respectively. There will be an induced intrinsic metric h_{ab} on the surface Σ, and n^a shall denote the unit normal vector field on Σ pointing from M^- to M^+. Figure 14 illustrates these ideas. The induced metric on Σ may be expressed as,

$$h_{ab} = g_{ab} - n_a n_b , \tag{3.28}$$

and the extrinsic curvature is given by,

$$K_{ab} = h_a^c \nabla_c n_b . \tag{3.29}$$

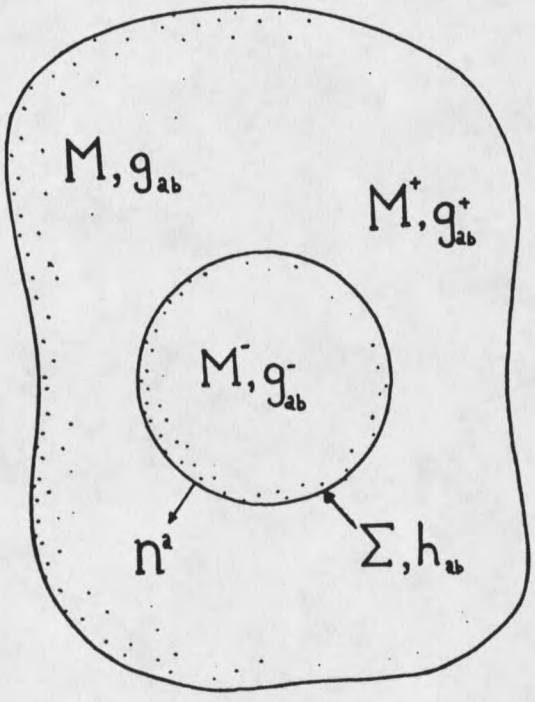

Figure 14 M is a Riemannian manifold with metric function g_{ab}. The manifold is divided into two pieces M^- and M^+, by a smooth, closed surface Σ. The metric function in M^- and M^+ is given by $g_{ab}{}^-$ and $g_{ab}{}^+$ respectively. h_{ab} is the induced metric on Σ, and n^a is a unit, normal vector field, on Σ, pointing from M^- to M^+.

The Israel matching conditions on the surface Σ are,

$$h^+_{ab} - h^-_{ab} = 0 \quad , \tag{3.30}$$

and

$$K^+_{ab} - K^-_{ab} = -8\pi(t_{ab} - \tfrac{1}{2} t\, h_{ab}); \tag{3.31}$$

where the + and - superscripts indicate that the tensor quantities have been evaluated on the surface Σ, in the M^+ and M^- parts of the manifold respectively.

We may now apply these methods to the decays from de Sitter to Minkowski space and Minkowski to anti-de Sitter space.

"Thin-wall" Decay from Minkowski Space to Anti-de Sitter Space

To analyze the "thin-wall" decay from Minkowski to anti-de Sitter space we will have to patch together an interior bubble of Euclideanized anti-de Sitter spacetime (M^-), to an exterior of Euclideanized Minkowski spacetime (M^+). So, inside the bubble, M^- is Euclideanized anti-de Sitter space, with coordinates (ξ,χ,θ,ϕ), and metric,

$$g_{ab}^{-} = \text{diag}(1 , \rho^2, \rho^2 \sin^2\chi , \rho^2 \sin^2\chi \sin^2 \theta) ; \qquad (3.32)$$

where $\rho^2 = \Lambda^2 \sinh^2\left[\frac{\xi}{\Lambda}\right]$, and Λ is the radius of curvature of the Euclideanized anti-de Sitter space. The unit normal vector field evaluated in M^- is ,

$$n_a^{-} = (1, 0, 0, 0) \quad , \qquad (3.33)$$

which gives,

$$h_{ab}^{+} = \text{diag}(0 , \rho^2, \rho^2 \sin^2\chi , \rho^2 \sin^2\chi \sin^2 \theta) \qquad (3.34)$$

The extrinsic curvature tensor , $K_{ab} = h_a^c \nabla_c n_b$, is quite trivial to calculate because n_a^- is a constant vector field. Thus,

$$K_{ab} = \Gamma_{ab}^{\xi} \quad , \qquad (3.35)$$

with the result that,

$$K_{ab}^{-} = \frac{1}{\Lambda} \coth\left(\frac{\xi}{\Lambda}\right) h_{ab}^{-} \qquad (3.36)$$

Outside the bubble, M^+ is Minkowski space, with coordinates (Ξ,X,Θ,Φ), and metric,

$$g_{ab}^{+} = \text{diag}(1 , \Xi^2, \Xi^2 \sin^2\chi , \Xi^2 \sin^2\chi \sin^2 \theta) \qquad (3.37)$$

The unit normal vector field evaluated in M^+ is simply,

$$n_a^{+} = (1, 0, 0, 0) \quad , \qquad (3.38)$$

which gives

$$h_{ab}^{+} = \text{diag}(0 , \Xi^2, \Xi^2 \sin^2\chi , \Xi^2 \sin^2\chi \sin^2 \theta) \qquad (3.39)$$

The extrinsic curvature tensor , $K_{ab} = h_a^c \nabla_c n_b$, is again quite trivial to calculate in this case because n_a^+ is again a constant vector field. Thus

$$K_{ab} = \Gamma_{ab}^{\Xi} \quad , \qquad (3.40)$$

with the result that

$$K_{ab}^{+} = -\frac{1}{\Xi} h_{ab}^{+} \ . \qquad (3.41)$$

The matching condition, $[h_{ab}^{+} - h_{ab}^{-}]_\Sigma = 0$, implies that

$$\Xi_\Sigma = \Lambda \sinh\left(\frac{\xi_\Sigma}{\Lambda}\right) \quad , \qquad (3.42)$$

where ξ_Σ and Ξ_Σ are the respective coordinates of Σ in M^- and M^+. Taking the induced stress energy tensor for the thin wall at Σ to be

$$t_{ab} = \gamma\, h_{ab}^{+} \quad , \tag{3.43}$$

then the matching condition, $[\, K_{ab}^{+} - K_{ab}^{-} \,]_\Sigma = -8\pi(t_{ab} - \frac{1}{2} t\, h_{ab})$, gives

$$\frac{1}{\xi_\Sigma}\left[\, 1 - \cosh\left(\frac{\Xi_\Sigma}{\Lambda}\right)\right] h_{ab}^{+} = 4\pi\gamma\, \xi_\Sigma\, h_{ab}^{+} \quad ; \tag{3.44}$$

re-arranging this expression we have

$$\left[\, 1 + \frac{\xi_\Sigma^2}{\Lambda^2}\right]^{1/2} = 1 + 4\pi\gamma\, \xi_\Sigma \quad , \tag{3.45}$$

and finally

$$\Xi_\Sigma = \frac{8\pi\gamma}{16\pi^2\gamma^2 - \frac{1}{\Lambda^2}} \tag{3.46}$$

This result may be re-expressed in terms of the variables that are more physical; thus if we let the radius of the bubble in the presence of gravity be denoted by ρ_w , and the corresponding radius in the absence of gravity be denoted by ρ_0 , then

$$\rho_w = \frac{\rho_0}{1 - \left(\frac{\rho_0}{2\Lambda}\right)^2} \quad , \tag{3.47}$$

where

$$\rho_0 = 3\gamma/\varepsilon \qquad (3.48)$$

The radius of curvature of the Euclideanized anti-de Sitter space (i.e., Λ) is given by $\Lambda = 3m_p^2/8\pi\varepsilon$, where ε is the energy density of the associated spacetime. Thus the zero gravity radius of the bubble (i.e., ρ_0) is defined in the limit $m_p \rightarrow \infty$ (i.e., the gravitational constant G.$\rightarrow$0). A comparison with the previous "thin-wall" result for the ϕ^{2-3-4} potential gives the relationship

$$\gamma = \frac{\psi_+^2}{3\sqrt{2}} \qquad (3.49)$$

We may now address the question of the Euclidean action for the nucleating bubble within this "thin-wall" model. The Euclidean action is naturally split into two pieces, the action for the bubble interior and the action for the bubble wall. For the decay from Minkowski to anti-de Sitter space, the initial spacetime without the bubble (i.e., Minkowski space) has a vanishing action and so there is no subtraction term in the evaluation of B.

From Eq.(3.16) we may calculate the Euclidean action of the bubble interior as follows:

$$S_E^{Int} = -2\pi^2 \int_0^{\rho_w} d\xi\, \rho^3\, \tilde{U} \qquad (3.50)$$

$$= 2\pi^2\varepsilon \int_0^{\rho_w} \rho^3 \left[1 + \left[\frac{\rho}{\Lambda}\right]^2\right]^{-1/2} d\rho \qquad (3.51)$$

$$= \frac{9}{64\varepsilon}\left\{\frac{2}{3}\left[1+\frac{\rho_w^2}{\Lambda^2}\right]^{3/2} - 2\left[1+\frac{\rho_w^2}{\Lambda^2}\right]^{1/2} + \frac{1}{2}\right\} \qquad (3.52)$$

We now make the substitutions, $\Lambda^2 = \frac{3}{8\pi\varepsilon}$, where ε is the energy density of the anti-de Sitter space, and Eq.(3.47) for ρ_w, giving

$$S_E^{Int} = \frac{3}{32\varepsilon}\left\{\left[\frac{\varepsilon+6\pi\gamma^2}{\varepsilon-6\pi\gamma^2}\right]^3 - 3\left[\frac{\varepsilon+6\pi\gamma^2}{\varepsilon-6\pi\gamma^2}\right] + 2\right\} \qquad (3.53)$$

Leaving us finally with

$$S_E^{Int} = \frac{27}{2\varepsilon}\frac{\pi^2\gamma^4}{(\varepsilon-6\pi\gamma^2)^3}(3\varepsilon - 6\pi\gamma^2) \qquad (3.54)$$

We next require the Euclidean action for the bubble wall, this consists of two terms, the "surface energy" term, and a contribution from the scalar curvature associated the bubble wall.

$$S_E^{wall} = \frac{1}{8\pi}\int\left(\gamma - \frac{K}{8\pi}\right)h^{1/2}d^3x \qquad , \qquad (3.55)$$

where K is the scalar curvature associated with the wall, obtained from the trace of $(K_{ab}^{+} - K_{ab}^{-})$. With $K=12\pi\gamma$, we have

$$S_E^{wall} = -\pi^2\sigma\rho_w^3 \qquad (3.56)$$

$$= -\frac{27\pi^2\gamma^4}{[\varepsilon-6\pi\gamma^2]^3} \qquad (3.57)$$

The Euclidean action for the nucleating bubble is then given by

$$S_E = S_E^{Int} + S_E^{wall} \qquad (3.58)$$

$$= \frac{27\,\pi^2\,\gamma^4}{2\,\varepsilon^3}\,\frac{1}{\left[1 - \dfrac{\rho_0^2}{4\,\Lambda^2}\right]^2} \quad ; \qquad (3.59)$$

or, in terms of the value for B in the absence of gravity (which we shall denote by B_0),

$$B = B_0\,\frac{1}{\left[1 - \dfrac{\rho_0^2}{4\,\Lambda^2}\right]^2} \qquad (3.60)$$

We observe that for the decay from Minkowski to anti-de Sitter space the value for B is increased from the flat-space value of B_0, and therefore the decay rate is decreased. If $\rho_0=2\Lambda$ then B becomes infinite (i.e., the decay rate is reduced to zero) and we now lie on the boundary of the Coleman and De Luccia forbidden region. The radius of the bubble also becomes infinite in this situation. The decay rate is similarly reduced to zero for any larger values of ρ_0, the reason for this (as explained by Coleman and De Luccia) is that the gravitational contribution to the energy of the bubble prevents any finite sized bubble from having zero total energy.

"Thin-Wall" Decay from de Sitter Space to Minkowski space

Figure 15 shows a diagrammatic representation of the patching together of a bubble of Euclideanized Minkowski space (M^-), to Euclideanized de Sitter space (M^+); corresponding to the "thin-wall" decay from de Sitter to Minkowski space. Inside the bubble, M^- is Minkowski space, with coordinates $(\xi,\chi,\theta,\varphi)$, and metric,

$$g_{ab}^{-} = \mathrm{diag}(1 , \xi^2, \xi^2 \sin^2\chi , \xi^2 \sin^2\chi \sin^2 \theta). \qquad (3.61)$$

The unit normal vector field evaluated in M^- is,

$$n_a^{-} = (1, 0, 0, 0) \quad ; \qquad (3.62)$$

which gives

$$h_{ab}^{-} = \mathrm{diag}(0 , \xi^2, \xi^2 \sin^2\chi , \xi^2 \sin^2\chi \sin^2 \theta) \quad . \qquad (3.63)$$

The extrinsic curvature tensor , $K_{ab} = h_a^c \nabla_c n_b$, is quite trivial to calculate in this case because n_a^- is a constant vector field. Thus

$$K_{ab} = \Gamma^{\xi}_{ab} \quad , \qquad (3.64)$$

with the result that

$$K_{ab}^{-} = -\frac{1}{\xi} h_{ab}^{-} \quad . \qquad (3.65)$$

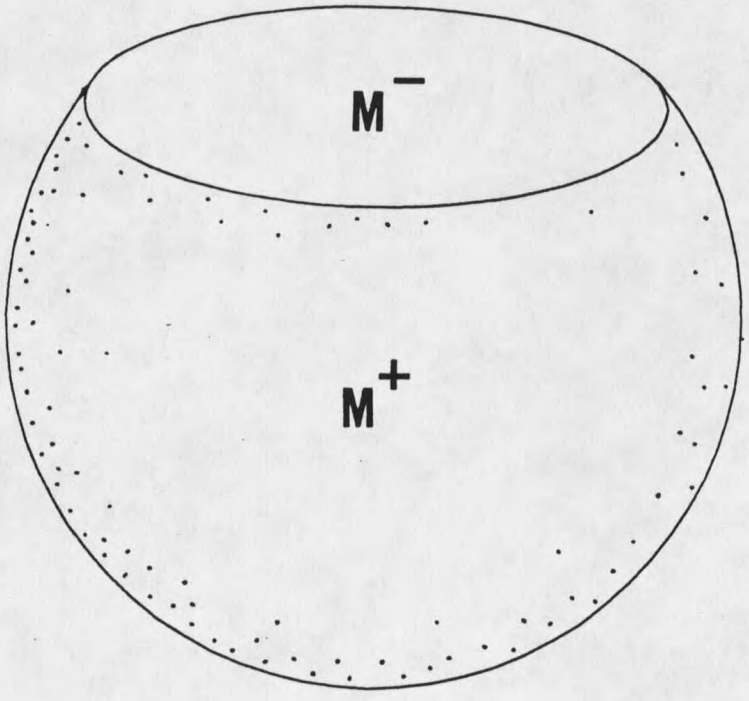

Figure 15 "Thin-wall" decay from de Sitter to Minkowski space. This diagram illustrates the ideas behind the Israel formalism, in which we "patch" together an interior bubble of Euclideanized Minkowski space to an exterior of Euclideanized de Sitter space.

We proceed in a similar manner for the Euclideanized de Sitter space: M^+ is Euclideanized de Sitter space, with coordinates (Ξ,X,Θ,Φ), and metric

$$g^{+}_{ab} = \mathrm{diag}(1 , \rho^2, \rho^2 \sin^2 X , \rho^2 \sin^2 X \sin^2 \Theta) \quad , \qquad (3.66)$$

where $\rho^2 = \Lambda^2 \sin^2\left(\frac{\Xi}{\Lambda}\right)$, and Λ is the radius of the Euclideanized de Sitter space. The unit normal vector field evaluated in M^+ is

$$n_a^+ = (1, 0, 0, 0) \quad , \tag{3.67}$$

which gives

$$h_{ab}^+ = \mathrm{diag}(0 , \rho^2, \rho^2 \sin^2 X , \rho^2 \sin^2 X \sin^2 \Theta) \quad . \tag{3.68}$$

The extrinsic curvature tensor , $K_{ab} = h_a^c \nabla_c n_b$, is again quite trivial to calculate because n_a^+ is a constant vector field. Thus

$$K_{ab} = \Gamma^{\Xi}_{ab} \quad , \tag{3.69}$$

with the result that

$$K_{ab}^+ = - \frac{1}{\Lambda} \cot\left(\frac{\Xi}{\Lambda}\right) h_{ab}^+ \quad . \tag{3.70}$$

The matching condition, $[h_{ab}^+ - h_{ab}^-]_\Sigma = 0$, implies that

$$\xi_\Sigma = \Lambda \sin\left(\frac{\Xi_\Sigma}{\Lambda}\right) \quad , \tag{3.71}$$

where ξ_Σ and Ξ_Σ are the respective coordinates of Σ in M^- and M^+. Taking the induced stress energy tensor for the thin wall at Σ to be

$$t_{ab} = \gamma h_{ab}^- \quad , \tag{3.72}$$

then the matching condition, $[K_{ab}^+ - K_{ab}^-]_\Sigma = -8\pi(t_{ab} - \frac{1}{2} t h_{ab})$, gives

$$\frac{1}{\xi_\Sigma} \left(1 - \cos\left(\frac{\Xi_\Sigma}{\Lambda}\right) \right) h_{ab}^- = 4\pi\gamma \xi_\Sigma h_{ab}^- \quad . \tag{3.73}$$

Re-arranging this expression we have

$$\left[1 - \frac{\xi_\Sigma^2}{\Lambda^2}\right]^{1/2} = 1 + 4\pi\gamma\,\xi_\Sigma \quad , \tag{3.74}$$

and finally

$$\xi_\Sigma = \frac{8\pi\gamma}{16\pi^2\gamma^2 + \frac{1}{\Lambda^2}} \quad . \tag{3.75}$$

This result may be re-expressed in terms of the radius of the bubble in the presence of gravity denoted by ρ_w , and the corresponding radius in the absence of gravity be denoted by ρ_0. Thus

$$\rho = \frac{\rho_0}{1 + \left[\frac{\rho_0}{2\Lambda}\right]^2} \quad , \tag{3.76}$$

where

$$\rho_0 = \frac{3\gamma}{\varepsilon} \quad . \tag{3.77}$$

A comparison with the previous thin wall result for the ϕ^{2-3-4} potential gives the relationship

$$\gamma = \frac{\psi_+^2}{3\sqrt{2}} \quad . \tag{3.78}$$

The calculation of the Euclidean action for the decay from de Sitter to Minkowski space proceeds in a similar manner to that of the decay from Minkowski to

anti-de Sitter space; remembering that we now have a subtraction piece due to the non-vanishing Euclidean action of the initial spacetime (i.e., de Sitter space). This final expression for B is given by

$$B = B_0 \frac{1}{\left[1 + \frac{\rho_0^2}{4\Lambda^2}\right]^2} \quad , \qquad (3.79)$$

i.e., the decay rate from de Sitter to Minkowski space is increased over the corresponding decay rate in the absence of gravity due to a decrease in B.

Exact Numerical Results for the Decay from de Sitter Space to Minkowski Space.

For the $\phi^{2\text{-}3\text{-}4}$ potential under consideration the "thin-wall" formulae become

$$B = \frac{\pi^2 \psi_+^8}{24\,\tilde{\varepsilon}^3}\left[1 + \frac{\pi\, m^2 \psi_+^4}{3\, m_P^2\, \tilde{\varepsilon}}\right]^{-2} \quad , \qquad (3.80)$$

and

$$\rho = \frac{\psi_+^2}{\sqrt{2}\,\tilde{\varepsilon}}\left[1 + \frac{\pi\, m^2 \psi_+^4}{3\, m_P^2\, \tilde{\varepsilon}}\right]^{-1} \quad . \qquad (3.81)$$

We have the prediction that as the mass of the field is increased, where $\tilde{\varepsilon}$ and ψ_+ are kept constant, the bubble radius decreases and the decay rate increases (i.e., there is a

decrease in B). These results are now compared with the exact numerical results in order to estimate the validity of the approximation scheme.

To proceed with the numerical analysis (n.b., see Appendix for a detailed explanation of the numerical methods) it is necessary to take note of an important difference between the false vacuum decay from de Sitter to Minkowski space and false vacuum decays both in the absence of gravity and for the decay from Minkowski to anti-de Sitter space. The spacetime outside a nucleating bubble is that of the false vacuum, thus for the decay from de Sitter to Minkowski space the exterior spacetime is (Euclideanized) de Sitter space. This spacetime is closed and has the topology of a four sphere. There is a maximum value for ξ within this spacetime, which occurs at the "south pole" if there origin of coordinates (i.e., ξ=0) is located at the "north pole". We may consider the nucleating bubble, without any loss of generality, to be centered on the "north pole" of this four sphere. As a result of this the boundary condition (Eq.(3.13)) requiring $\sigma \rightarrow 0$ as $\xi \rightarrow \infty$ is not valid for the decay of de Sitter space as this value of ξ is never attained within the Euclideanized de Sitter space; we therefore replace this boundary condition with the requirement that at the "south pole" (i.e., where ξ takes its maximum value) the field derivative σ' must vanish, for the same reason that this quantity must vanish at the "north pole" (i.e., to prevent singular behavior in the Euclideanized scalar field equation) .

Figure 16 shows the bubble profile evolution (i.e., solution curves to Eq.(3.11)) as the mass of the field is increased, with potential parameters $\tilde{\varepsilon}$=0.5 and ψ_+=1.0. We observe that as the mass of the field is increased, the nucleating bubble profile flattens out and eventually reaches an equilibrium state, where a further increase in the mass has no effect upon the profile. The final state is described by the field having a constant value throughout the Euclideanized spacetime, this constant value corresponds to the

field lying at the top of the potential barrier. This however is the Hawking-Moss(1982) tunneling mode! Thus, as the mass of the field is increased, the Coleman-De Luccia tunneling mode evolves continuously into the Hawking-Moss tunneling mode.

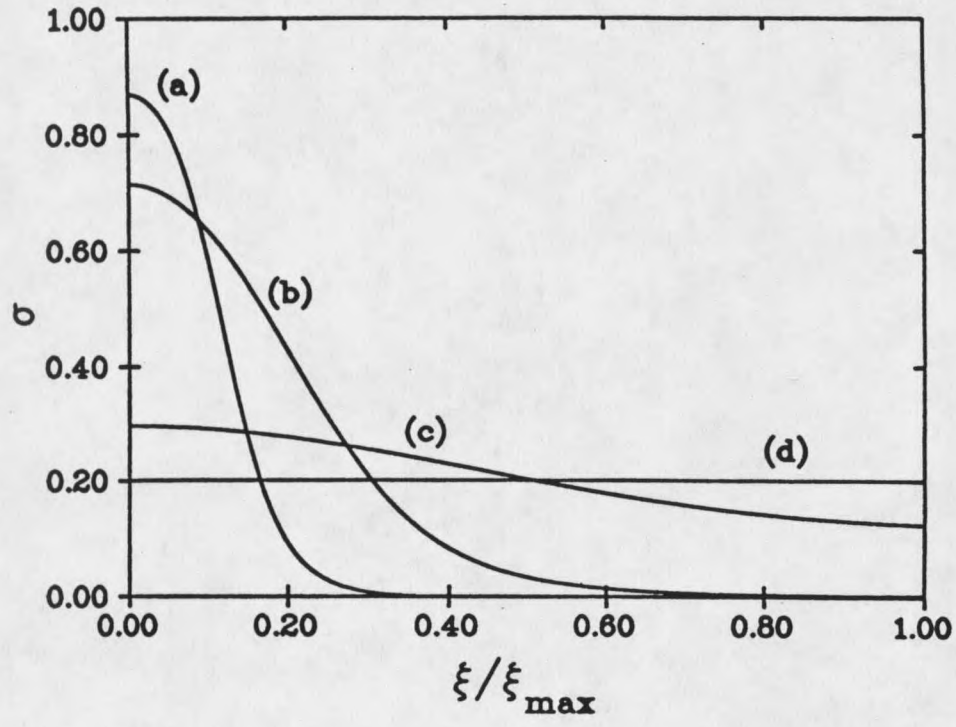

Figure 16 Bubble profiles associated with the decay from de Sitter to Minkowski space for several values of the field mass. The potential parameters ω and ψ_+ are kept at the constant values of 0.5 and 1.0 respectively. The masses associated with the bubble profiles are: (a) m=0.1, (b) m=0.2, (c) m=0.3, and (d) m=0.4. All bubble profiles with m>0.4 are well described by the Hawking-Moss tunneling mode; i.e., σ takes the constant value corresponding to the top of the inverted potential.

The Hawking-Moss tunneling mode corresponds to the entire Universe tunneling at an instant from the false vacuum state to the top of the potential barrier. This simply results in another de Sitter Universe, though one that is unstable to field

perturbations, with a larger vacuum energy density. After such a transition has taken place, perturbations push the field off the potential hill and the field then evolves classically to the true vacuum state. The expression for B corresponding to the Hawking-Moss mode is fairly easy to calculate, requiring just the volume of the respective Euclideanized de Sitter space multiplied by the associated energy density and is given by,

$$B_{HM} = \frac{3\, m_p^4}{8\, m^4} \{ \tilde{\varepsilon}^{-1} - \tilde{\varepsilon}_{top}^{-1} \} \quad . \qquad (3.82)$$

The evolution of the bubble profile and tunneling process resulting in this transition is certainly not evident from the "thin-wall" approximation, though such a transition has been previously suggested by Jensen and Steinhardt (1984,1989).

It may be argued that with $\tilde{\varepsilon}$=0.5 the "thin-wall" approximation is not valid anyway (i.e., the energy density difference between the true and false vacua is not a small quantity); however, a similar transition takes place with smaller values of $\tilde{\varepsilon}$ for which the "thin-wall" approximation is valid. We may also apply the symmetry transformations Eqs.3.17-19 to shift $\tilde{\varepsilon}$ from 0.5 to a value applicable to the "thin-wall" approximation; remembering that these (exact) transformations leave the solutions $\sigma(\xi)$ and $\rho(\xi)$ invariant.

Though the transition from the Coleman-De Luccia mode to the Hawking-Moss mode is continuous, there do appear to be three distinct regimes associated with this decay:

As the mass of the field is initially increased from zero, the end-point for the bubble profile, $\sigma(\xi_{max})$, remains very close to σ=0 and we may characterize these as strong Coleman-De Luccia modes. There then occurs a rapid transition where an

increase in the mass of the field results in the end-point of the bubble profile evolving rapidly from $\sigma=0$ to $\sigma=\sigma_{top}$, where σ_{top} is the field value corresponding to the top of the potential barrier. Finally we arrive at the Hawking-Moss mode where the bubble profile takes the constant value of σ_{top} throughout the spacetime. A further increase in the field mass does not change the characteristics of the nucleating bubble profile, i.e., the nucleating bubble appears via the Hawking-Moss mode.

Figure 17 shows the difference between the Euclidean action for the bubble spacetime and the initial spacetime (i.e., B), (a) for the exact, numerical bubble solutions, (b) for the 'thin-wall' approximation, and (c) for the Hawking-Moss mode. The Hawking-Moss mode, for small field masses, has a larger action than that of the 'thin-wall'; however, as the field mass is increased, there is a cross-over point beyond which the Hawking-Moss action is smaller.

The behavior of the exact action, determined numerically, is quite striking. For small field masses the exact action is characteristic of the form given by the "thin-wall" approximation; with a finite value at m=0 and a gradual decrease as the mass of the field is increased (n.b., better numerical agreement would be achieved if the value of $\tilde{\varepsilon}$ under consideration was smaller). At the point defined by $B_{HM} = B_{TW}$ the phase transition process undergoes what may be described as a "cross-over" in the way in which the phase transition proceeds, beyond this point $B_{Exact} \simeq B_{HM}$.

At first sight the evolution of the bubble profile does not appear to exactly follow the transition in B. For example, a field mass m=0.3 places B_{Exact} in the Hawking-Moss region, however, the bubble profile for m=0.3 (Figure 17, curve (c)) has not yet fully transformed into the Hawking-Moss form. This may be explained by the fact that the Hawking-Moss solutions correspond to the field lying at the extremum of the potential. Thus, first-order variations in the field change B only at higher orders

(remembering that B involves the integral of the field potential for the nucleating bubble throughout the spacetime). The bubble profile for m=0.3 therefore gives a value for B very close to the Hawking-Moss value because its profile is only a small variation away from the Hawking-Moss solution.

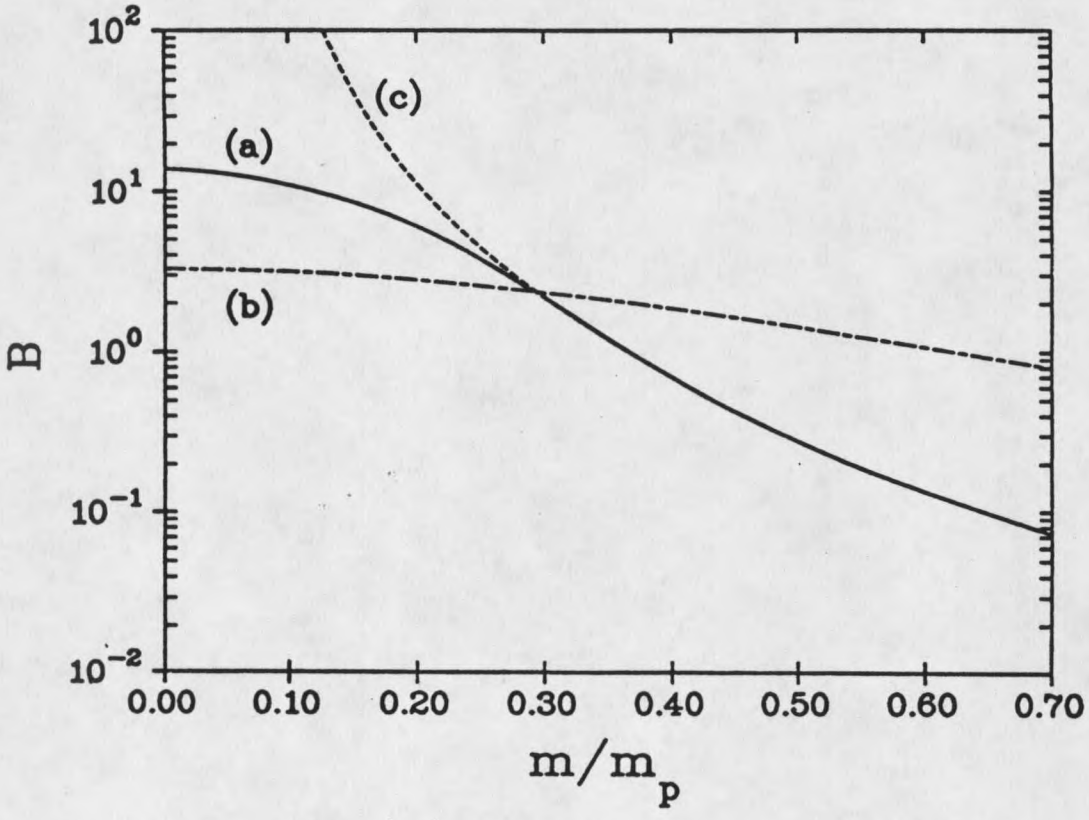

Figure 17 Difference between the Euclidean action for the bubble spacetime and the empty spacetime (i.e., B) for the decay from de Sitter to Minkowski space as a function of the field mass 'm'; where the potential parameters ω and ψ_+ are kept at the constant values of 0.5 and 1.0, respectively. Curve (a) shows the exact value of B obtained numerically, curve (b) shows "thin-wall" approximation, and curve (c) shows B for the Hawking-Moss tunneling mode.

Exact Numerical Results for the Decay from Minkowski Space to Anti-de Sitter Space.

For the ϕ^{2-3-4} potential the "thin-wall" formulae become

$$B = \frac{\pi^2 \psi_+^8}{24\,\tilde{\varepsilon}^3}\left(1 - \frac{\pi\, m^2 \psi_+^4}{3\, m_p^2\, \tilde{\varepsilon}}\right)^{-2} , \qquad (3.83)$$

and

$$\rho = \frac{\psi_+^2}{\sqrt{2}\,\tilde{\varepsilon}}\left(1 - \frac{\pi\, m^2 \psi_+^4}{3\, m_p^2\, \tilde{\varepsilon}}\right)^{-1} . \qquad (3.84)$$

Eq.(3.83) implies that for the decay from Minkowski to anti-de Sitter space the action may diverge for certain values of the parameters, and at this point the bubble radius becomes infinite. In particular, if we keep $\tilde{\varepsilon}$ and ψ_+ constant and increase the mass of the scalar field from zero, a critical mass will be reached at which point the action becomes infinite and the decay rate goes to zero. No bubble solutions exist for a greater field mass. Alternatively, if we keep the mass of the field and the dimensionless field distance between the two vacuum states (i.e., ψ_+) constant, then a reduction in $\tilde{\varepsilon}$ will also bring about this divergence in B and prevent any subsequent vacuum decay. The critical mass in this situation is given by

$$m_c = \frac{1}{\psi_+^2}\left(\frac{3\,\tilde{\varepsilon}}{\pi}\right)^{1/2} m_p \qquad (3.85)$$

For most fields in nature, we might expect the dimensionless quantities $\tilde{\varepsilon}$ and ψ_+ to typically be of order unity or at most a few orders of magnitude; thus from Eq.(3.85) we see that the associated critical mass will be close to the Planck mass and certainly well away from the masses that we observe for fields today.

Coleman and De Luccia argue that there is a simple physical interpretation for the existence of this critical mass: The nucleating bubble is required to have zero energy. In flat spacetime, as we increase the radius of a bubble the volume will grow at a greater rate than the surface area. Thus, as the volume gives a negative contribution to the energy of the bubble, and the surface area gives a positive contribution to the energy of the bubble, we may reduce the energy of the bubble by increasing its radius. Therefore, we are always able to generate a zero energy bubble in flat spacetime. However, in anti-de Sitter spacetime (for sufficiently large radii) the volume grows at the same rate as the surface area. Thus we may find that in some situations we are unable to generate a zero energy bubble.

Figures 18 and 19 show the evolution of a nucleating bubble profile as the mass of the field is increased, with the potential parameters being fixed at $\tilde{\varepsilon}$=0.5 and ψ_+=1.0 ; these obviously do not correspond to thin wall profiles. We notice that as the mass of the field approaches criticality, the starting point for the field $\sigma(\rho=0)$ approaches a limiting value of 1.0. We may explain this quite easily with reference to the analogy of "rolling off the hill" of the inverted potential. As the mass of the field is increased then, from Eq.(3.27), we see that the magnitude of the "frictional" term is increased. Thus more energy is required to reach the final point of $\sigma(\rho \rightarrow \infty)=0$, and so the field has to start from a higher point on the hill. If the mass of the field becomes sufficiently large then we could expect the "frictional" term to be sufficient to prevent the field from ever reaching $\sigma=0$ at a finite ρ.

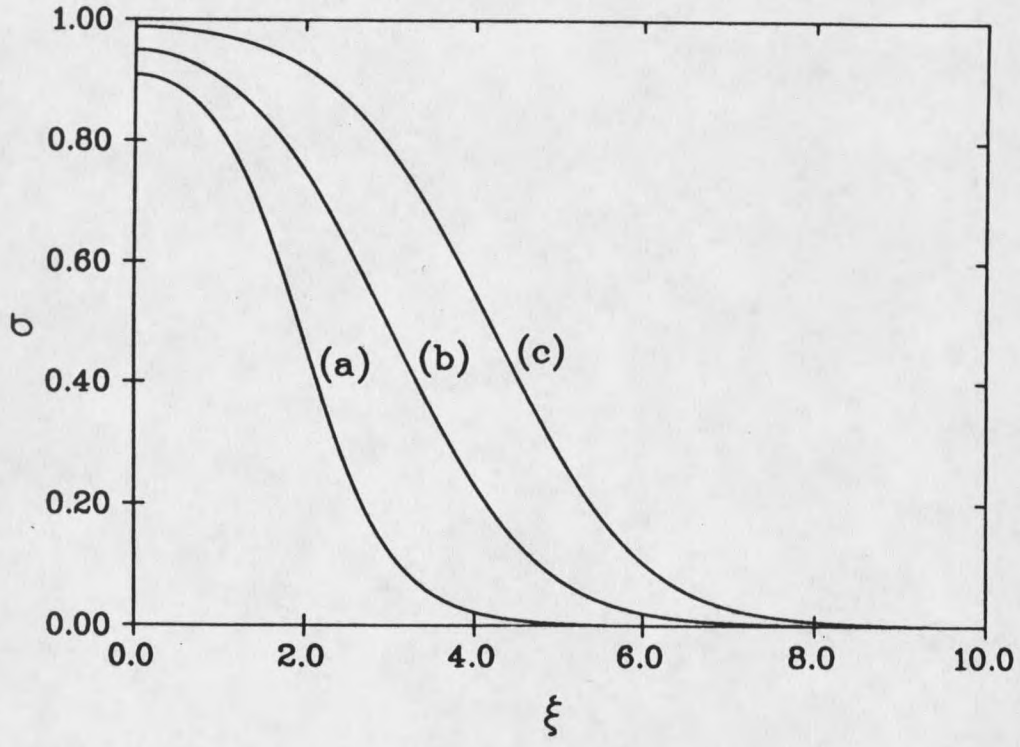

Figure 18 Bubble profiles $\sigma(\xi)$ for the decay from Minkowski to anti-de Sitter space for several values of the field mass. The potential parameters ω and ψ_+ are kept at the constant values of 0.5 and 1.0, respectively. The masses of the field for the three curves are (a) m=0, (b) m=0.82, and (c) m=0.85. The critical mass m_c is approximately 0.865 for this choice of potential parameters.

In the absence of gravity the "frictional" term was inversely proportional to the Euclidean time and so there was always a value of ρ for which the "frictional" term was small enough that the field could roll off the hill and reach σ=0. However, in the presence of gravity the "frictional" term contains a piece which does not depend upon ρ and is only a function of the field mass and shape of the potential; thus we cannot play the "thin-wall" game of waiting long enough in Euclidean time for the "friction" to become negligible.

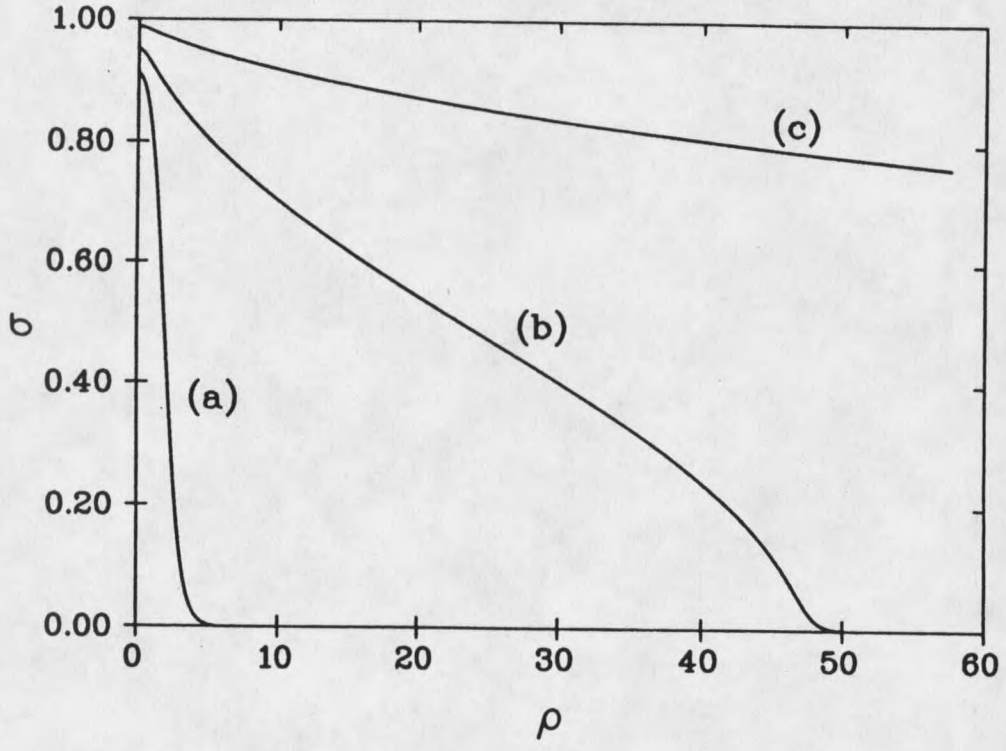

Figure 19 Bubble profiles $\sigma(\rho)$ for the decay from Minkowski to anti-de Sitter space. The potential and mass parameters for the three curves are the same as for Figure 18. The $\sigma(\rho)$ profile evolution has a marked difference to the $\sigma(\xi)$ profile evolution as criticality is approached, which may be explained in terms of the solution curves to the Einstein equations, shown in Figure 20

The bubble profiles, $\sigma(\rho)$, undergo a dramatic evolution as the mass of the field is increased; this may be explained with reference to the solution curves, $\rho(\xi)$, for the Einstein equation, shown in Figure 19. For all decays from Minkowski space to anti-de Sitter space there will be a potential barrier which has a positive energy density; thus, when the bubble profile evolves through this barrier the spacetime will undergo a de Sitter-like stage of evolution. This appears in the $\rho(\xi)$ profiles as a flattening out of the

curves, and this phenomenon increases in prominence as the mass of the field is increased. Eventually, if the mass of the field is increased sufficiently, there will be a point where the $\rho(\xi)$ profile will reach a plateau, where $\rho'=0$; this may be thought of as the bubble profile running into the de Sitter horizon (though in the Euclideanized spacetime this is more accurately described as the "equator"). This scenario defines the critical mass associated with the decay from Minkowski to anti-de Sitter space.

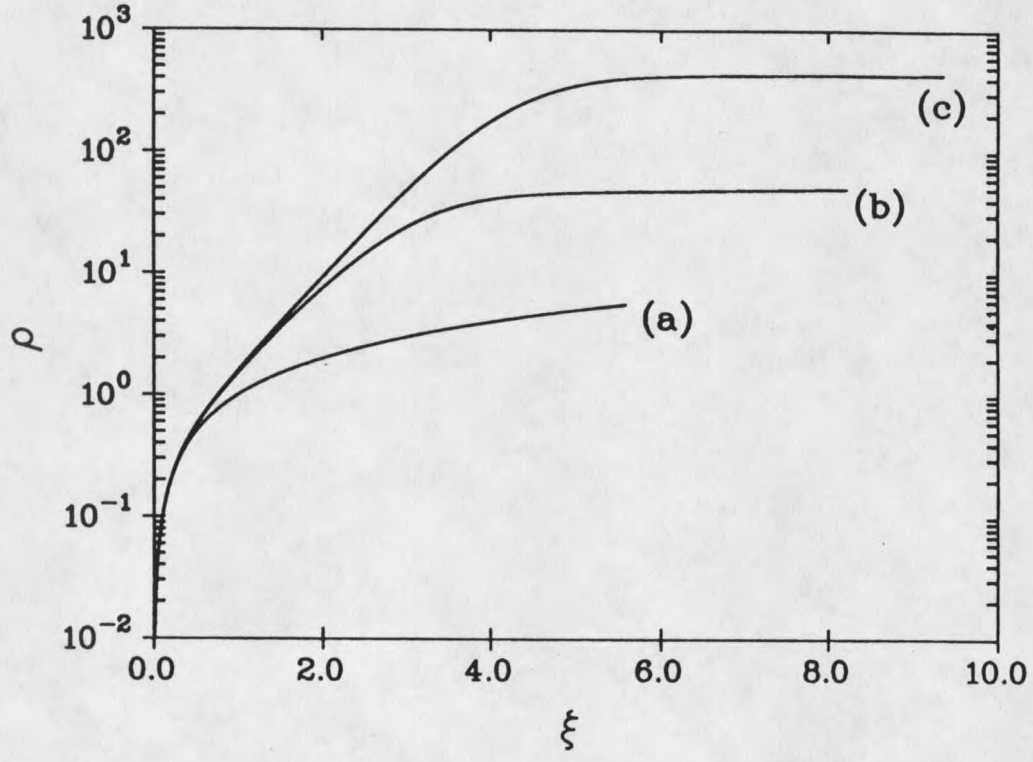

Figure 20 Solution curves for the Einstein equation giving the $\rho(\xi)$ evolution for the three bubble profiles shown in Figures 18 and 19. As criticality is approached, the ρ evolution reaches a "plateau" which may be pictured as the bubble profile "running into a de Sitter horizon" (a point where $\rho'=0$). The plateau corresponds to a de Sitter phase of evolution and occurs when the bubble profile runs through the potential barrier where the energy density is positive.

Figure 21 shows the critical mass as a function of $\tilde{\varepsilon}$, the lower curve corresponding to the "thin-wall" critical line and the upper curve corresponding to the exact critical line. For small $\tilde{\varepsilon}$ (i.e., the "thin-wall" regime), the "thin-wall" approximation gives a remarkably good prediction for the critical mass, as illustrated with the exact critical mass being asymptotic to the approximate critical line in this region. Beyond the "thin-wall" regime the exact critical line diverges from the approximate critical line, such that the exact critical mass always lies above the approximate critical mass. Thus, there are decays which the "thin-wall" approximation would label as forbidden, but which could actually occur.

Figure 22 shows the evolution of the ratio of B_{TW} to B_{exact} as the mass of the field is increased, where the potential parameter ψ_+ is kept at 1.0 and $\tilde{\varepsilon}$ takes on the values 0.1, 0.3 and 0.5 for the three curves (a),(b) and (c) respectively. We observe that the "thin-wall" approximation initially underestimates B, though the agreement with B_{exact} improves as $\tilde{\varepsilon}$ is decreased; as expected. As the mass of the field is increased B_{TW} is found to diverge before B_{exact}. This occurs because the critical mass for the "thin-wall" approximation always lies below the exact critical mass.

Figure 23 shows the evolution of the ratio of the "thin-wall" bubble radius to the exact bubble radius for the same set of parameters as in Figure 22. Though the radius is well defined for "thin-wall" bubbles, this is not the case for the exact bubble profiles; we define the bubble radius to be $\rho(\sigma_{initial} / 2)$ where $\sigma_{initial}$ is the starting value of σ at $\rho=0$. The qualitative behavior of the bubble radius evolution is very similar to that of the evolution of B. The divergence in the "thin-wall" radius again occurs before the exact divergence as a result of the "thin-wall" critical mass lying below the exact critical mass.

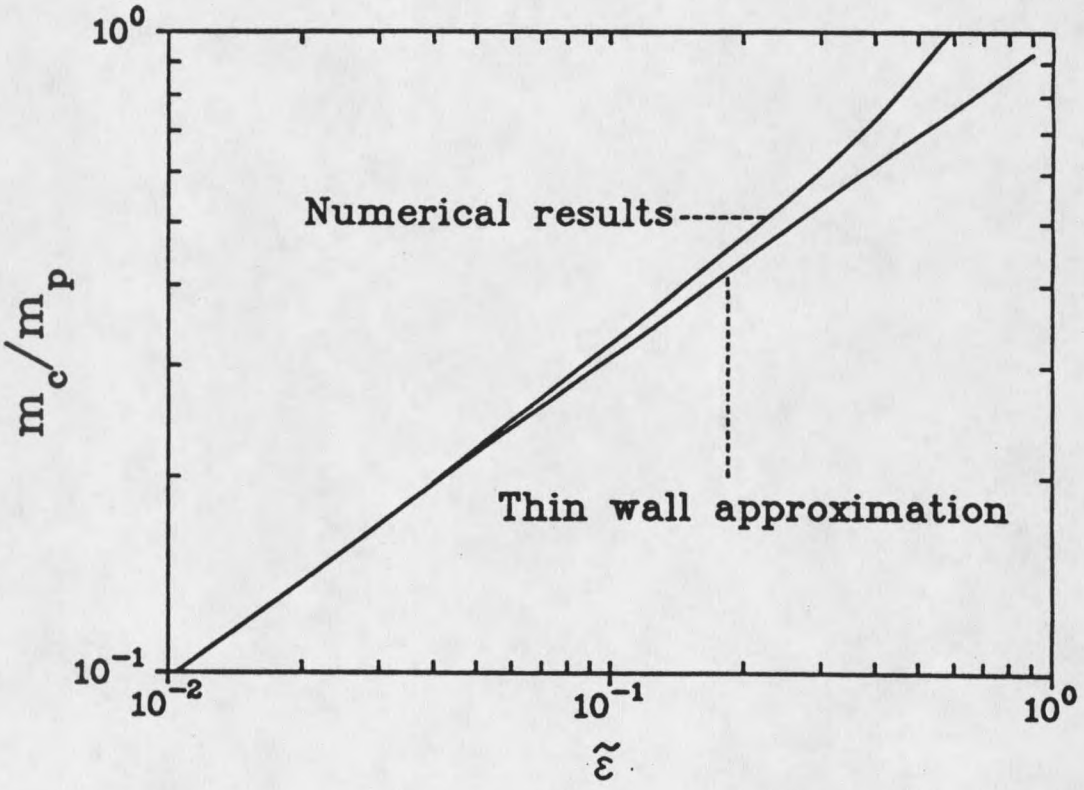

Figure 21 Critical mass associated with the decay from Minkowski to anti-de Sitter space, above which no O(4)-symmetric decays are permitted. In the "thin-wall" regime, corresponding to a small value of ω, the exact critical mass asymptotically approaches the value given by the "thin-wall" approximation and there is good agreement between the exact results and the approximate results. Away from the "thin-wall" regime, as ω becomes larger, the exact critical line deviates from and lies above the approximate critical line.

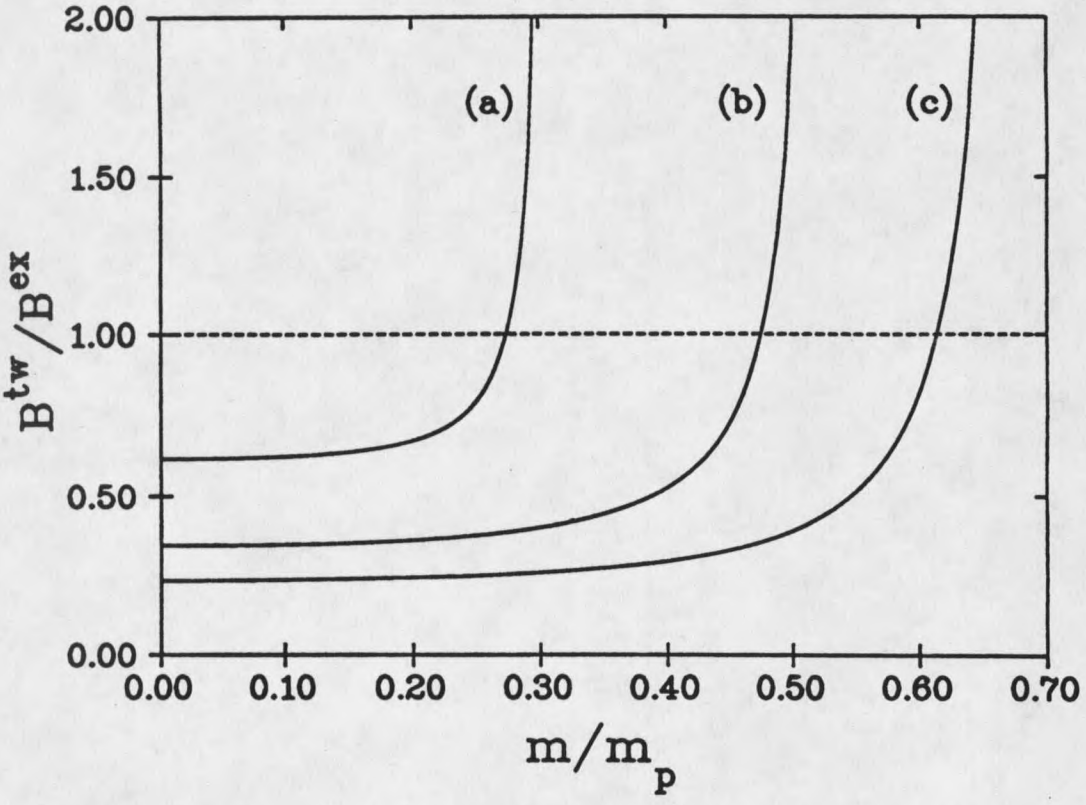

Figure 22 Evolution of the ratio of B_{tw} to B_{exact}, for the decay from Minkowski to anti-de Sitter space, as the mass of the field is increased. The three curves have different values of ω given by (a) ω=0.1, (b) ω=0.3, and (c) ω=0.5; ψ_+=1.0 in all three cases. The "thin-wall" approximation initially underestimates B; however, as the "thin-wall" critical mass lies below the exact critical mass, the "thin-wall" expression for B diverges prior to the divergence in the exact value for B.

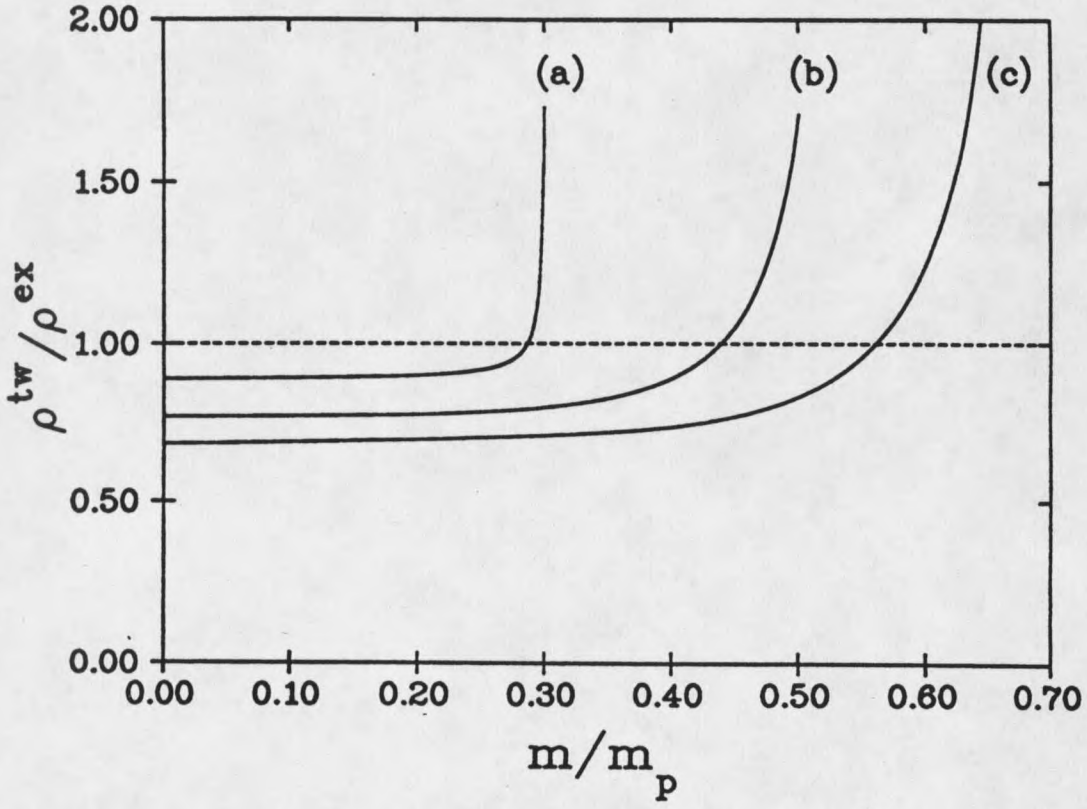

Figure 23 Evolution of the ratio of the bubble "radius" computed in the "thin-wall" approximation to the exact bubble radius [defined by $\rho(\sigma_{initial}/2)$, where $\sigma_{initial}$ is the starting value of σ at $\rho=0$] for the decay from Minkowski to anti-de Sitter space, as the mass of the field is increased. The three curves have different values of ω given by (a) $\omega=0.1$, (b) $\omega=0.3$, and (c) $\omega=0.5$. $\psi_+=1.0$ in all three cases.

CHAPTER 4

THE EFFECT OF GRAVITATIONALLY COMPACT OBJECTS ACTING AS SITES FOR BUBBLE NUCLEATION

Nucleation Sites

A characteristic of first-order phase transitions in everyday matter is their ability to be initiated by nucleation sites. An example of this is the preferential formation of rain-drops around atmospheric dust particles; similarly, bubbles of carbon dioxide in a glass of soda will tend to originate at definite points on the surface of the glass, these corresponding to defects or impurities. We are therefore led to ask whether such nucleation sites might occur for first-order phase transitions in quantum fields. In particular, could gravitationally compact objects act as nucleation sites for false-vacuum decay?

Hiscock (1987), and Mendell and Hiscock (1989), considered the effects of gravitationally compact objects on false-vacuum decay within the "thin-wall" approximation. In particular, Hiscock considered the effect of black holes, and Mendell and Hiscock considered the effect of gravitationally compact objects such as neutron stars. Their analysis utilized the Israel (1966) formalism for the "patching" together of spacetimes, in a similar manner to the analysis in Chapter 3. Thus, for example, when considering the effect of a black-hole on the false vacuum decay from Minkowski to anti-de Sitter space, one would "patch" together an interior core of Schwarzschild-anti-de Sitter spacetime to and exterior of Schwarzschild spacetime. Their analysis found

that gravitationally compact objects have the effect of reducing B, the difference between the Euclidean action for the spacetime with, and without, the nucleating bubble. It would therefore appear that such objects may, in certain situations, increase the false-vacuum decay rate.

The "thin-wall" analysis of Hiscock, and Mendell and Hiscock, had the attractive feature of inherently taking into account the self-gravity of the quantum field undergoing the phase transition; however, as we have seen in Chapters 2 and 3, the "thin-wall" approximation does not usually describe false-vacuum decay processes very well. Therefore, by adopting a different approach to the "thin-wall" approximation we may be able to gain further insight into the effect of gravitationally compact objects acting as nucleation sites. Such an approach should also allow us to confirm some of the predictions of the "thin-wall" analysis.

It will be useful to construct a simple model to explain why gravitationally compact objects might act as nucleation sites for false-vacuum decay. The Euclidean action for an O(4)-symmetric nucleating bubble in the "thin-wall" approximation may be written as follows,

$$\mathcal{S} = \sigma \mathcal{A} - \varepsilon \mathcal{V} \quad , \quad \text{with } \sigma,\varepsilon > 0 \quad ; \tag{4.1}$$

where $\mathcal{A}$ corresponds to the surface-area of the nucleating bubble and $\mathcal{V}$ to its volume (remembering that these are "three-areas" and "four-volumes"). It is assumed that we have a fixed background spacetime and so the spacetime does not contribute, as such, to B (i.e., the difference between the Euclidean action for the spacetime with, and without, the nucleating bubble); thus we may write $B=\mathcal{S}$. The "decay rate", which is proportional to exp(-B), may be enhanced by reducing B; so if we could find a way of increasing $\mathcal{V}$ while keeping $\mathcal{A}$ constant (with σ and ε also constant) then this reduction in B would be

achieved. Obviously, in a flat spacetime once we have fixed the value of $\mathcal{A}$ then $\mathcal{V}$ is automatically defined; however, this need not be true in a curved spacetime. Figure 24 illustrates this idea by showing that the volume contained within a surface area $\mathcal{A}$ may be increased by a curved spacetime. Such a volume surplus will occur in the spacetimes of a "star"; the use of the word "star" will from now on refer to the generic group of gravitationally compact objects (e.g., neutron stars, planets, boson stars, monopoles etc.).

Euclideanized Scalar Field Equation in the Presence of a Gravitationally Compact Object

We may make use of the generalized formula

$$g^{-\frac{1}{2}} \partial_\mu [\, g^{\frac{1}{2}} g^{\mu\nu} \partial_\nu \,] \phi = \frac{dU}{d\phi} \quad , \tag{4.2}$$

to express the Euclideanized scalar field equation in the presence of a gravitationally compact object. The solution to Eq.(4.2) will provide us with the scalar field profile for the nucleating bubble together with its Euclidean action.

The Euclideanized metric for a static, spherically symmetric spacetime containing a gravitationally compact object may be written as

$$g_{\mu\nu} = \mathrm{diag}[\, f(r) \,,\, h(r) \,,\, r^2 \,,\, r^2 \sin^2\theta \,] \quad , \tag{4.3}$$

with determinant,

$$g^{\frac{1}{2}} = (\, fh \,)^{\frac{1}{2}} r^2 \sin\theta . \tag{4.4}$$

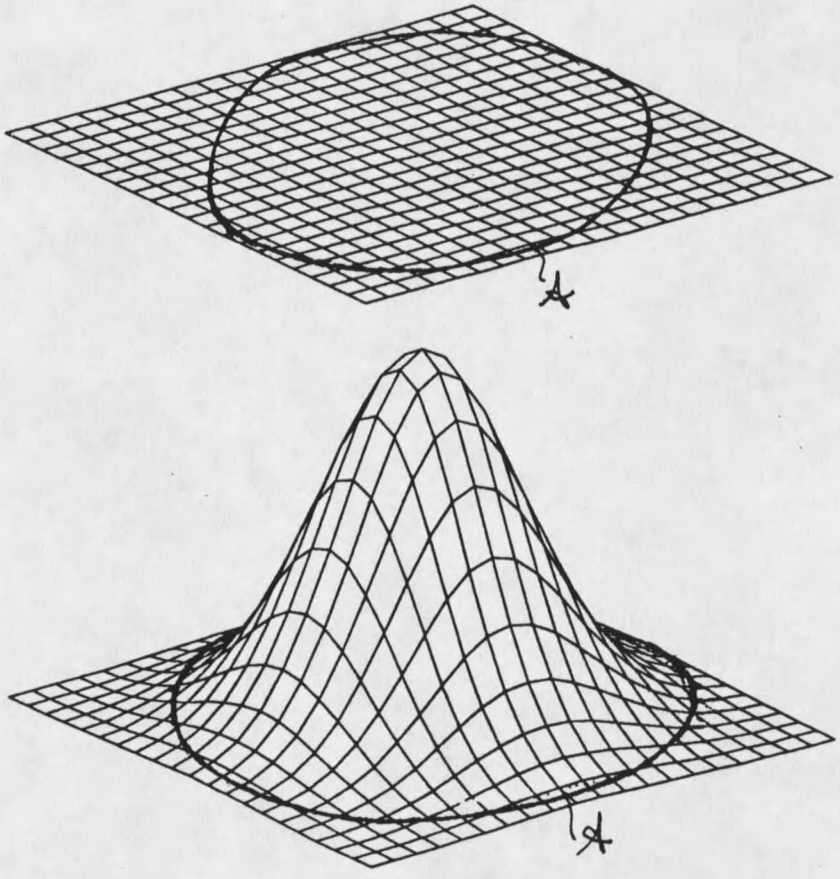

Figure 24 "Embedding diagrams" to illustrate the idea that a curved spacetime can have a greater volume contained within a proper area $\mathcal{A}$ than the corresponding flat spacetime. The top illustration shows the "flat spacetime" (where one spatial dimension has been suppressed); thus the proper area is represented by the length of the circle and the proper volume is given by the surface area contained within the circle. The bottom illustration shows a "curved spacetime", in this situation there is a greater proper volume contained within the surface area, $\mathcal{A}$.

This metric is O(3)-symmetric about the origin of the "spatial" coordinates and so we would not expect the O(4)-symmetry of the nucleating bubble in a flat O(4)-symmetric spacetime to hold in this situation, though there are good reasons to believe that the bubble with the smallest Euclidean action will have the O(3)-symmetry of the metric. If we plug this expression for the metric into Eq.(4.2) for the scalar field equation we have (assuming that ϕ depends only upon τ and r),

$$\frac{1}{f}\frac{\partial^2\phi}{\partial\tau^2}+\frac{1}{h}\frac{\partial^2\phi}{\partial r^2}+\frac{1}{h}\left\{\frac{2}{r}+\frac{1}{2f}\frac{df}{dr}-\frac{1}{2h}\frac{dh}{dr}\right\}\frac{\partial\phi}{\partial r}=\frac{dU}{d\phi} \qquad (4.5)$$

This equation (a 2-dimensional, elliptic, partial differential equation; also, in the case of interest here, is non-linear due to the term , $dU/d\phi$) is substantially more difficult to solve than any of the equations involved with the O(4)-analysis of Chapters 2 and 3. There is even uncertainty about the appropriate boundary conditions necessary to solve the equation: we would expect that as $r\rightarrow\infty$ the field, ϕ, should return to the value corresponding to the false vacuum (i.e., $\phi\rightarrow 0$ for the $\phi^{2\text{-}3\text{-}4}$ theory of Chapters 2 and 3). However, the boundary condition for finite r, as $\tau\rightarrow\infty$ (and similarly, $\tau\rightarrow(-)\infty$), is uncertain. A "cylinder" solution with the O(3)-symmetry of the metric may have $(\partial\phi/\partial\tau)=0$ at all values of τ, which would complete our required boundary information. We may also consider oscillating cylindrical solutions, with the O(3)-symmetry of the metric; and even solutions where $\phi\rightarrow$(false vacuum value) as $\tau\rightarrow(+/-)\infty$ (for all values of r), where the solution would again have the O(3)-symmetry of the metric. In this last situation the nucleating bubble might look like a prolate or oblate spheroid; with rotational symmetry about the τ axis. Each of these possibilities would correspond to different sets of boundary conditions.

A Perturbative Analysis of the Effect of a Gravitationally Compact Object on the Nucleating Bubble.

The line element corresponding to the metric of Eq.(4.3) may be written

$$ds^2 = f(r)\, d\tau^2 + h(r)\, dr^2 + r^2\, d\Omega^2 \quad , \tag{4.6}$$

where $d\Omega$ is the line element on the unit two-sphere. If f(r)=h(r)=1 (i.e., in the absence of a star) the spacetime returns to its O(4)-symmetric state, and the analysis of Chapter 2 is appropriate for determining the field profile and Euclidean action of the nucleating bubble.

Consider the situation where we have a star, which is not too compact, in our spacetime (this would rule out black holes for example). We may put this notion on a more precise footing by writing the metric f(r) and h(r) functions as

$$f(r) = 1 + F(r) \quad , \tag{4.7}$$

and,

$$h(r) = 1 + H(r) \quad ; \tag{4.8}$$

and demand that $|F(r)| \ll 1$, and $|H(f)| \ll 1$, for all r.

We are now forced to make an important assumption about the nucleating bubble in the spacetime of the star. As F(r) and H(r) move away from zero (i.e., from a "flat" spacetime to a spacetime corresponding to a very "dilute" star), we assume that the nucleating bubble will move away from its O(4)-symmetric state to an O(3)-symmetric state, corresponding to the O(3)-symmetry of the metric, in a *continuous* manner. What we mean by this is that when $|F(r)|$ and $|H(r)|$ are very small, the

nucleating bubble will have the form of either an oblate or prolate spheroid (i.e., we shall consider the lowest, non-vanishing, multipole perturbation of the O(4)-bubble, this will correspond to the "quadrupole" spherical harmonics); the perturbations are required to have the O(3)-symmetry of the metric (i.e., the τ axis shall be the axis of rotational symmetry for the spheroid). This assumption appears to be reasonable as it would seem unlikely that the O(4)-symmetric bubble corresponding to F=H=0 would, for example, suddenly transform into an infinite cylinder around the τ-axis, for an infinitesimally small F(r) and H(r). Such a scenario would perhaps imply an instability of the O(4)-symmetric, flat-spacetime bubble to fluctuations in the metric.

The O(4)-symmetric bubble had a field profile given by

$$\phi_4 = \phi(\rho) , \tag{4.9}$$

with

$$\rho^2 = \tau^2 + r^2. \tag{4.10}$$

We shall now consider the prolate/oblate spheroidal solution,

$$\phi_3 = \phi[\,\tilde{\rho}] \quad , \tag{4.11}$$

with

$$\tilde{\rho}^2 = \rho^2 + A\,\rho^2 \cos^2\theta + B\,\rho^2 \sin^2\theta \quad , \tag{4.12}$$

where θ shall be the angle measured from the r-axis in the two-dimensional (τ,r)-space; i.e., $\theta = \tan^{-1}(\tau / r)$. Thus the solution to the perturbative analysis will require the determination of the two coefficients A and B. It will be convenient for us to re-write Eq.(4.12) as $\tilde{\rho}^2 = w_\tau\,\tau^2 + w_r\,r^2$, requiring the determination of the coefficients w_τ and w_r.

The two constraints which allow us to determine the coefficients, w_τ and w_r, are the requirements that the nucleating bubble have zero energy and that the Euclidean action for the nucleating bubble be an extremum. The energy of the nucleating bubble is given by (see, for example, Wald (p.286))

$$E = \int_\Sigma T_{\mu\nu}\ t^\nu\ d\sigma^\mu \quad , \tag{4.13}$$

where $T_{\mu\nu}$ is the stress-energy tensor for the scalar field, $d\sigma^\mu$ provides the measure for the 'surface' integral (remembering that this is a three-surface) and is a normal vector to the hypersurface Σ, and t^ν is the time-translation Killing vector field.

The stress-energy tensor for a minimally coupled scalar field takes the form

$$T_{\mu\nu} = \partial_\mu \phi\, \partial_\nu \phi - \frac{1}{2} g_{\mu\nu}\, g^{\alpha\beta}\, \partial_\alpha \phi\, \partial_\beta \phi + g_{\mu\nu}\, U \quad . \tag{4.14}$$

Taking Σ to be the τ=0 hypersurface, we will have $d\sigma^\mu = (f^{-\frac{1}{2}}, 0,0,0)\, d\sigma$, and $t^\nu = (1,0,0,0)$. The expression for the energy then reduces to

$$E = 4\pi \int_0^\infty r^2 (fh)^{\frac{1}{2}} \left\{ \frac{1}{2h} \left[\frac{\partial \phi}{\partial r} \right]^2 + U \right\} dr \quad . \tag{4.15}$$

As we have taken Σ to be the τ=0 hypersurface then the $(\partial\phi/\partial\tau)$ term vanishes due to a reflection symmetry of the bubble profile about this hypersurface.The energy will be a function only of the parameter w_r, and the requirement of zero energy (i.e., E=0) will therefore allow us to fix this parameter. With w_r known, the Euclidean action will now be a function only of the parameter w_τ. Therefore, by evaluating the

Euclidean action for a series of values of w_τ , we may determine the value of w_τ which extremises the Euclidean action, and hence corresponds to the nucleating bubble.

Thus we have a framework by which we may perform a perturbative analysis of the effects of a gravitationally compact object on false vacuum decay. In order to perform an actual calculation, however, it will be necessary to have the metric functions f(r) and h(r) for the star.

The Metric Functions for a "Toy" Star.

It would not be sensible to construct a realistic star as a first step in an attempt to model the effects of a gravitationally compact object on false-vacuum decay. This is because the determination of the metric functions f(r) and h(r) for a realistic stellar model is quite a complex task, requiring a knowledge of the equations of state for the matter that comprises the star, for example. What we require is a simple model star, where we are not overburdened by a large number of free, stellar parameters; thus a simple model which would only have two parameters such as the mass of the star and the compactness of the star would be appropriate.

We may expect (and this will later be verified) that if a star is going to have a significant effect on the nucleating bubble then the size of the star would have to be comparable to the size of the nucleating bubble. In a cosmological setting this would imply that the star would have to have a size corresponding to a "grand unified length scale"; thus we are dealing with "stellar" candidates such as boson stars and monopoles. The model star should also be a reasonable model for these candidates.

Exact analytic solutions to the Einstein equations do exist for stellar models, e.g., for a constant energy density star. These solutions are undesirable for our "star" because they do not act as good models for boson stars and monopoles. Also, the radial derivatives of the metric functions, f(r) and h(r), are not continuous at the stellar boundary; this may lead to complications in the numerical analysis, which would not be an attractive feature in an initial model.

The following functions will be used for the metric of the "model star",

$$h(r) = \frac{1}{1 - \frac{2\kappa}{r}\left\{1 - \exp\left[-\left(\frac{r}{2\kappa\gamma}\right)^3\right]\right\}} \tag{4.16}$$

$$f(r) = 1 - \frac{2\kappa}{r} \qquad r \geq 2\kappa\gamma \tag{4.17}$$

$$= 1 - \frac{e^{1/2}}{\gamma}\exp\left[-\tfrac{1}{2}\left(\frac{r}{2\kappa\gamma}\right)^2\right] \qquad r < 2\kappa\gamma \tag{4.18}$$

These metric functions are desirable because they possess a simple algebraic form; they are continuous, together with their derivative functions (i.e., sufficiently smooth to realistically model a boson star); they have a small parameter space (i.e., only two parameters κ and γ); and generally provide a reasonable model for a stellar candidate such as a boson star (see, for example, Seidel and Suen (1990) for a discussion of boson star metrics).

The mass of the star is given by the parameter κ, and the parameter γ represents the compactness of the star. The star does not possess a well defined boundary; however, a characteristic size of the star (as we may observe below in Eq.(4.19)) is

given by $2\kappa\gamma$; this illustrates the role that γ plays in representing the compactness of the "star".

We may write the mass function for the star as follows,

$$M(r) = \kappa\left\{ 1 - \exp\left[- \left(\frac{r}{2\kappa\gamma}\right)^3 \right] \right\} \quad . \tag{4.19}$$

This expression gives the mass of the star contained within the radius "r", so

$$M(r\rightarrow\infty) = \kappa \quad , \tag{4.20}$$

and the fraction of the mass contained within the "boundary" of the star is given by

$$M(r=2\kappa\gamma) = (1 - e^{-1}) \approx 63\% \quad . \tag{4.21}$$

The (t,t)-component of the stress-energy tensor for the metric provides the information about the local energy-density for the matter which comprises the star. This may be expressed in terms of the metric h(r) function using the Einstein equations

$$8\pi T_{tt} = \frac{1}{rh^2}\frac{dh}{dr} + \frac{1}{r^2}\left[1 - \frac{1}{h} \right] \quad . \tag{4.22}$$

For the metric under consideration this reduces to

$$T_{tt} = \rho = \frac{3}{32\,\pi\,\kappa^2\,\gamma^3} \exp\left[- \left(\frac{r}{2\kappa\gamma}\right)^3 \right] \quad , \tag{4.23}$$

where ρ represents the energy density. This tells us that we have an exponentially decaying energy density as we move away from the center of the star. Figures 25, 26

and 27 give pictorial representations of the metric functions, f(r) and h(r), together with the corresponding energy-density for the model star.

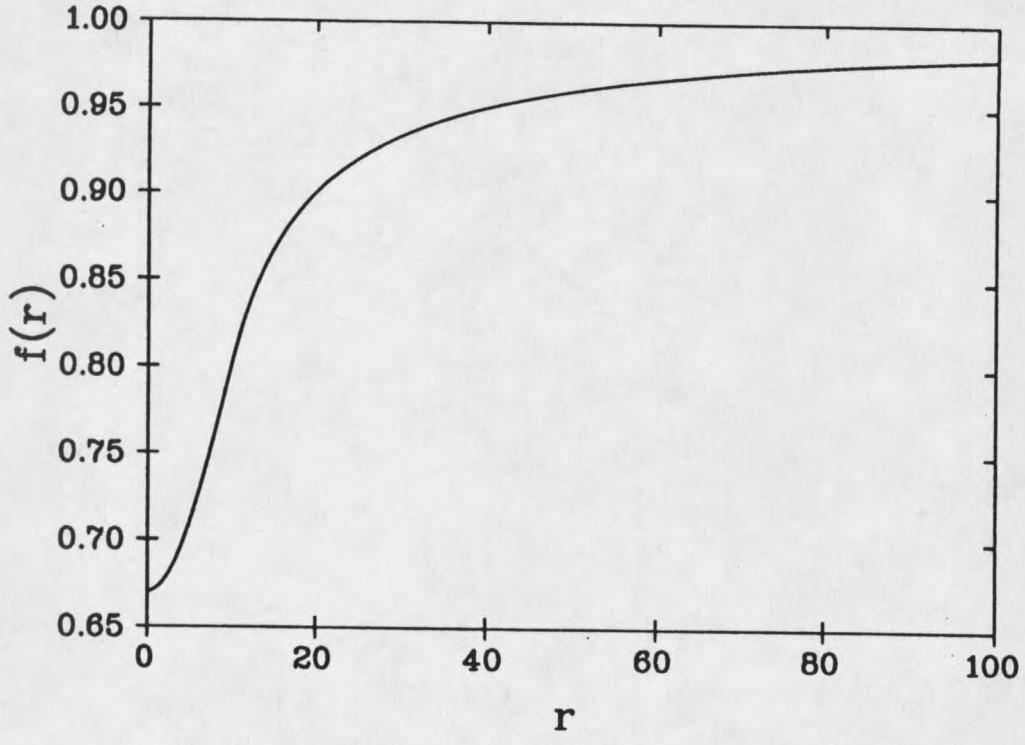

Figure 25 Metric function f(r), with metric parameters κ=1.0 and γ=5.0; this would result in a stellar radius, r_{star} = 10 (in dimensionless units).

The metric function, f(r), is piecewise constructed, such that "outside" the star (i.e., $r > 2\kappa\gamma$) the metric function corresponds to the exterior Schwarzschild solution (n.b., the metric function, h(r), does not correspond to the Schwarzschild solution "outside" the star; thus we do not have a complete, exterior, Schwarzschild solution). At $r=2\kappa\gamma$ an interior function is joined to the exterior Schwarzschild function so that the overall metric function, f(r), together with its derivative, df/dr, are continuous at this

point. The form of the interior function is such that it admits a maximum value for the γ parameter, beyond which the perturbative analysis intrinsically breaks down. This value of γ is $e^{1/2} \cong 1.65$, for which f(r=0)=0 (i.e., F(r)=-1, which violates the condition, $| F(r) | << 1$, necessary for the perturbative analysis). Of course, the validity of the perturbative analysis will be brought into question before this value of γ is reached.

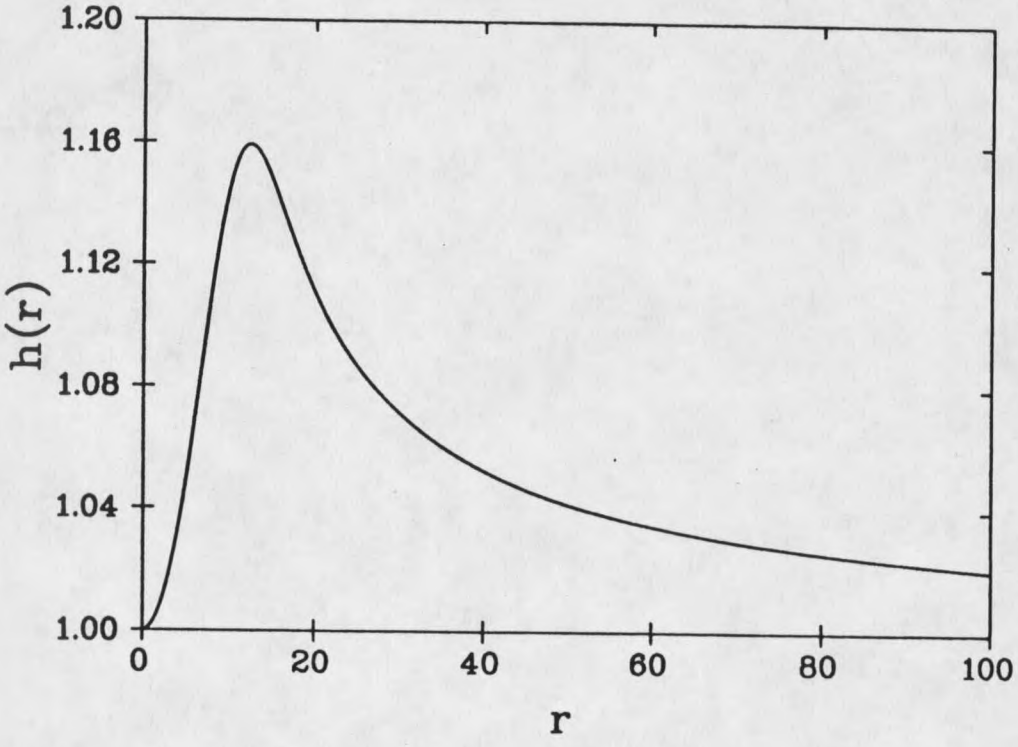

Figure 26 Metric function h(r), with metric parameters κ=1.0 and γ=5.0; this would result in a star of radius r_{star}=10 (in dimensionless units).

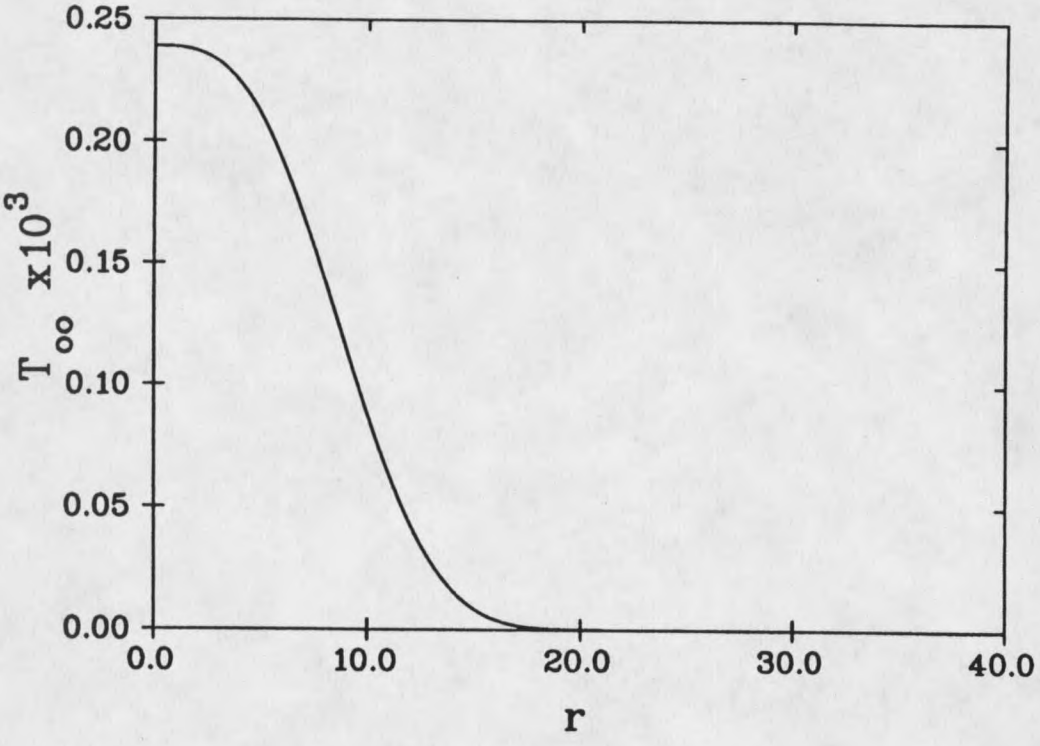

Figure 27 The (t,t) component of the stress-energy tensor, giving the energy density for the matter comprising the star, with metric parameters κ=1.0 and γ=5.0; corresponding to a star of (dimensionless) radius, r_{star}=10.

Results

Figure 28 shows the ratio of S_3 to S_4 (evaluated numerically) as a function as the stellar mass, κ, for a series of γ values; the scalar field potential parameters being fixed at the values of $\tilde{\varepsilon}$=1.0 and ψ_+=1.0. S_3 is the Euclidean action for the bubble in the spacetime of the gravitationally compact object and S_4 is the Euclidean action for the bubble in the flat spacetime. Note that as the analysis adopts a fixed background

spacetime, there is no contribution from the spacetime, as such, to the value of B (the difference between the Euclidean action for the spacetimes with and without the nucleating bubble); we may therefore write $B_3=S_3$ and $B_4=S_4$.

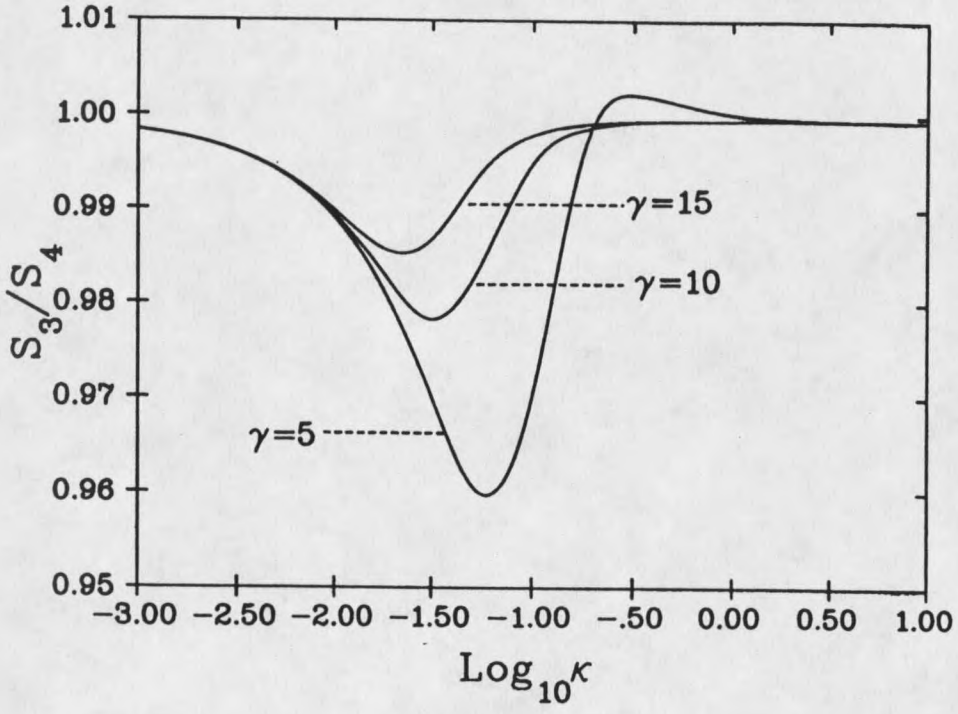

Figure 28 A plot of S_3 / S_4 for a range of metric parameters κ and γ, the scalar field potential parameters are fixed at the values of ω=1.0 and ψ_+=1.0.

We observe a phenomenon which may be described as a "resonance" for the B_3 / B_4 curves. As the mass of the star goes to zero the Euclidean action of the nucleating bubble approaches the O(4)-symmetric value, as would be expected. Similarly, for large mass stars, with a constant value of γ (e.g., this might correspond to a bubble of "nuclear" dimensions forming at the center of the Earth), the Euclidean action for the nucleating bubble approaches the O(4)-symmetric value. However, there

is a range of masses for which the Euclidean action of the nucleating bubble drops below the O(4)-symmetric value. The prominence of this drop away from the O(4)-symmetric value increases with a decrease in the value of γ, i.e., the effect increases with an increase in the compactness of the star. The value of κ at which the minimum in the Euclidean action occurs is dependent upon the compactness of the star, i.e., upon γ; we shall later find the exact relationship between κ and γ for the minimum in the Euclidean action.

Figures 29 and 30 show the w_r and w_τ values corresponding to the metric and potential parameters of Figure 28. These curves imply that the nucleating bubble located at the "resonance trough" is a prolate spheroid. The O(3)-radius (i.e., the size of the bubble on the τ=0 slice) is slightly less than the corresponding radius for the O(4)-symmetric bubble (i.e., $w_r > 1$). We may think of this as the effect of the gravitational field "pulling in" the bubble wall. The "size" of the bubble along the τ–axis is larger than that corresponding O(4)-symmetric bubble, thus giving a prolate appearance. Figure 32 illustrates the evolution of the shape of the nucleating bubble from the O(4)-symmetric configuration to the O(3)-symmetric, resonant configuration.

When the star is much larger than the nucleating bubble (i.e., $2\kappa\gamma$ is much larger than the dimensionless radius of the bubble) , we may write the metric line element, as seen by the bubble nucleating at the center of the star, in an following approximate form,

$$ds^2 = f_0\, d\tau^2 + dr^2 + r^2\, d\Omega^2 \quad , \tag{4.24}$$

where,

$$f_0 = 1 - \frac{e^{1/2}}{\gamma} \quad ; \tag{4.25}$$

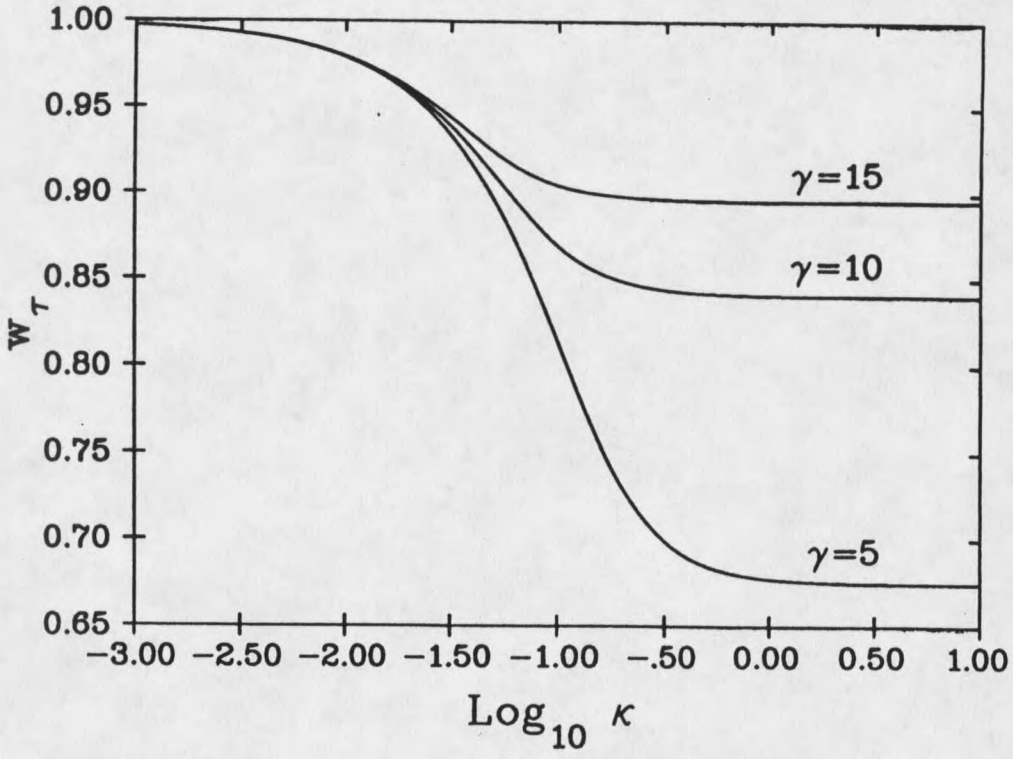

Figure 29 Plot of w_τ curves for a range of metric parameters κ and γ, the scalar field potential parameters are fixed at the values of ω=1.0 and ψ_+=1.0.

i.e., $f_0 = f(r=0)$, for the given set of metric parameters. We may make this approximation because the variation in f(r) over the spatial extent of the bubble will be negligible. Similarly, the coefficient of dr^2 is taken to be $h(r=0)=1$, the spatial variation of this metric function is also negligible over the spatial extent of the bubble.

Defining a new variable, $\bar{\tau} = f^{\frac{1}{2}}\,\tau$, we may re-write the approximate line element as,

$$ds^2 = d\bar{\tau}^2 + dr^2 + r^2\, d\Omega^2 \qquad (4.26)$$

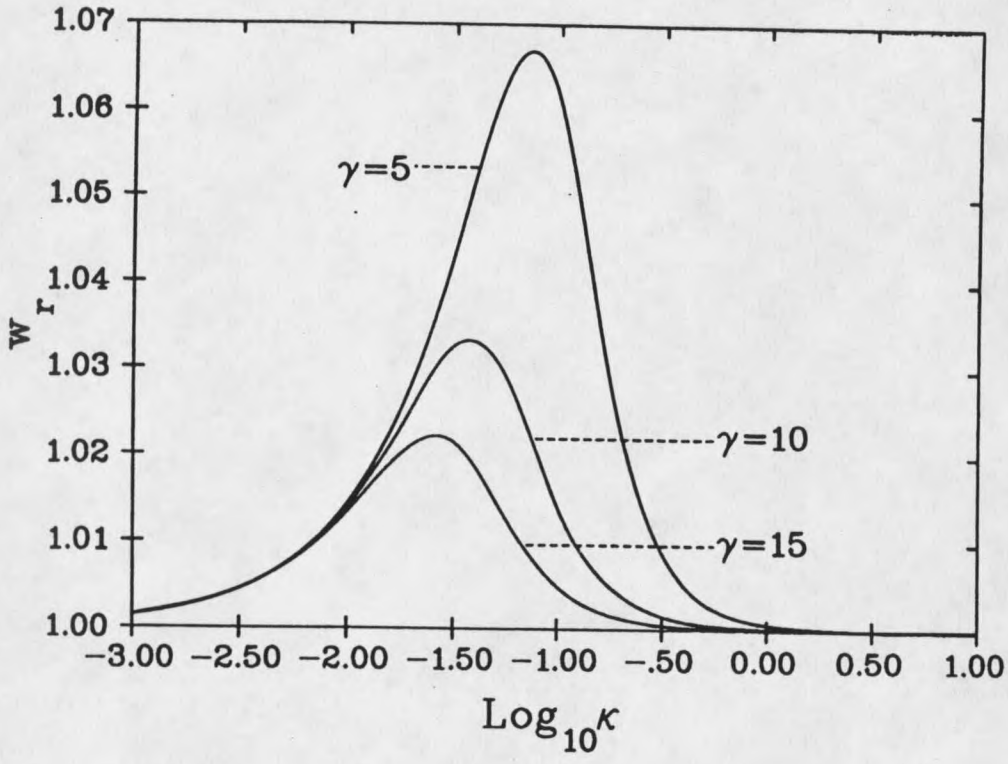

Figure 30 Plot of w_r curves for a range of metric parameters κ and γ, the scalar field potential parameters are fixed at the values of ω=1.0 and ψ_+=1.0.

This line element is O(4)-symmetric in the $(\bar{\tau},r,\theta,\psi)$-space, and so the solution to the Euclideanized scalar field equation is just the usual $\phi(R)$, where $R^2 = \bar{\tau}^2 + r^2$. In terms of the original (τ,r,θ,ψ) coordinate system, the nucleating bubble solution is again $\phi(R)$, where we now express R^2 as $R^2 = f_0 \tau^2 + r^2$. Thus the nucleating bubble will be a prolate spheroid, with the τ-axis being the axis of rotational symmetry; the perturbation parameters, w_τ and w_r, take the values f_0 and 1.0, respectively. Figures 29 and 30 verify this analysis, where, for large κ, $w_r \to 1$ and $w_\tau \to f_0$.

If the nucleating bubble is much larger than the characteristic size of the star (i.e., $\kappa \to 0$) then the volume "surplus" due to the star will be negligible compared to

the volume of the bubble. In this case we would not expect the star to have a significant effect upon the nucleating bubble. This is verified with the results shown in Figures 28, 29 and 30, where $w_r \to 1$, $w_\tau \to 1$, and $B_3 \to B_4$ as $\kappa \to 0$.

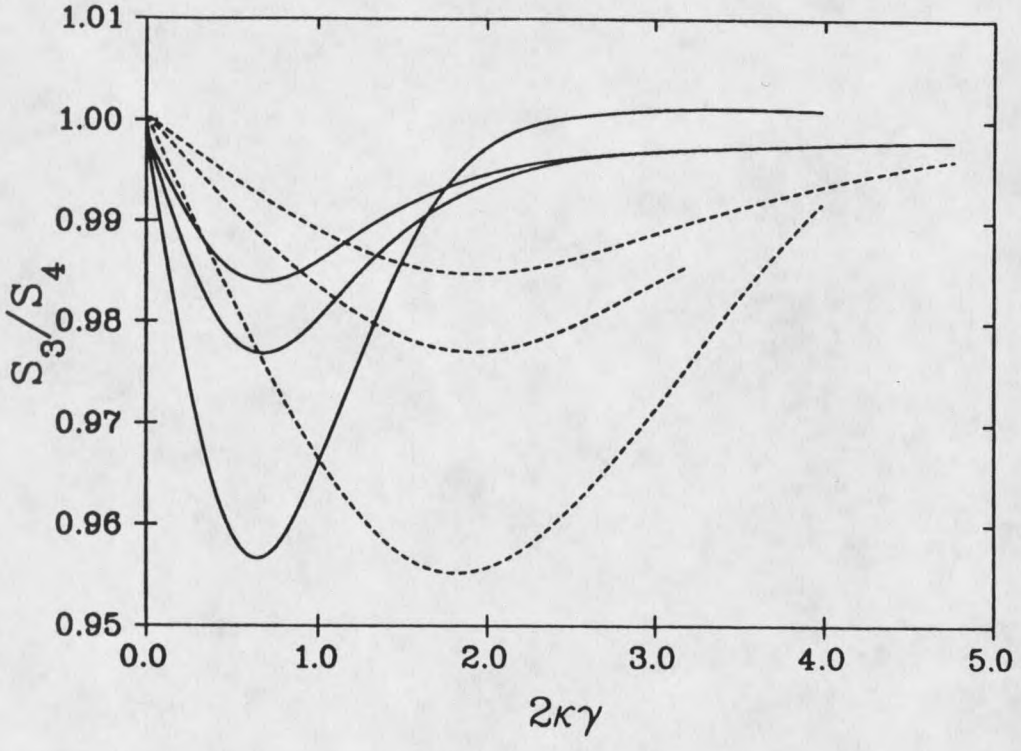

Figure 31 Superposition of two sets of S_3 / S_4 curves; the solid curves corresponding to potential parameters ω=1.0 and ψ_+=1.0, and the dashed curves corresponding to potential parameters ω=0.2 and ψ_+=1.0. (S_3 / S_4) is plotted against $2\kappa\gamma$, which gives a characteristic size for the star. The curves, for a given set of potential parameters, correspond to the γ parameters: γ=5 (highest peak), γ=10 (middle peak) and γ=15 (lowest peak). The potential parameters, (ω=1.0 , ψ_+=1.0), result in a nucleating bubble of characteristic (dimensionless) radius r_{bubble} = 1.3 , and the potential parameters, (ω=0.2 , ψ_+=1.0), result in a nucleating bubble of characteristic (dimensionless) radius r_{bubble} = 4.3. Thus we observe that at "resonance" the star is typically about half the size of the nucleating bubble.

The quantity $(2\kappa\gamma)$ represents the characteristic size of the star. It may, therefore, be useful to plot the ratio (S_3 / S_4) against $(2\kappa\gamma)$ to provide some insight into the relationship between the stellar size and the "resonance" phenomenon. Figure 31 provides such a plot in which we have superimposed the solution curves corresponding to two sets of potential parameters, namely $\tilde{\varepsilon}=1.0$ and $\tilde{\varepsilon}=0.2$; both with $\psi_+=1.0$. The first thing that is noticed from Figure 31 is that the "resonance troughs" all occur at roughly the same value of $(2\kappa\gamma)$ for a given set of potential parameters. In particular, if we refer to the size of the O(4)-symmetric bubble for the given set of potential parameters, we notice that the "resonance" occurs when the star is roughly half the size of the nucleating bubble. This is what one would expect from general intuitive arguments. Again, as with Figure 30, the depth of the "resonance trough" increases with an increase in the compactness of the star; this also agrees with general intuitive arguments.

For the scalar field potential parameters under consideration, a stellar compactness of $\gamma=5$ results in a characteristic 4% to 5% reduction in the Euclidean action of the nucleating bubble, as compared to the O(4)-symmetric bubble action. This is in qualitative agreement with the predictions of the "thin-wall" analysis. It is not possible to make a direct quantitative comparison between the perturbative results and the "thin-wall" results due to fundamental differences in the formulation of the two analyses. However, the "thin-wall" analysis of Mendell and Hiscock, in which the effect of a neutron star on false-vacuum decay was considered, resulted in values of B_3 which were characteristically 30% to 50% lower than B_4. If we considered smaller values of γ in the perturbative analysis (i.e., more compact stars) then we might expect reductions in B_3 which would be closer to the "thin-wall" analysis. However, the validity of the perturbative approach may then be brought into question.

The "thin-wall" analysis of Hiscock, and Mendell and Hiscock, considered solutions to the coupled Euclideanized scalar field and Einstein equations (via the Israel formalism) which had the form of infinite, oscillating cylinders; where the τ-axis was the axis of symmetry. The perturbative analysis has shown that the nucleating bubble, at resonance, takes the form of a prolate spheroid (Figure 32 illustrates the evolution of the O(4)-symmetric bubble in the flat spacetime to the form of a prolate spheroid in the stellar spacetime). The extent of this prolation is increased with an increase in the stellar compactness. It is therefore conceivable that a transition takes place where the nucleating bubble transforms from a prolate spheroid to an the oscillating cylinder of the "thin-wall" analysis for a sufficiently compact star.

We may now address the question of whether a gravitationally compact objects will have a significant effect on false-vacuum decay.

False-Vacuum "Decay Rate" in the Presence of a Gravitationally Compact-Object.

In a flat, O(4)-symmetric spacetime, the number of O(4)-symmetric nucleating bubbles per unit four volume, associated with false-vacuum decay is given by

$$\Gamma = A \exp(-B_4) \quad , \tag{4.27}$$

where B_4 is the difference between the Euclidean action for the spacetime with and without the nucleating bubble. The coefficient A typically has an order of magnitude given by the field mass to the fourth power, i.e., m^4.

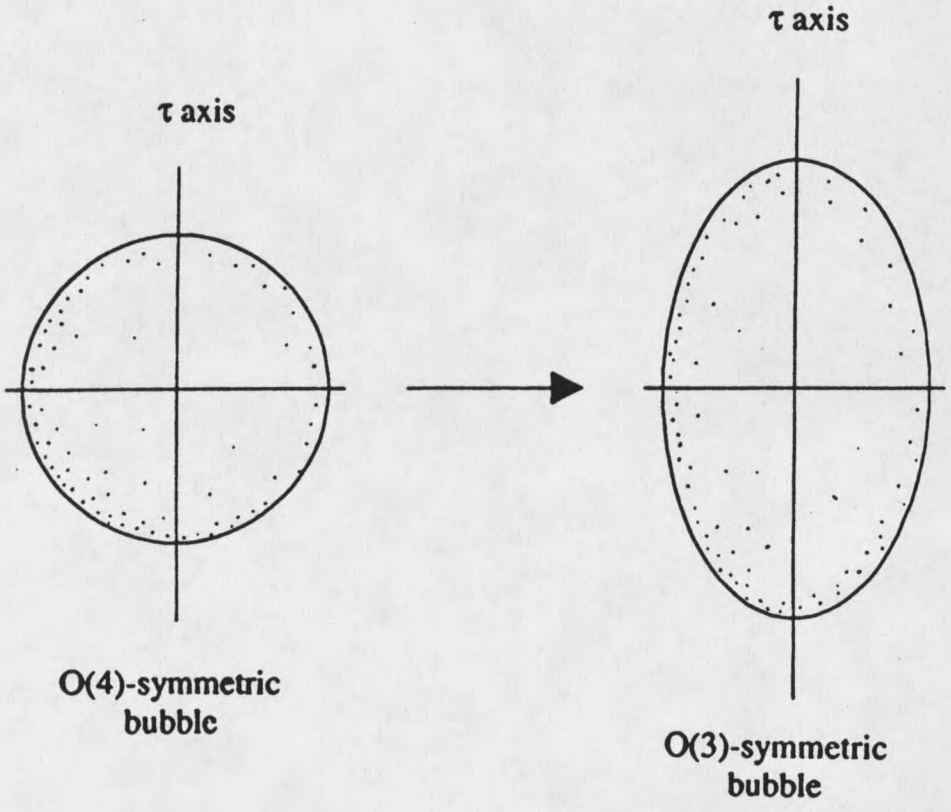

Figure 32 Characteristic evolution of the shape of the nucleating bubble at, and near, resonance, from the O(4)-symmetric form in a flat spacetime to a prolate spheroid (with τ as the rotational symmetry axis), in the spacetime of a "dilute" gravitationally compact object.

So, for example, if we had a square box with sides of length L, and volume L^3, the characteristic time that one would have to wait for a nucleating bubble to appear is,

$$T_4 = L^{-3}\, m^{-4} \exp(B_4) \ . \qquad (4.28)$$

Of course, the nucleating bubble may appear anywhere within the box; there is no preferred location for the formation of the bubble. However, when we consider the effect of a gravitationally compact object on false-vacuum decay, we make the assumption that the bubble will be forming around the compact object. The nucleating

bubble field profile and Euclidean action are obtained under this assumption. We must therefore use a modified form of Eq. 4.28 to calculate the characteristic time associated with the formation of a nucleating bubble around the compact object. Of course the nucleating bubble could form anywhere within the stellar spacetime. However, the Euclidean action, B_3, and the associated "decay rate" formula relate to the formation of the bubble around the star. We may use, as a good approximation, Eq.(4.28) to estimate the rate of bubble nucleation in a stellar spacetime for bubbles not forming around the star.

If we place one compact object (star) into our originally flat, O(4)-symmetric spacetime, where the Euclidean action for a nucleating bubble around the star is given by B_3, then the characteristic time associated with the formation of the nucleating bubble around the star is,

$$T_3 = C \exp(B_3) \quad , \tag{4.29}$$

where the coefficient C typically has an order of magnitude given by m^{-1}. If there is more than one star in the spacetime then we may make a "dilute gas" approximation in order to calculate T_3. The dilute gas approximation basically assumes that the stars do not interfere with one another, with regards to the bubble formation process. This requires the typical distance between the stars to be much greater than the characteristic size of the stars, and also much greater than the characteristic size of the nucleating bubbles. Thus the spacetime "between the stars" is also approximately flat.

If there are N similar stars (i.e., same values of κ and γ within our stellar model) in an otherwise empty spacetime, and B_3 is the Euclidean action associated with the formation of a nucleating bubble around a star, then the characteristic time for a single bubble to form around one of the stars is,

$$T_3 = N^{-1}\, m^{-1} \exp(-B_3) \qquad (4.30)$$

To address the question of whether gravitationally compact objects play an important role in false vacuum decay, it is necessary to compare to characteristic times for nucleating bubble formation, i.e., T_3 and T_4. Thus, if $T_3 < T_4$ then gravitationally compact objects will dominate the false-vacuum decay process. However, if $T_3 > T_4$ then gravitationally compact objects will not play an important role in false-vacuum decay. It is not sufficient to merely compare the values of B_3 and B_4 in order to determine the dominant mechanism for false-vacuum decay.

Consider a spacetime with three-volume, V, and N similar stars. The ratio of T_3 to T_4 is given by

$$\frac{T_3}{T_4} = \frac{V\, m^3}{N} \exp(B_3 - B_4) \qquad (4.31)$$

For known values of m, B_3 and B_4, this expression provides us with the number density of stars needed for the gravitationally compact objects to play the dominant role in false-vacuum decay (i.e., stars will play the dominant role in the decay mechanism if $(N/V) > m^3 \exp(B_3 - B_4)$).

In Chapter 5 we shall make use of Eq.(4.31) in an attempt to place bounds upon the number density of some astrophysical objects, such as boson stars and microscopic black holes, within the Universe.

CHAPTER 5

ASTROPHYSICAL APPLICATIONS

Post-Nucleation Evolution of a Bubble of True Vacuum

The nucleation of a bubble of true-vacuum within the medium of false-vacuum is merely the first stage in the process of false-vacuum decay. Following the nucleation of a bubble there is a subsequent evolution in which the bubble expands, converting the remainder of the false-vacuum to the true-vacuum state.

The post-nucleation evolution of the bubble is primarily classical, unlike the quantum processes which are responsible for the creation of the bubble. The evolution is therefore governed by the Lorentzian classical scalar field equation, though when gravity is important we require the coupled Lorentzian scalar field and Einstein equations.

We shall not consider the effects of gravity on the post-nucleation evolution of the bubble, but rather, assume that we have a fixed background spacetime which is flat (i.e., Minkowski space). The line element for the Euclideanized Minkowski space may be expressed as,

$$ds^2 = d\tau^2 + dr^2 + r^2\, d\Omega_2{}^2 \quad ; \tag{5.1}$$

where $d\Omega_2$ is the line element on the unit two-sphere. As Euclideanized Minkowski space is O(4)-symmetric, we may define an O(4)-radial variable, ξ, via

$$\xi^2 = \tau^2 + r^2 \quad , \tag{5.2}$$

the line element, Eq.(5.1), then becomes

$$ds^2 = d\xi^2 + \xi^2\, d\Omega_3{}^2 \quad ; \tag{5.3}$$

where $d\Omega_3$ is the line element on the unit three-sphere. The scalar field equation in this spacetime may be obtained from the general expression for the scalar field equation

$$g^{-\frac{1}{2}}\, \partial_\mu \left[\, g^{\frac{1}{2}}\, g^{\mu\nu}\, \partial_\nu \,\right] \phi = \frac{dU}{d\phi} \quad ; \tag{5.4}$$

which gives for the Euclideanized Minkowski space

$$\frac{d^2\phi}{d\xi^2} + \frac{3}{\xi}\frac{d\phi}{d\xi} = \frac{dU}{d\phi} \tag{5.5}$$

The solution to the Euclideanized scalar field equation, with the appropriate boundary conditions, provides us with $\phi(\xi)$ for $\xi \geq 0$. This not only gives the field profile of the nucleating bubble but also the field profile to the exterior of the lightcone, and on the lightcone centered at the nucleation site, for all Minkowski time, $t \geq 0$. We assume here, without loss of generality, that the bubble is nucleated at $t=0$ within our (t,r,θ,ϕ) coordinate system.

The evolution of this bubble after its nucleation is given by the solution to the Lorentzian scalar field equation in the Minkowski spacetime. The line element for the (non-Euclideanized) Minkowski spacetime is given by

$$ds^2 = -dt^2 + dr^2 + r^2\, d\Omega_2{}^2 \quad . \tag{5.6}$$

We may again define a variable, ξ, (though no longer an O(4)-radial variable) by

$$\xi^2 = -t^2 + r^2 \quad , \tag{5.7}$$

and the line element is now given by

$$ds^2 = -d\xi^2 + \xi^2 \, d\Omega_3^2 \tag{5.8}$$

The Lorentzian scalar field equation may also be obtained from the generalized formula of Eq.(5.4) (n.b., in the Lorentzian sector, the term $g^{1/2}$ in Eq. 5.4 is replaced by $(-g)^{1/2}$, and similarly for the $g^{-1/2}$ term), giving

$$\frac{d^2\phi}{d\xi^2} + \frac{3}{\xi}\frac{d\phi}{d\xi} = -\frac{dU}{d\phi} \tag{5.9}$$

The Lorentzian scalar field equation differs from the Euclideanized scalar field equation only by the sign in which the potential derivative appears. In terms of the particle motion analogy of Chapter 2, we now have a particle of unit mass moving in the potential U (rather than the inverted potential -U); with a frictional term which is inversely proportional to the "time", ξ. The Lorentzian scalar field equation will provide us with the scalar field profile in the interior of the lightcone centered at the nucleation site (i.e., $\phi(\xi)$ for $\xi<0$).

It is convenient to define a new variable, y, given by

$$y = \xi^2 \quad , \tag{5.10}$$

such that the spacetime exterior to the lightcone centered on the bubble corresponds to $y>0$, and the interior of the lightcone corresponds to $y<0$; where the lightcone is represented by $y=0$. The Lorentzian scalar field equation, in terms of the y coordinate, is given by

$$y\frac{d^2\phi}{dy^2} + 2\frac{d\phi}{dy} = -\frac{1}{4}\frac{dU}{d\phi} \qquad (5.11)$$

The value of the field at y=0 is the same as that for ξ=0, however, the field derivative at y=0 is no longer zero (i.e., though $d\phi/D\Xi = 0$ at ξ=0 , $d\phi/dy$ is not zero at y=0). The field derivative at y=0 is instead given by,

$$\frac{d\phi}{dy}(y=0) = -\frac{1}{8}\frac{dU}{d\phi} \qquad (5.12)$$

The interior lightcone evolution of a thin-wall bubble is notably different from the corresponding evolution of a non-thin-wall bubble. In the "thin-wall" approximation the core of the bubble at the moment of nucleation has a field value corresponding to the true-vacuum state. Thus (dU/dy)=0 at y=0 and there is no interior lightcone evolution of the field (i.e., the field takes the constant value corresponding to the true vacuum state throughout the interior of the lightcone). Figure 33 illustrates the field profile for a bubble within the "thin-wall" approximation, for y ranging from the interior of the lightcone (i.e., y<0) to the exterior of the lightcone (i.e., y>0). Within the framework of the $\phi^{2\text{-}3\text{-}4}$ model of Chapter 2, this "thin-wall" bubble corresponds to the potential parameters, $\tilde{\varepsilon}$=1. 0 and ψ_+=1. 0.

Non-thin-wall bubbles have field profiles which do not reach the true vacuum state at y=0. There is, therefore, a subsequent field evolution to the interior of the lightcone, where the field evolves to the true vacuum state. Figure 34 illustrates an exact field profile (for the $\phi^{2\text{-}3\text{-}4}$ model of Chapter 2, with potential parameters $\tilde{\varepsilon}$=1. 0 and ψ_+=1. 0) for a range of y values, in a similar manner to Figure 33. We observe that in the interior of the lightcone the field initially oscillates about the true vacuum state (σ=1), this oscillation is damped due to the damping term in the scalar field equation. The field eventually "comes to rest" at the true vacuum state.

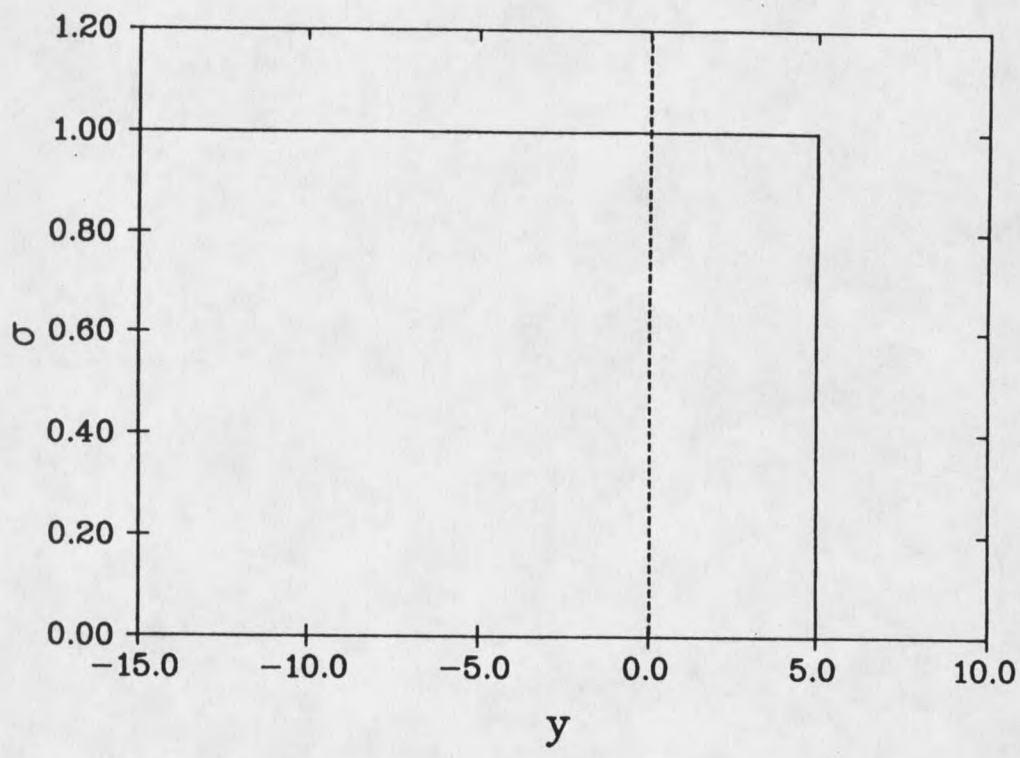

Figure 33 Field profile for a "thin-wall" bubble. y=0 corresponds to the light-cone centered at the nucleation site for the bubble; y>0 corresponds to the exterior of the lightcone; and y<0 corresponds to the interior of the lightcone. When the bubble nucleates, the center of the bubble ($\sigma(y=0)$) has a field value corresponding to the true vacuum state ($\sigma=1$); there is, therefore, no interior lightcone evolution of the field. The field profile shown here is "idealized", and corresponds to the "thin-wall" approximation. There will, however, be exact field profiles which will resemble this profile in situation where the two vacuum states are nearly degenerate.

Consider a false-vacuum decay in a cosmological setting. Such phase transitions are believed to have occurred in the past of our Universe (within the inflationary Universe scenarios). If the energy density gap between the true and false-vacuum states was small then the bubble profile would have a form similar to that of Figure 33 (i.e., a "thin-wall" profile); whereas, if the energy density difference were

large then the profile of Figure 34 would be a better representation of the actual field profile.

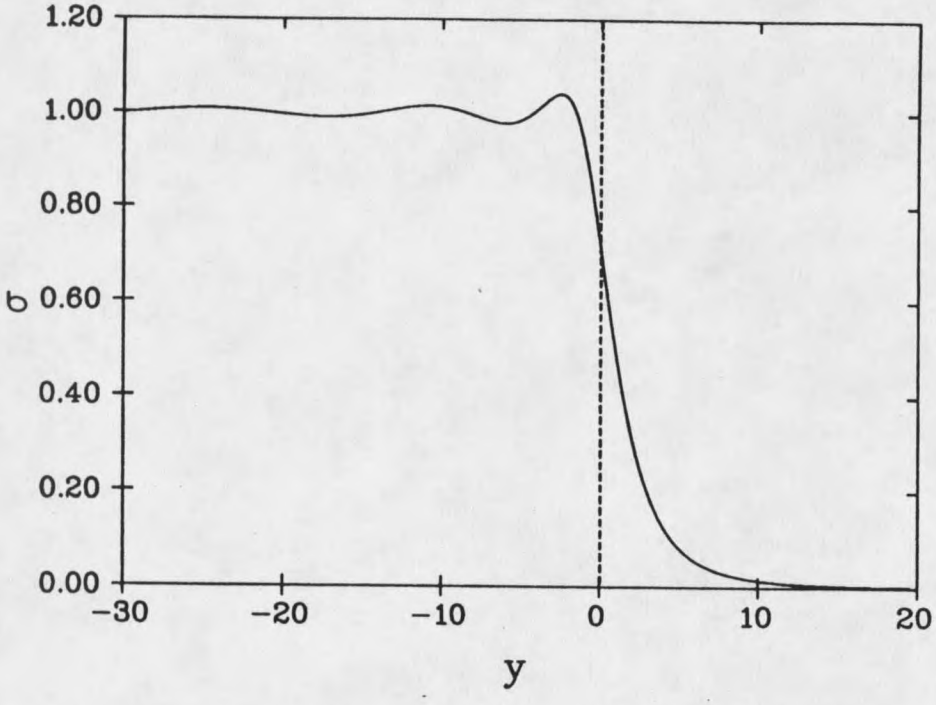

Figure 34 Field profile for a thick-wall bubble. y=0 corresponds to the light-cone centered at the nucleation site for the bubble; y>0 corresponds to the exterior of the lightcone; and y<0 corresponds to the interior of the lightcone. When the bubble nucleates, the center of the bubble ($\sigma(y=0)$) has a field value which has not yet reached the true vacuum state ($\sigma=1$); there is therefore an interior lightcone evolution of the field. Within the formulation of the $\phi^{2\text{-}3\text{-}4}$ model of Chapter 2, this bubble profile corresponds to the potential parameters $\omega=1.0$ and $\psi_{+}=1.0$.

Within the inflationary Universe models, the fields that undergo the vacuum phase transitions are the Higgs fields. These Higgs fields couple to other particle fields and this coupling is believed to provide the mass generation mechanism for these fields. Thus, for example, the Lagrangian density for the Standard Model contains terms of the

form $\{g\phi\,[\Psi]^2\}$, where g is a coupling constant, ϕ is the value of the Higgs field, and Ψ represents some other field (e.g. , a fermionic field such as the electron). We may re-write this term as $\{m^2[\Psi]^2\}$, where "m" now represents the mass of the Ψ field (assuming that $(g\phi)$ is the only coefficient of the quadratic term in the Ψ field). So, when the Higgs field is in its symmetric state (i.e., $<\phi>=0$) the Ψ field is massless, but when the Higgs field is in its broken symmetry phase (i.e., $<\phi>=\phi_0$, where ϕ_0 is the field value corresponding to the broken symmetry vacuum state), the Ψ field becomes massive, with mass $m=(g\phi_0)^{1/2}$.

For a Higgs field bubble profile of the form shown in Figure 33, a fermionic field Ψ would be massless outside the bubble but would have a mass inside the bubble. The Ψ field equation would then take the form,

$$\Box\,\Psi = 0 \quad , \qquad \text{Outside of bubble,} \tag{5.13}$$

and,

$$(\Box + m^2)\,\Psi = 0 \quad , \qquad \text{Inside of bubble.} \tag{5.14}$$

In terms of classical wave theory, we have here the characteristic problem of "impedance mismatching" for the Ψ field at the bubble wall. This will result in a reflection and transmission coefficient associated with the ψ field passing through the bubble wall; the larger the value of "m" then the greater this effect will be. The partial reflection of the ψ field will provide a back-reaction on the bubble wall and hence have an effect on the evolution of the bubble wall.

With a Higgs field bubble profile of the form shown in Figure 34, the mass of the Ψ field will no longer undergo a sudden jump at the location of the bubble wall. The mass will now vary continuously, i.e., $m^2(y)=g\phi(y)$, and so $m^2(y)$ will have the same "shape" as the bubble field-profile. There will again be a reflection and transmission coefficient associated with the Ψ field propagating through the bubble

wall; however, this effect will be weaker than in the "thin-wall" case because of the less abrupt change in the mass of the Ψ field (we call upon intuitive arguments from classical wave mechanics to make this observation). The pressure (back-reaction) on the bubble wall due to the Ψ field will therefore be less for a thick-wall bubble than for a thin-wall bubble. This may result in differences in the post-nucleation evolution of the bubbles in the two scenarios.

The interior lightcone oscillation of the Higgs field for thick-wall bubbles (see Figure 34) will also result in a back-reaction in any field coupled to the Higgs field. Such an oscillation may result in particle creation in other fields, thus transferring energy from the Higgs field to other fields, and possibly contribute to the re-heating process in the bubble interior.

Other physically interesting effects associated with the behavior of quantum fields at the bubble wall, including particle creation, have been suggested. For example, Mc Lerran et. al. (1991) and Dine et. al. (1991), have considered the possibility that the baryon-anti-baryon asymmetry observed within the Universe today may have been the result of quantum effects associated with the bubble-wall of an electroweak phase transition (within these models the GWS electroweak phase transition is assumed to be first-order).

Within these scenarios the degree of particle creation, re-heating or any other phenomenon associated with fields coupled to the (bubble) Higgs field *will be strongly model dependent*. We shall, therefore, leave this for further study.

Bounds on Fermion Masses within the Standard Model

The masses of the electroweak gauge bosons [γ , { W^+,W^-,Z^0}] and the fermions [{ (e,ν_e), (μ,ν_μ), (τ,ν_τ) } , { (u,d), (c,s), (t,b) }] are generated via the Higgs mechanism within the Glashow (1961), Weinberg (1967) and Salaam (1968) theory [GWS theory]. The theory does not, *per Se*, put any bounds upon the fermionic masses but it has been found that very heavy fermionic masses can de-stabilize the vacuum state within the theory.

The 1-loop, renormalized, effective potential for the Higgs field within the GWS theory is given by

$$V(\phi) = -\frac{1}{2}\mu^2\phi^2 + \frac{1}{4}\lambda\phi^4 + \Xi\,\phi^4 \ln(\frac{\phi^2}{M^2}) \quad , \qquad (5.15)$$

where $\frac{1}{2}\phi^2 = \Phi^+\Phi$ (Φ = Higgs doublet) , M is the renormalization mass scale, and $\frac{1}{2}\mu^2$ and $\frac{1}{4}\lambda$ are the quadratic and quartic coefficients of the tree-level potential, respectively. The coefficient Ξ is given by

$$\Xi = \frac{1}{64\pi^2}\left[\sum_{\text{gauge bosons}} 3g_i^4 - \sum_{\text{fermions}} f_i^4 \right] \quad , \qquad (5.16)$$

$$= \frac{1}{64\pi^2}\left[3\{ 2g^4 + (g^2 + g'^2)^2 \} - \left(\frac{g}{2M_w}\right)^4 \sum_{\text{fermions}} m_f^4 \right] \quad , \qquad (5.17)$$

where

$$g = \frac{e}{\sin \Theta_w} \quad , \tag{5.18}$$

and

$$g' = \frac{e}{\cos \Theta_w} \quad . \tag{5.19}$$

Θ_w is the electroweak mixing angle, and M_w ($\approx$ 77 GeV) is the mass of the W-boson. The m_f terms represent the masses of the fermions.

If the coefficient Ξ is positive semi-definite then the 1-loop effective potential is bounded from below. However, if the coefficient Ξ becomes negative then the 1-loop effective potential is rendered unbounded from below. This is generally regarded as being unphysical, and may illustrate a breakdown in the theory. Figure 35 illustrates this potential for the values, Ξ=0 and Ξ=-1, demonstrating that the potential becomes unbounded for negative Ξ.

From Eq.(5.17) we observe that if there is a sufficiently massive fermion within the theory then it is possible that Ξ may become negative. The known fermions do not have sufficient mass to make Ξ negative; however, there is no definitive experimental bound on the top-quark mass at this time. Thus the top-quark may bring news of catastrophe with its eventual discovery! (i.e., the possibility that the Universe we live in might be unstable to quantum decay into a spacetime that would be unstable to gravitationally singular behavior, and in which the "Cauchy problem" is not well defined)

We may place a theoretical upper-bound upon the top-quark mass by demanding that it not have sufficient mass to render Ξ negative. This was one of the first steps taken in placing such a bound. There are also various phenomenological arguments for placing bounds on the top-quark mass (e.g., based on the K_L-K_S mass difference, see for example, Buras (1981)), but these are not very strong bounds.

A subsequent analysis of the two-loop effective potential by Mahanthappa and Sher (1980) revealed that there is a range of unbounded one-loop potentials which become bounded at the two-loop level. The two-loop potential is a complex object and cannot be written down in closed form, though it may be studied in an approximate form via the use of "running coupling constants" within a renormalization group prescription.

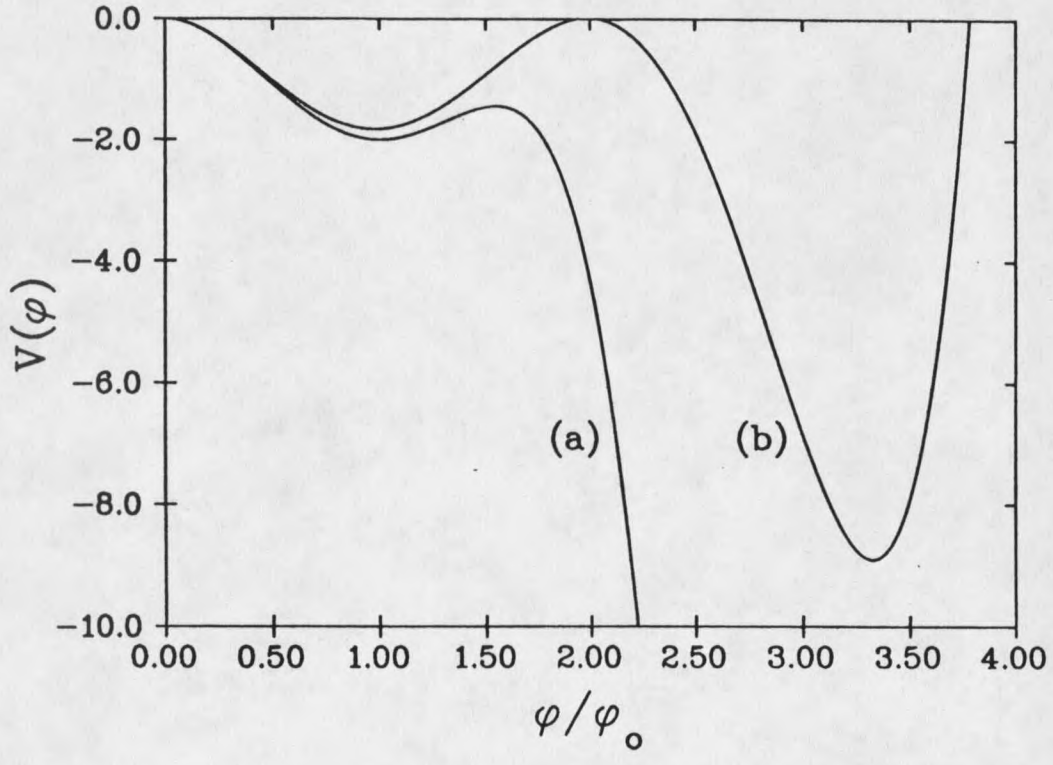

Figure 35 The one-loop, renormalized, effective potential for the Standard Model; for two values of the potential parameter, Ξ. Positive semi-definite values of Ξ result in bounded potentials; therefore Ξ=0 corresponds to the last bounded potential, and Ξ=-1 is an example of an unbounded potential.

The set of unbounded one-loop potentials which become bounded at the two-loop level have an additional vacuum state lying beyond the vacuum state of the one-

loop potential. If the actual potential within the Standard Model is described by one of these new potentials then our current vacuum state would be a false-vacuum state, and unstable to quantum decay. Figure 36 illustrates a one-loop unbounded potential that becomes bounded at the two-loop level.

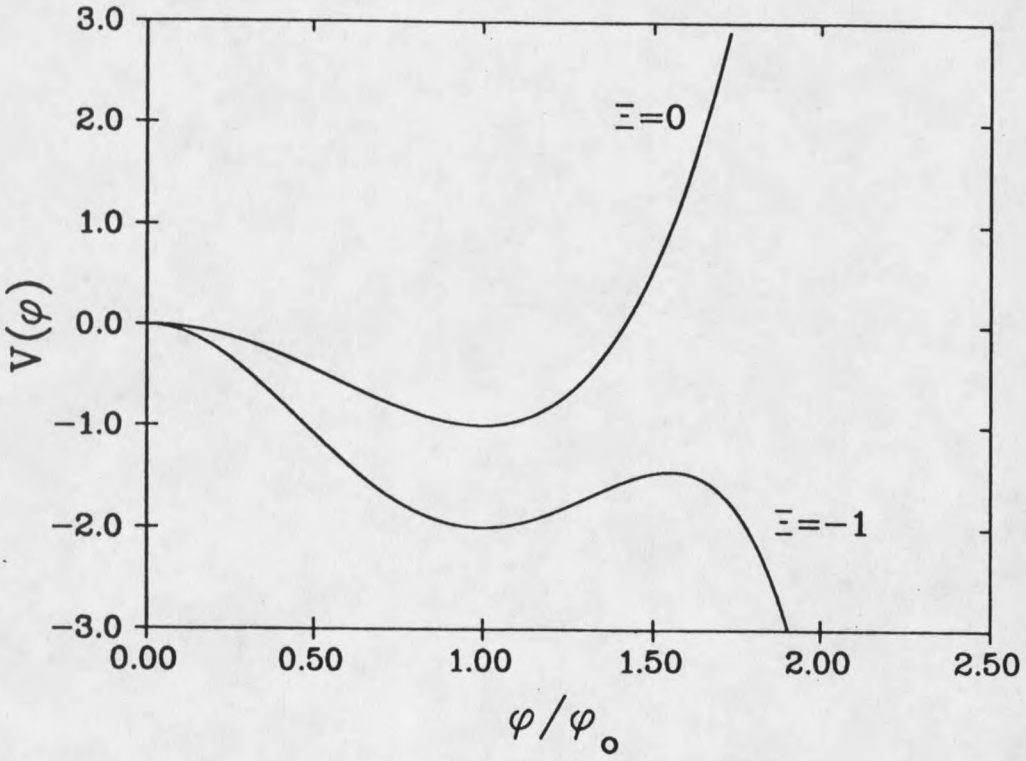

Figure 36 An unbounded one-loop potential, (a), becomes bounded at the two-loop level. Though the one-loop potential would be regarded as unphysical and forbidden, the two-loop potential is allowed. We also observe that the two-loop potential has a second vacuum state rendering the old vacuum state unstable to quantum decay.

We may place theoretical bounds upon the top-quark mass, within the two-loop analysis, as follows:

(1) If the top-quark is sufficiently massive then it will render the two-loop effective potential unbounded; we demand that the mass be insufficient for this to occur.

(2) There is a range of top-quark masses for which our present vacuum state is a false vacuum state, and is therefore unstable to quantum decay. The lifetime of the false-vacuum state will be a function of the two-loop effective potential which in turn is a function of the top-quark mass. We demand that the lifetime of the false-vacuum state be at least 10^{10} years; corresponding to the "age" of such a vacuum state.

Flores and Sher (1983) have placed a bound upon the top-quark mass based upon criterion (2); i.e., the top-quark mass may be sufficiently massive to make our vacuum state a false vacuum-state, but the lifetime of such a false-vacuum state must at least correspond to the age of the Universe (about 10^{10} years). Their calculation utilized an approximate form of the two-loop effective potential (using a renormalization group improved, one-loop, effective potential, with running coupling constants). The relationship between the effective potential and the lifetime of the false-vacuum state was obtained via the Coleman "thin-wall" approximation.

We may question the sensitivity of the bound on the top-quark mass to the use of the "thin-wall" approximation; as compared to a bound obtained from an exact calculation of the lifetime of the false-vacuum state. We may also ask whether possible astrophysical nucleation sites such as microscopic black-holes and boson stars could strengthen the bound on the top-quark mass. To correctly address these questions we would need the complete two-loop effective potential for the Higgs field, or at least a renormalization group improved one-loop potential. Instead of becoming model specific and involve ourselves with the complexities of the two-loop potential of the Standard Model we shall consider the above questions in a more generalized "toy" model, in the spirit of our calculations of Chapters 2,3 and 4.

The "toy" model shall have a potential with similar characteristics to the two-loop effective potential of the Standard Model. We shall consider bounds placed upon a hypothetical particle via the "thin-wall" approximation, in the situation where we are currently living in a false-vacuum state. The "thin-wall" bounds shall then be compared to the bounds obtained via an exact numerical evaluation of the lifetime of the false-vacuum state. Finally, we shall assume that the universe has "stellar" nucleation sites present, and we shall determine the bounds placed upon the hypothetical particle mass by possible induced false-vacuum decay via the "stellar" nucleation sites.

The Model

Consider the potential

$$U(\phi) = m_a^2 \phi^2 - m_a \phi^3 + \left\{ \frac{m_a^2 + m_c^2 - m_b^2}{m_a^2} \right\} \phi^4 \quad , \tag{5.20}$$

where ϕ will represent our Higgs field, m_a = mass of Higgs field, m_b=mass of fermionic field (which we shall place a bound on), and m_c=mass of bosonic field. 'm_c' shall be set to a constant value; and to define a scale within the model we shall set m_c to 100 GeV.

We note that our potential is merely the ϕ^{2-3-4} potential used in the analysis of Chapters 2 and 3, but with a different set of parameters. The potential may be written in a dimensionless form as follows

$$\tilde{U}(\phi) = \psi^2 - \psi^3 + \left\{ \frac{m_a^2 + m_c^2 - m_b^2}{m_a^2} \right\} \psi^4 \quad , \tag{5.21}$$

where $\psi = m^{-1}\phi$, and $\tilde{U} = m^{-4}\, U$.

The requirement that this potential be bounded is given by

$$m_a^2 + m_c^2 - m_b^2 > 0 \quad , \tag{5.22}$$

i.e., the coefficient of the quartic term in the potential must be greater than zero. Eq. (5.22) implies that

$$m_b < [\, m_a^2 + m_c^2 \,]^{1/2} \quad . \tag{5.23}$$

This is our first constraint on the mass of the 'b'-particle; the constraint is a function of the 'a'-particle mass. This is analogous to the constraint placed upon the top-quark mass, which is a function of the unknown Higgs particle mass.

We also note that if

$$m_b < [\, \tfrac{3}{4} m_a^2 + m_c^2 \,]^{1/2} \quad , \tag{5.24}$$

then our current vacuum state, located at $\psi = 0$, becomes the true vacuum state (i.e., in this case either the second vacuum state has a greater energy than our vacuum state or, for sufficiently small m_b, there is not even a second vacuum state.)

When m_b lies in the range

$$[\, \tfrac{3}{4} m_a^2 + m_c^2 \,]^{1/2} < m_b < [\, m_a^2 + m_c^2 \,]^{1/2} \quad , \tag{5.25}$$

then our current vacuum state, located at $\psi=0$, is a false vacuum state (i.e., there is a vacuum state with lower energy lying beyond our present vacuum state). The false-vacuum will be separated from the true vacuum via a potential barrier and therefore the false-vacuum decay will proceed via a first order phase transition. Figure 37 illustrates the three "regions" for the potential, for a range of m_b and m_a. In region (a) our current vacuum state, located at $\phi=0$, is a true-vacuum state, and therefore has absolute stability (m_a and m_b in this region are allowed). In region (b) our current vacuum state is a false-vacuum (i.e., there is a deeper lying vacuum state beyond our present vacuum state). Values of m_a and m_b in this region may be allowed, as long as the corresponding potential has a false-vacuum state with a lifetime greater than 10^{10} years. In region (c) the potential is unbounded; therefore, values of m_a and m_b in this region are not allowed.

We may relate the potential coefficients of Eq.5.21 to those of the analysis of Chapter 2 (i.e., $\tilde{\varepsilon}$ and ψ_+) as follows:

$$\text{with} \quad \lambda = \left\{ \frac{m_a^2 + m_c^2 - m_b^2}{m_a^2} \right\} \quad , \tag{5.26}$$

we have

$$\psi_+ = \frac{3}{8\lambda} + \frac{1}{8\lambda} [\, 9 - 32\,\lambda \,]^{1/2} \quad , \tag{5.27}$$

and

$$\tilde{\varepsilon} = -\,\psi_+^2 [\, \lambda\,\psi_+^2 - \psi_+ + 1 \,] \quad . \tag{5.28}$$

The "thin-wall" Euclidean action for the nucleating bubble may be expressed in terms of the $\tilde{\varepsilon}$ and ψ_+ parameters by

$$B_{tw} = \frac{\pi^2 \psi_+^8}{24 \tilde{\varepsilon}^3} \quad . \tag{5.29}$$

The exact Euclidean action for the nucleating bubble differs from the "thin-wall" value as explained in Chapter 2.

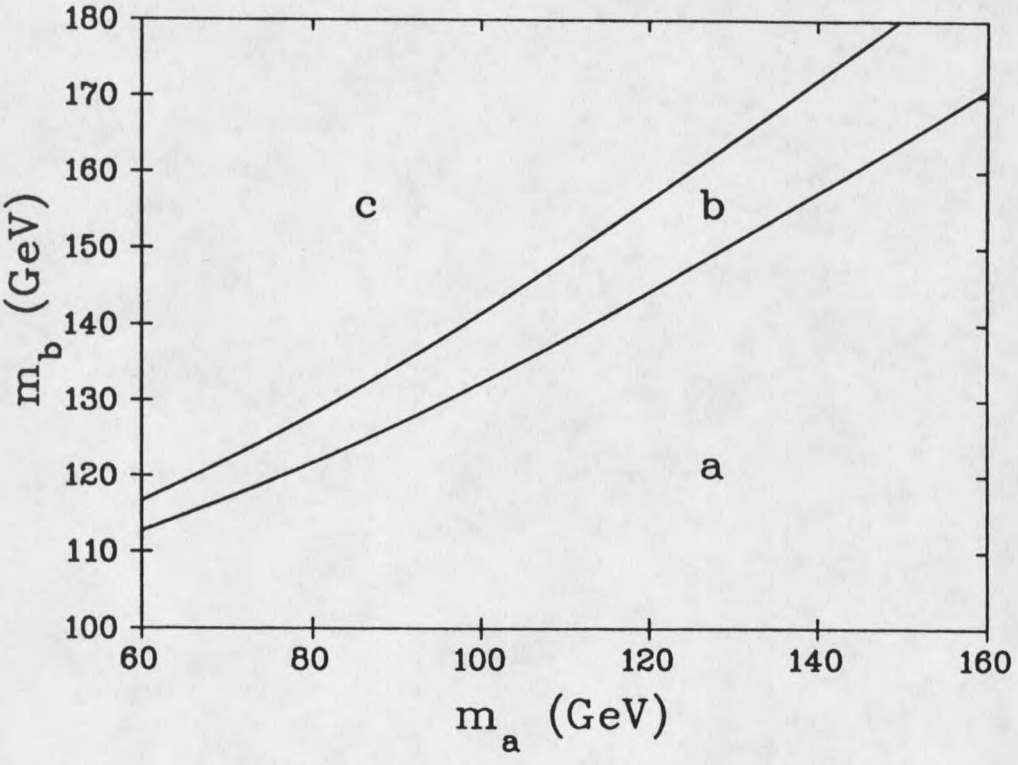

Figure 37 The three distinct "regions" in the parameter space of the potential given by Eq. 5.20. In region (a) our current vacuum state, located at ϕ=0, is a true-vacuum state; and therefore has absolute stability (m_a and m_b in this region are allowed). In region (b) our current vacuum state is a false-vacuum (i.e., there is a deeper lying vacuum state beyond our present vacuum state). Values of m_a and m_b in this region may be allowed, as long as the corresponding potential has a false-vacuum state with a lifetime greater than 10^{10} years. In region (c) the potential is unbounded; therefore, values of m_a and m_b in this region are not allowed.

The characteristic time associated with the nucleation of an O(4)-symmetric bubble is given by

$$T_4 = V^{-1}\, m^{-4} \exp[B_{o(4)}] \quad , \tag{5.30}$$

where V is the three-volume in which the bubble nucleation may occur, 'm' is the mass scale of the field undergoing the false-vacuum decay, and $B_{o(4)}$ is the Euclidean action of the O(4)-symmetric nucleating bubble. If we set VT_4 equal to the four-volume associated with our past-lightcone then we may obtain a critical value for $B_{o(4)}$. The Euclidean action for an O(4)-symmetric nucleating bubble associated with a given potential must be larger than this critical value so that the false-vacuum state would have survived to this present time.

The critical value for B_{o4} may be expressed as

$$B_{o4}^{crit} = 4\, \mathrm{Log}_e\, [Lm] \quad , \tag{5.31}$$

where L is the characteristic length-scale associated with our past lightcone (i.e., approximately 10^{10} years or 10^{28} cm). For our model, the term 'm' in Eq. (5.31) would be replaced by 'm_a', which is the characteristic length scale of the (Higgs) field that is undergoing the phase transition.

A new bound, within the framework of the "thin-wall" approximation, may therefore be placed upon the mass of the 'b'-particle from the constraint

$$B_{o4}^{tw} > B_{o4}^{crit} \quad . \tag{5.32}$$

Of course B_{o4}^{tw} is only an approximation to the exact Euclidean action associated with the O(4)-symmetric decay. The actual bound to the 'b'-particle mass, associated with O(4)-symmetric false-vacuum decay, is based upon the constraint,

$$B_{o4}^{exact} > B_{o4}^{crit} \qquad (5.33)$$

Figure 38 shows both the exact and the "thin-wall" bound placed on m_b associated with the lifetime of a false-vacuum state to decay via O(4)-symmetric bubble nucleation. The lower dashed curve shows the bound placed on m_b from the "thin-wall" approximation, and the upper dashed curve shows the exact bound placed on m_b. Values of m_b below the respective dashed curve, but still lying in the false vacuum region (i.e., above the lower solid line), are allowed because the lifetime of the corresponding false-vacuum is greater than the age of the Universe.

The bound from the "thin-wall" approximation is not vastly different to the exact bound. The reason for this is that with 'm_a' in the 100 GeV mass range the value of B_{o4}^{crit} is approximately 400. Within the $\phi^{2\text{-}3\text{-}4}$ model, values of the Euclidean action in the region of 400 place us in the regime where the "thin-wall" approximation is reasonably good. Thus we a have relatively good agreement between the "thin-wall" bound and the exact bound on m_b.

Finally, we shall make an estimate of the importance of possible astrophysical nucleation sites for false-vacuum decay. This is achieved via a bound on m_b associated with induced false-vacuum decay via the astrophysical nucleation sites.

The characteristic time associated with the nucleation of bubble around a nucleation site is given by,

$$T_3 = m^{-1} \exp(B_3) \quad , \tag{5.34}$$

where B_3 is the Euclidean action for a bubble nucleating around the nucleation site, and 'm' is the characteristic length scale of the field undergoing the phase transition. We shall make the assumption that the Universe is empty, apart from N similar nucleation sites. By similar, we shall mean that the same Euclidean action is associated with the nucleation of a bubble around each of the nucleation sites.

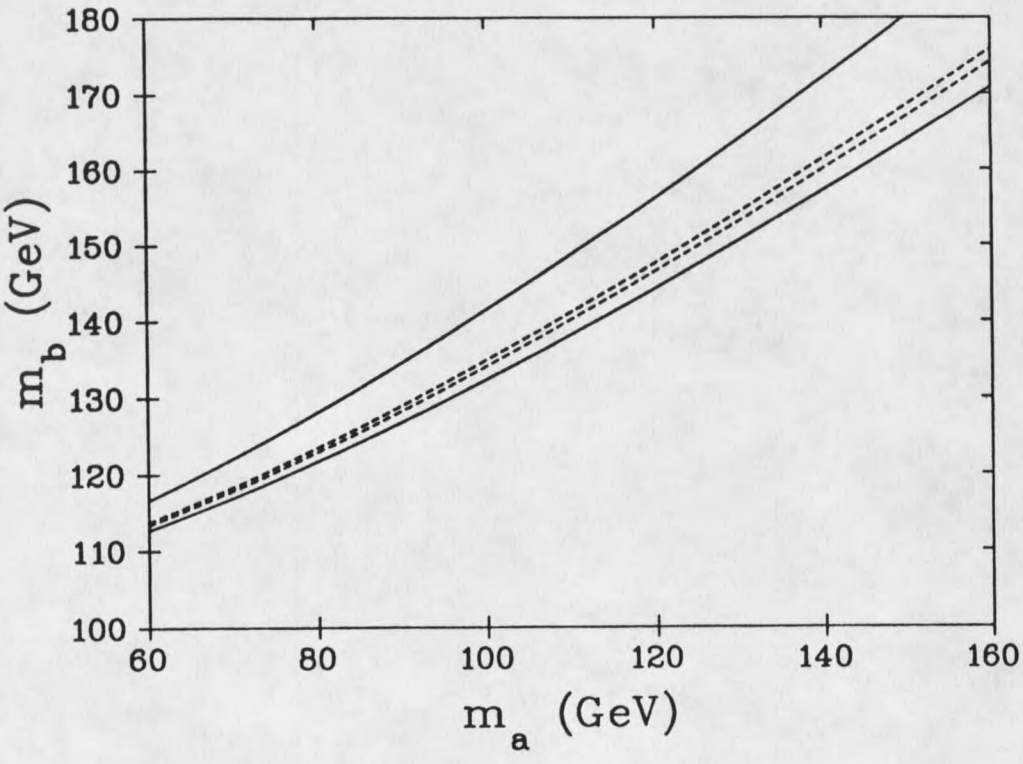

Figure 38 The exact bound and the "thin-wall" bound placed on m_b associated with the lifetime of a false-vacuum state to decay via O(4)-symmetric bubble nucleation. The upper dashed curve corresponds to the exact bound and the lower dashed curve corresponds to the "thin-wall" bound.

The time associated with the nucleation of a bubble around any of the nucleation sites is

$$T_{3,N} = (Nm)^{-1} \exp(B_3) \qquad (5.35)$$

There is a critical value for B_3 obtained by setting $T_{3,N}$ to the characteristic age of the Universe. Thus we will require B_3 to be greater than the corresponding critical value so that the false-vacuum would have survived to the present day.

The effect of a nucleation site upon the Euclidean action for a nucleating bubble may be characterized by a parameter α. This will represent the deficit between the O(4)-symmetric bubble Euclidean action (i.e., in the absence of a nucleation site) and the O(3)-symmetric bubble Euclidean action (i.e., in the presence of a nucleation site). We define α by,

$$B_3 = (1 - \alpha) B_4 \qquad (5.36)$$

The analysis of Chapter 4 suggests that values of α in the range of 0. 01 to 0. 05 are possible within the perturbative analysis. The analysis of Hiscock (1987) suggests that values of α up to 0. 25 are possible within the "thin-wall" approximation for black-hole nucleation sites; and the Mendell and Hiscock (1989) analysis suggests that even larger values of α may be possible within the "thin-wall" approximation for compact objects such as neutron stars.

In order to consider induced false-vacuum decay we need to know the number density spectrum of nucleation sites within the universe. We may, however, place an upper bound on m_b by assuming a state of "maximum efficiency" for nucleation sites within the Universe. A nucleating bubble associated with false-vacuum decay will have a characteristic size which will depend upon the "shape" of the Higgs field potential,

and therefore be a function of m_a and m_b. A nucleation site is most efficient (i.e., causes the largest reduction in the Euclidean action) when it is comparable in size to the nucleating bubble. Therefore, for the term "maximum efficiency", we shall mean that the entire mass density of the Universe will be attributed to nucleation sites which are of a characteristic size given by the size of the nucleating bubble. We attribute a nucleation efficiency parameter, α, to these nucleation sites.

The maximum allowed mass density of the Universe, within observational constraints, is $\rho_{max} \approx 10^{-28}$ g cm^{-3}. The most efficient nucleation site, as we have seen in Chapter 4, will have a characteristic size which is roughly the same as the size of the nucleating bubble. If we have a model for the nucleation site (e.g. , black-hole, boson star, etc.) then its mass will be determined once its "size" is known. We may, therefore, place a bound on the number density, n, of nucleation sites by

$$n \approx \frac{\rho_{max}}{M_{nuc.\ site}} \tag{5.37}$$

For example, if m_a is in the 100 GeV mass range, then $M_{nuc.\ site}$ is typical of the order of 10^{11} Kg for a "maximum efficiency" black hole or boson star. We shall crudely assume that N=nV, where V is our present horizon volume; this of course ignores the fact that we are living in an expanding Universe.

Figure 38 shows the bounds on m_b for several values of α. The solid line represents the exact O(4)-symmetric bound. We observe that α has to be at greater than about 0.5 for the nucleation sites dominate over the O(4)-symmetric decay, and hence place a stronger bound on m_b. Such a value of α would rule out the nucleation sites considered in the perturbative analysis of Chapter 4. We may similarly exclude black holes (within the "thin-wall approximation) as these typically result in values of α less

than 0.25. However, the compact objects considered in the analysis of Mendell and Hiscock (1989) were capable of producing values of α greater than 0.5.

Of course, in our Universe, not all of the mass is contained within "maximum efficiency" nucleation sites; also, the mass density of the Universe may quite easily be an order or magnitude, or more, smaller than ρ_{max}. Both of these would diminish the importance of nucleation sites to false-vacuum decay.

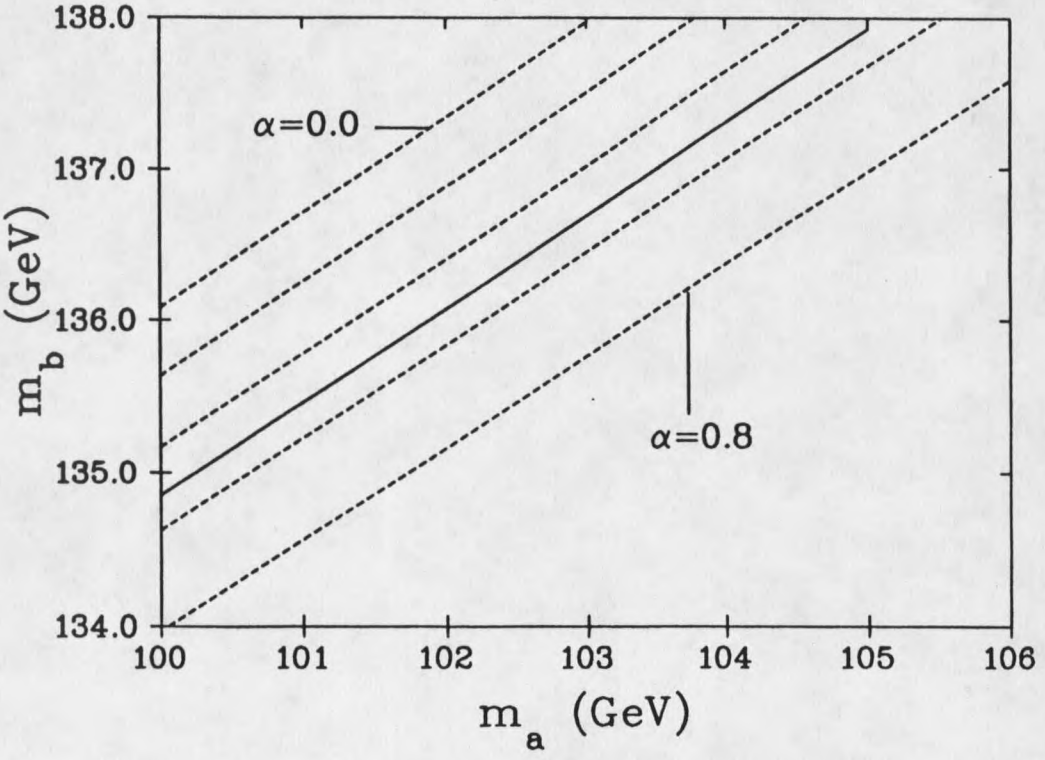

Figure 39 Bounds on m_b as a result of induced false-vacuum decay via possible astrophysical nucleation sites. α represents the nucleation efficiency of the nucleation sites and is defined by, $B_3 = (1-\alpha)\, B_4$. The dashed curves correspond (in sequence) to $\alpha = 0.0$, 0.2 , 0.4 , 0.6 , and 0.8. We observe that a value of α greater than about 0.5 is required for the induced vacuum decay to dominate over non-nucleated decay. Also, when this is the case, a stronger bound is obtained for m_b.

The conclusions of this section are actually quite insensitive to the model for the (Higgs) potential. This is because the results are really only functions of the four-volume associated with our past lightcone, the mass scale of the field undergoing the phase transition and the number density and efficiency of the nucleation sites. Thus it would not be unreasonable to make use of the "thin-wall" approximation to place bounds upon the top-quark mass based on the lifetime of possible false-vacuum states associated with the full two-loop potential of the GWS electroweak theory. It would also be reasonable to assume that the possible existence of suitable astrophysical nucleation sites (i.e., gravitationally compact objects with a radius in the 100 GeV range) will not strengthen the bounds upon the top-quark mass.

CHAPTER 6

CONCLUSIONS

The validity of the "thin-wall" approximation in most situations is questionable. In the absence of gravity we observe that the approximation scheme is at best a zeroth order approximation. The Euclidean action for a nucleating bubble given by the "thin-wall" approximation rapidly diverges from the exact Euclidean action as the energy density difference between the true and false-vacuum moves away from degeneracy.

A new approximation scheme is seen to considerably improve upon the results of the "thin-wall" approximation. The Euclidean action for the nucleating bubble obtained from the new approximation improves upon the "thin-wall" estimate by typically one to two orders of magnitude. The new approximation scheme is seen to be robust rather than model specific (i.e., the approximation scheme is not limited to specific field potentials). The new approximation is also well defined, unlike the "thin-wall" approximation; and requires about the same degree of calculation to obtain the Euclidean action as the "thin-wall" approximation.

In the presence of gravity the "thin-wall" approximation is again of limited validity. For the decay from de Sitter space to Minkowski space there is a transition from the Coleman-De Luccia "thin-wall" tunneling mode to the Hawking-Moss tunneling mode. This transition takes place as the mass of the field undergoing the transition is increased. The "thin-wall" approximation does not even hint at this transition in the tunneling mode.

Two symmetry transformations are presented; one associated with the $\phi^{2\text{-}3\text{-}4}$ potential and the other associated with the coupled Euclideanized scalar field and Einstein equations (independent of the functional form of the potential). These symmetries allow the results of the numerical analysis to be extended over a large range of the field potential parameter space without further calculation.

The "thin-wall" approximation predicts a forbidden region for the decay from Minkowski space to anti-de Sitter space. Associated with this decay is a critical mass, above which the false-vacuum decay from Minkowski space to anti-de Sitter space is forbidden. The "thin-wall" approximation is seen to give a good approximation for this critical mass, for field masses well below the Planck scale. When the approximation breaks down then it does so in such a way as to underestimate the critical mass, i.e., the "thin-wall" approximation overestimates the size of the forbidden region.

In a perturbative analysis, gravitationally compact objects are shown to be able to reduce the Euclidean action for a bubble of true-vacuum nucleating around them (i.e., *gravitationally compact objects may act as nucleation sites for first-order phase transitions within quantum fields*). This reduction in the Euclidean action is significant when the gravitationally compact object is comparable in size to the nucleating bubble. The maximum reduction occurs when the compact object has a radius which approximately half the radius of the nucleating bubble. Within the perturbative analysis, reductions in the Euclidean action of up to 5% are observed; as compared with the Euclidean action of the O(4)-symmetric nucleating bubble in a flat spacetime.

The importance of possible astrophysical nucleation sites such as microscopic black-holes and boson stars to cosmological false-vacuum phase transitions will depend upon their number density within the Universe. For phase transitions with an associated mass scale in the 100 GeV range, it appears that the number density of

possible nucleation sites is too small to have a significant effect on our present vacuum state (if our present vacuum happens to be a false-vacuum state). Nucleation sites would have to produce Euclidean action deficits of at least 50% to 60% (compared to the O(4)-symmetric nucleating bubble Euclidean actions) in order to start competing with non-induced vacuum decay. Such deficits are, by definition, outside the range of consideration of the perturbative analysis; and even push the bounds of O(3) -"thin-wall" models for nucleated false-vacuum decay, for which Euclidean action have been calculated to date.

The interior lightcone evolution of a bubble of true vacuum basically falls into two regimes. If the potential associated with the false-vacuum decay has nearly degenerate vacua then the "thin-wall" approximation will be valid. The scalar field at the center of a thin-walled nucleating bubble lies at (or very close to) the true-vacuum state. As a result there is no (or very little) interior lightcone evolution of the field. The scalar field at the center of a thick-wall bubble does not, however, reach the true-vacuum state. Thus there is an evolution of the field towards the true-vacuum state in the interior of the lightcone Such an evolution results in the damped oscillation of the field about the true-vacuum state to the interior of the light-cone.

In a cosmological setting, the oscillation of the Higgs field to the interior of the lightcone may result in particle creation and re-heating (via couplings to other quantum fields) in the lightcone interior. The degree of particle creation and re-heating will be very model dependent. However, the exact form of the Higgs potential, within a given unified field scenario, would allow for a determination of the bubble profile and hence an estimate of the degree of particle creation.

The bubble wall may also be a place for other interesting physics. Particle physics, utilizing a Feynman diagram approach (i.e., a perturbative expansion), requires the presence of a vacuum state to define a particle spectrum. To the outside of a "bubble" lies a well defined (false) vacuum state, and therefore, well defined "particle physics"; similarly for the inside of the bubble. However, there is no vacuum state, per se, in the bubble wall; this is because much of the bubble wall corresponds to the potential barrier in the Higgs field potential. Certain particle physics phenomenology is dependant upon the properties (e.g., symmetries) of the vacuum state. For example, the interior bubble vacuum state may result in CP-violation (Charge-Parity), while the exterior bubble vacuum state may not exhibit CP violation. However, the status of CP-violation in the bubble wall is, to some degree, indeterminate; CP-violation may very well be violated to a greater degree in the bubble wall than in the interior bubble vacuum. As a bubble-wall may lie to the past of our light-cone then any interesting physical effects associated with the bubble wall may have had an effect on our observable universe. A detailed study of the physics of the wall would therefore appear to be appropriate.

BIBLIOGRAPHY

Allen B. , Phys. Rev. D33, 3640, (1986)

Berezin V.A. , Kuzmin V.A. , and Tkachev I.I. , Phys. Rev. D43 , R3112 , (1991)

Birrell N.D. , and Davies P.C.W. , Quantum Fields in Curved Space , Cambridge University Press, (1982)

Buras A. , Phys. Rev. Lett. 46 , 1354 , (1981)

Callan C. G. , and Coleman S. , Phys. Rev. D16 , 1762 , (1977)

Coleman S. , Phys. Rev. D15 , 2929 , (1977)

Coleman S. , and De Luccia F. , Phys. Rev. D21 , 3305 , (1980)

Coleman S. , Glazer V. , and Martin A. , Commun. Math. Phys. 58 , 211 , (1978)

Dine M. , Huet P. , Singleton R. , and Susskin, L. , Phys. Lett B257 , 351 , (1991)

Duncan M.J. , Philippe R. , and Sher M. , Phys. Lett. B153, 165 , (1985)

Flores R. , and Sher M. , Phys. Rev. D27 , 1679 , (1983)

Glashow S.L. , Nucl. Phys. 22 , 597 , (1961)

Guth A.H. , Phys. Rev. D23 , 347 , (1981)

Hawking S.W. , and Moss I.G. , Phys. Lett. B110 , 35 , (1982)

Higgs P.W. , Phys. Rev. Lett. 12, 132, (1964)

Hiscock W.A. , Phys. Rev. D35 , 1161 , (1987)

Israel W. , Nuovo Cimento B44 , 1 , (1966) , and Nuovo Cimento B48 , 463 , (1967)

Jensen L.G. , and Steinhardt P.J. , Nucl. Phys. B237 , 176 , (1984)

Jensen L.G. , and Steinhardt P.J. , Nucl. Phys. B317 , 693 , (1989)

La D , Steinhardt P.J. , Phys. Rev. Lett. 62 , 376 , (1989)

Linde A.D. , Rep. Prog. Phys. , Vol. 42 , (1979)

Mahanthappa K.T. , and Sher M. , Phys. Rev. D22 , 1711 , (1980)

Mc Lerran L. , Shaposhnikov M. ,
Turok N. , and Voloshin M. , Phys. Lett. B256 , 451 , (1991)

Mendell G. , and Hiscock W.A. , Phys. Rev. D39 , 1537 , (1989)

Politzer H.D. , and Wolfram S. , Phys. Lett. B82 , 242 , (1976)

Press W.H., Flannery B.R., Teukolsky S.A., and Vetterling W.T. ,
Numerical Recipes in C , Cambridge University Press, (1988)

Salam A. , Elementary Particle Theory, Ed. N. Swartholm, p. 367,
(Almqvist and Wiksell, Stockholm, 1986)

Samuel D.A. , and Hiscock W.A. , Phys. Lett. B261 , 251 , (1991)(a)

Samuel D.A. , and Hiscock W.A. , Phys. Rev. D44 , 3052 , (1991)(b)

Seidel E. , and Suen Wai-Mo , Phys. Rev. D42 , 384 , (1990)

Shen T.C. , Phys. Rev. D37 , 3537 , (1988)

Wald R.M. , General Relativity, The University of Chicago Press, (1984)

Weinberg, S. , Phys. Rev. Lett. 19 , 1264 , (1967)

APPENDIX

NUMERICAL METHODS

The results in this dissertation have required the numerical solution of various differential equations (e.g. , the Euclideanized scalar field and Einstein equations). In this appendix an outline of the numerical methods adopted shall be reviewed, and a "source code primitive" shall be presented.

For our analysis of the O(4)-symmetric false vacuum decay with gravity, we are presented with the following set of differential equations:

$$\frac{d^2\psi}{d\xi^2} + \frac{3}{\rho}\frac{d\rho}{d\xi}\frac{d\psi}{d\xi} = \frac{d\tilde{U}}{d\psi} \qquad \text{A.1}$$

$$\left(\frac{d\rho}{d\xi}\right)^2 = 1 + \frac{8\pi}{3}\frac{m^2}{m_p{}^2}\rho^2\left[\frac{1}{2}\left(\frac{d\psi}{d\xi}\right)^2 - \tilde{U}\right] \qquad \text{A.2}$$

We may re-express the above equations in terms of a set of coupled first order equations as follows:

$$\frac{d\psi}{d\xi} = \chi \qquad \text{A.3}$$

$$\frac{d\chi}{d\xi} = \frac{d\tilde{U}}{d\psi} - \frac{3}{\rho}\frac{d\rho}{d\xi}\chi \qquad \text{A.4}$$

$$\left[\frac{d\rho}{d\xi}\right] = \left\{ 1 + \frac{8\pi}{3}\frac{m^2}{m_p{}^2}\rho^2\left[\frac{1}{2}\left[\frac{d\psi}{d\xi}\right]^2 - \tilde{U} \right]\right\}^{1/2} \qquad \text{A.5}$$

This procedure has required the inclusion of only one extra "dummy" variable, namely χ , which corresponds to the field derivative with respect to the O(4)-radial variable.

The analysis of false vacuum decay in the absence of gravity requires a simple specialization of these equations, in which we set the field mass "m" to zero (equivalent to letting the Planck mass, in the Einstein equation, go to infinity). In this situation the solution to the Einstein equation is trivial and we only require the numerical solution to the Euclideanized scalar field equation.

The three equations (A.3,4,5) , each require a starting condition at ξ=0 in order to be integrated. For Eqs. (A.4) and (A.5) the starting conditions are known in advance, these being, χ=0 and ρ=0 at ξ=0. If we had the starting value for ψ (i.e., for Eq. (A.3)) , at ξ=0, then the nucleating bubble profile would be defined.

Consider the decay from Minkowski to anti-de Sitter space. If we had the starting value for ψ then integration of the differential equations would eventually leave us with ψ=0 and χ=0 as $\xi \to \infty$; if the false vacuum state were located at ψ=0, as it is in our analysis of Chapters 2 and 3. It is instructive at this point to make use of the analogy, as described in Chapters 2 and 3, of the particle moving in the inverted potential. If we guess an initial value for ψ that is "too small", then the particle will have insufficient energy to overcome the "friction" and hence will not reach ψ=0. We may "detect" this scenario in the integration of the differential equations via the occurrence of a positive value for χ; if we had the correct starting value for ψ then χ

would be negative semi-definite for all values of $\xi>0$. If we guess an initial value for ψ that is "too high" (remembering that we must not choose a starting value that is beyond the true vacuum value), then the "friction" is insufficient to overcome the excess energy and the particle will "overshoot". This scenario may be "detected" by a negative value for ψ, remembering that the false vacuum is located at $\psi=0$, and the true vacuum is at $\psi>0$. Thus we may "home in" on the starting value for ψ via a method of : (1) guess a starting value for ψ, (2) integrate differential equations until either $\chi>0$ or $\psi<0$, (3) update the starting value for ψ with the knowledge that the previous value resulted in either an "undershoot" or "overshoot"; repeat this procedure. Utilizing a method of bisection, this procedure will improve the accuracy of the known starting value for ψ by a factor of two for each iterative loop; thus if we require $\psi_{initial}$ to be known to m significant digits then it is necessary to perform the iteration $[\, m / (\log_{10} 2) \,]$ times.

Even if $\psi_{initial}$ were known to arbitrary precision (via some analytical method for example), it would still not be possible to numerically integrate the differential equations out to $\xi=\infty$; unless of course we introduce some "compactified" O(4)-radial variable, e.g. , $\Xi=\tan^{-1}\xi$. We are therefore going to have some maximum value for ξ associated with the integration of the differential equations. As the integration of the differential equations will always fail in practice via an "overshoot" or "undershoot" then we must decide upon a method to bring the integration of the differential equations to an end, after the desired degree of accuracy has been obtained for $\psi_{initial}$. This decision is to some extent arbitrary; we shall therefore let the terminating scenario be one of an overshoot, and the maximum value for ξ shall be that corresponding to the location where $\psi=0$.

The integration of the differential equations proceeds via the fourth-order Runge-Kutta, adaptive-step-size, method. An error estimate is obtained through the

propagation of the dependent variables over a step size $\delta\xi$ and then again utilizing two steps of size $\delta\xi/2$; as these two sets of propagations will usually result in different increments in the dependent variables then we may calculate an estimate of the fractional error in the increment of a dependent variable as a result of the propagation over the interval $\delta\xi$. If this error does not satisfy the error per step constraint then a propagation over a smaller step size is attempted in order to meet the error per step constraint.

The integrated solutions are stored in an array at regular, uniform intervals in ξ (i.e., if the array size is given by 'n' and the maximum value for $\xi=\xi_{max}$ then the dependent variables ψ and ρ are stored at intervals of ξ_{max} / n).

For the decay from de Sitter to Minkowski space the numerical analysis will proceed in a similar manner, but with a few differences. We now have to integrate across the de Sitter horizon, or more precisely, across the "equator" in the Euclideanized de Sitter spacetime. This "equator" is defined by $(d\rho/d\xi)=0$ (i.e., the R.H.S. of equation (A.5) vanishes); beyond the "equator" the form of equation (A.5) is changed slightly, now being

$$\left(\frac{d\rho}{d\xi}\right) = -\left\{ 1 + \frac{8\pi}{3}\frac{m^2}{m_p{}^2}\rho^2\left[\frac{1}{2}\left(\frac{d\psi}{d\xi}\right)^2 - \tilde{U} \right] \right\}^{1/2} \qquad \text{A.6}$$

This equation implies that ρ will now decrease with an increase in ξ, this continues until we "close the sphere" , (i.e. , until ρ reaches zero); this will automatically define a ξ_{max} within the spacetime. Care has to be taken during the propagation of the dependent variables across the horizon.

We are also faced with a different terminating boundary condition for the decay from de Sitter to Minkowski space. The scenario now requires χ=0 both at the "north pole" (i.e., where ξ=0 and ρ=0) and at the "south pole" (i.e., where $\xi=\xi_{max}$ and ρ=0). This is necessary in order to prevent singular behavior in equation (A.4). However, we may use an adapted method of "overshoot" and "undershoot", in a similar manner to the analysis for the decay from Minkowski to anti-de Sitter space, in order to determine the starting value for ψ.

The calculation of the Euclidean action for the nucleating bubble utilizes the stored values of $\psi(\xi)$, and is estimated via the integral

$$S_E = -2\pi^2 \int_0^{\xi_{max}} \rho^3 \tilde{U}\, d\xi \qquad \text{A.7}$$

The integration is performed via an extended Simpson's rule which has an error that scales according to $(1/n^4)$, where n is the array size for the stored ψ values.

The array data $\psi(\xi)$ and $\chi(\xi)$ provide the starting point for the O(3)-analysis of the effect of a gravitationally compact object acting as nucleation site. In this analysis we adopt a perturbative approach, starting with the O(4)-symmetric nucleating bubble in the absence of gravity (i.e., $m_p \to \infty$ in the O(4)-analysis), and place this into the fixed background spacetime of a "star". Maintaining O(3)-symmetry, the O(4)-bubble is "prolated and oblated" until it satisfies the constraint of having zero energy and is an extremum of the Euclidean action.

The following pages provide a source code primitive, in the C language, for the analysis of the O(4)-symmetric false vacuum decay from Minkowski to anti-de Sitter space. The computer code for the analysis of the false vacuum decay from de Sitter to

Minkowski space and the O(3)-symmetric decay in a fixed "star" background are obtained from modifications of, and extensions to, this code.

```
/*****************************************************************************
```

Numerical analysis of bubble nucleation processes for first-order phase transitions within quantum scalar fields.

Computer code written in 'C'

```
*****************************************************************************/
```

Relationship between program variables and thesis notation :

epsilon_tilda = $\tilde{\varepsilon}$ sigma = σ ksi = ξ psi_plus = ψ_+

omega = ω rho = ρ field_mass = m

```
#include <math.h>
#include <stdio.h>
#include <conio.h>
```

Direct pre-processor to include standard libraries for math functions and input / output routines.

```
double pot ( double sigma,
             double omega,
             double psi_plus );

double dpot ( double sigma,
              double omega,
              double psi_plus );
```

Functions pot() and dpot() return the value of the field potential and potential derivative respectively.

```
double f1 ( double chi  );

double f2 ( double ksi,
            double chi,
            double sigma,
            double omega,
            double psi_plus,
            double field_mass,
            double rho );

double f3( double chi,
           double sigma,
           double omega,
           double psi_plus,
           double field_mass,
           double rho );
```

Functions f1() , f2() and f3() are Runge-Kutta, fourth order, single step propagation functions.

Representing:

f1: $\frac{d\phi}{d\xi} = \chi$

f2: $\frac{d\chi}{d\xi} = \frac{dU}{d\phi} - \frac{3}{\rho}\frac{d\rho}{d\xi}\chi$

f3: $\frac{d\rho}{d\xi} = \left[1 + \frac{8\pi m^2}{3 m_p^2} \left(\frac{1}{2}\chi^2 + U \right) \rho^2 \psi_+^2 \right]^{1/2}$

```
double sigma_initial_value (double omega,
                            double psi_plus,
                            double field_mass,
                            double bubble_info[]
                            );
```

Function sigma_initial_value() returns the necessary starting value for sigma at ksi=0. Thus after a call to this function all of the boundary conditions required to solve the differential equations are known.

```
double o4_euc_action (double sigma_data[],
                      double chi_data[],
                      double ksi_max ,
                      double omega,
                      double psi_plus );
```

Function o4_euc_action() returns the value of the Euclidean action for the O(4)-symmetric nucleating bubble.

Where:

$$S_E = -2\pi^2 \int \rho^3 \tilde{U}\, d\xi$$

```
double o4_integrand( int integrand_count,
                     double sigma_data[],
                     double rho_data[],
                     double omega,
                     double psi_plus );
```

Function o4_integrand() returns the integrand for the o(4)-symmetric Euclidean action integral.

```
void rk ( double ksi,
          double chi,
          double sigma,
          double rho,
          double omega,
          double psi_plus,
          double field_mass,
          double d_ksi,
          double inc[] );
```

Function rk() is a fourth-order, Runge-Kutta, single step propagation routine. Increments in the sigma, chi and rho variables are returned in the inc[] array; where the step size is set by the d_ksi variable.

```
void bubble_profile ( double omega,
                      double psi_plus,
                      double field_mass,
                      double sigma_ini,
                      double bubble_ksi_max,
                      double sigma_array[],
                      double chi_array[],
                      double rho_array[] );
```

Function bubble_profile integrates the differential equations (the boundary conditions and starting conditions are all known at this stage). The function returns the bubble profile sigma(ksi), chi(ksi) and rho(ksi) in three data arrays... sigma_array[], chi_array[] and rho_array[].

```
#define num_data_points 101
#define error_per_step 1e-8
#define iterations_required 30
#define pi 3.1415926535898
```

num_data_points = number of data points to be used in arrays for bubble profile storage.
error_per_step = maximun allowed error in a single step of fourth-order, Runge-Kutta, propagation.
iterations_required = number of trial 'shoots' of the differential eqs. in order to determine sigma_initial.

```
main()
{

 double  epsilon_tilda,          psi_plus,                 omega,
         field_mass,             sigma_initial,            o4_action,
         bubble_ksi_size,        bubble_ksi_max ,          bubble_info[2],
         sigma[num_data_points], chi[num_data_points],     rho[num_data_points];

 psi_plus = 1.0;

 epsilon_tilda=.550;

 omega = epsilon_tilda / pow( psi_plus , 2 );

 field_mass=1.0;


 sigma_initial = sigma_initial_value ( omega,      psi_plus,      field_mass,     bubble_info );

 bubble_ksi_size = bubble_info[0];
 bubble_ksi_max = bubble_info[1];

 bubble_profile( omega,                psi_plus,      field_mass,     sigma_initial,
                 bubble_ksi_max,       sigma,         chi,            rho );


o4_action = o4_euc_action( sigma,              chi,          rho,
                           bubble_ksi_max,     omega,        psi_plus );

/**********   OUTPUT ROUTINE ( e.g., GRAPHICS ) FOR DATA SHOULD GO HERE.   *******/

  return(0);

}
```

Set initial data

```
/*****************************************************************************
                    Function to return value of potential
*****************************************************************************/

double pot ( double sigma,
             double omega,
             double psi_plus
             )

{

 double potential_value;

 potential_value = ( pow(sigma,2)

                   - ( 2 + 4 * omega ) * pow( sigma , 3 )

                   + ( 1 + 3 * omega ) * pow( sigma , 4 )

                   ) * pow( psi_plus , 2 );

 return ( potential_value );

}

/*****************************************************************************
                    Function to return derivative of potential
*****************************************************************************/

double dpot ( double sigma,
              double omega,
              double psi_plus
              )

{

 double pot_deriv_value;

 pot_deriv_value = ( 2 * sigma

                   - ( 6 + 12 * omega ) * pow( sigma , 2 )

                   + ( 4 + 12 * omega ) * pow( sigma , 3 )

                  ) * pow( psi_plus , 2 );

 return ( pot_deriv_value );

}
```

Potential :

$$\tilde{U} = (\sigma^2 - 2 (1+2\omega) \sigma^3 + (1 + 3\omega) \sigma^4) \psi_+^2$$

Potential derivative:

$$\frac{d\tilde{U}}{d\sigma} = (2\sigma - 6(1 + 2\omega) \sigma^2 + 4(1 + 3\omega) \sigma^3) \psi_+^2$$

```
/*****************************************************************************
                Function to return Runge-Kutta propagation function f1
*****************************************************************************/

double f1 ( double chi )

{

return ( chi );

}
```

$$f1: \quad \frac{d\sigma}{d\xi} = \chi$$

```
/*****************************************************************************
        Function to return Runge-Kutta propagation function f2
*****************************************************************************/

double f2 ( double ksi,
            double chi,
            double sigma,
            double omega,
            double psi_plus,
            double field_mass,
            double rho )

{

 double pot_deriv,
        friction;

 pot_deriv = dpot ( sigma,
                    omega,
                    psi_plus );

 if ( rho == 0 ) return ( pot_deriv / 4 ) ;

 else  { friction = f3 ( chi,
                         sigma,
                         omega,
                         psi_plus,
                         field_mass,
                         rho );

         return ( pot_deriv - 3 * friction * chi / rho );
       };
}
```

$$f2: \quad \frac{d\chi}{d\xi} = \frac{d\tilde{U}}{d\sigma} - \frac{3}{\rho}\frac{d\rho}{d\xi}\chi$$

```
/*****************************************************************************
                Function to return Runge-Kutta propagation function f3
*****************************************************************************/

double f3 ( double chi,
            double sigma,
            double omega,
            double psi_plus,
            double field_mass,
            double rho )
```

$$f3: \quad \frac{d\rho}{d\xi} = \left(1 + \frac{8\pi m^2}{3 m_p^2} \left(\frac{1}{2}\chi^2 + U \right) \rho^2 \psi_+^2 \right)^{1/2}$$

```
{

 double potential,
        arg;

 potential = pot ( sigma,
                   omega,
                  psi_plus );

 arg = 1 + ( ( 8 * pi / 3 )

           * pow( field_mass , 2 )

           * pow( rho , 2 )

           * pow( psi_plus , 2 )

           * ( 0.5 * pow ( chi , 2 ) - potential ) );


 return ( sqrt( arg ) );

}


/*****************************************************************************
                              Runge-Kutta increment routine
                              Changes external variables...   sig_inc
                                                              chi_inc
*****************************************************************************/


void rk ( double ksi,
          double chi,
          double sigma,
          double rho,
          double omega,
```

```
        double psi_plus,
        double field_mass,
        double d_ksi,
        double increment[] )

{

double a[4],
       b[4],
       c[4],
       sig_temp,
       chi_temp,
       ksi_temp,
       rho_temp;

a[0] = f1( chi ) * d_ksi;

b[0] = f2( ksi,          chi,          sigma,          omega,
           psi_plus,     field_mass,   rho) * d_ksi;

c[0] = f3( chi,          sigma,        omega,          psi_plus,
           field_mass,   rho) * d_ksi;

  sig_temp = sigma + a[0] / 2;

  chi_temp = chi + b[0] / 2;

  ksi_temp = ksi + d_ksi / 2;

  rho_temp = rho + c[0] /2;


a[1] = f1( chi_temp ) * d_ksi;

b[1] = f2( ksi_temp,     chi_temp,     sig_temp,       omega,
           psi_plus,     field_mass,   rho_temp) * d_ksi;

c[1] = f3( chi_temp,     sig_temp,     omega,          psi_plus,
           field_mass,   rho_temp ) * d_ksi;

 sig_temp = sigma + a[1] / 2;

 chi_temp = chi + b[1] / 2;

 rho_temp = rho + c[1] /2;


a[2] = f1( chi_temp ) * d_ksi;
```

```
b[2] = f2( ksi_temp,        chi_temp,       sig_temp,       omega,
           psi_plus,        field_mass,     rho_temp ) * d_ksi;

c[2] = f3( chi_temp,        sig_temp,       omega,          psi_plus,
           field_mass,      rho_temp ) * d_ksi;

  sig_temp = sigma + a[2];

  chi_temp = chi + b[2];

  rho_temp = rho + c[2];

  ksi_temp = ksi + d_ksi;


a[3] = f1( chi_temp ) * d_ksi;

b[3] = f2( ksi_temp,        chi_temp,       sig_temp,       omega,
           psi_plus,        field_mass,     rho_temp ) * d_ksi;

c[3] = f3( chi_temp,        sig_temp,       omega,          psi_plus,
           field_mass,      rho_temp ) * d_ksi;


 increment[0] = ( a[0] + 2 * a[1] + 2 * a[2] + a[3] ) / 6;

 increment[1] = ( b[0] + 2 * b[1] + 2 * b[2] + b[3] ) / 6;

 increment[2] = ( c[0] + 2 * c[1] + 2 * c[2] + c[3] ) / 6;

}

/*****************************************************************************
                Routine to find starting value of sigma for nucleating bubble
*****************************************************************************/

double sigma_initial_value ( double omega,
                             double psi_plus,
                             double field_mass,
                             double bubble_data[]
                             )

{

 int number_iterations = 0,
     size_flag = 0;
```

```
double sig_max,      sig_min,      sig_ini,      sigma,
       ksi,          chi,          rho,          d_ksi,
       sig_error,    chi_error,    rho_error,    error_estimate,
       chi_inc[3],   sig_inc[3],   rho_inc[3],   increment[3];

sig_max = 1.0;

sig_min = 1 / ( 6 * omega + 2 );

sig_ini = ( sig_max + sig_min ) / 2;


do {
    ksi = 0.0;

    chi = 0.0;

    rho = 0.0;

    d_ksi = 0.001;

    sigma = sig_ini;


  while ( sigma > 0 && chi <= 0 )
   {
    do {

      rk( ksi,          chi,          sigma,
          rho,          omega,        psi_plus,
          field_mass,   d_ksi,        increment);

      sig_inc[0] = increment[0];

      chi_inc[0] = increment[1];

      rho_inc[0] = increment[2];


      rk( ksi,          chi,          sigma,
          rho,          omega,        psi_plus,
          field_mass,   d_ksi / 2,    increment);


      sig_inc[1] = increment[0];

      chi_inc[1] = increment[1];

      rho_inc[1] = increment[2];
```

```
rk( ksi+d_ksi/2,        chi + chi_inc[1],       sigma + sig_inc[1],
    rho + rho_inc[1],   omega,                  psi_plus,
    field_mass,         d_ksi / 2,              increment);

sig_inc[2] = increment[0];

chi_inc[2] = increment[1];

rho_inc[2] = increment[2];


if( sigma != 0 )

   sig_error = fabs( ( sig_inc[0] - sig_inc[1] - sig_inc[2] ) / sigma );

else sig_error = 0;


 if( chi != 0 )

   chi_error = fabs( ( chi_inc[0] - chi_inc[1] - chi_inc[2] ) / chi );

else chi_error = 0;


 if( rho != 0 )

   rho_error = fabs( ( rho_inc[0] - rho_inc[1] - rho_inc[2] ) / rho );

else rho_error = 0;


error_estimate = sqrt( pow(sig_error , 2) + pow(chi_error , 2) + pow(rho_error , 2) );


  d_ksi = d_ksi / 2;

} while( error_estimate > error_per_step );


d_ksi = d_ksi * 2;

sigma = sigma + sig_inc[0];

chi = chi + chi_inc[0];

rho = rho + rho_inc[0];

ksi = ksi + d_ksi;
```

```
  if ( ( sigma <= sig_ini/2 ) && ( size_flag==0 ) )
    {
     bubble_data[0] = ksi;

     size_flag = 1;
    };

   if ( error_estimate < 0.1 * error_per_step ) { d_ksi = d_ksi * 2;};

  }


 number_iterations = number_iterations + 1;


 if( ( sigma < 0 && chi < 0 )   &&   ( number_iterations != iterations_required ) )
   {
    sig_max = sig_ini;

    sig_ini = ( sig_max + sig_min ) / 2;
    };

 if( sigma > 0 && chi > 0 )
   {
    sig_min = sig_ini;

    sig_ini = ( sig_max + sig_min ) / 2;
    };


 if( ( number_iterations == iterations_required ) && ( sigma > 0 ) )
   {
    number_iterations = iterations_required - 1;
    };

} while( number_iterations < iterations_required );


if ( error_estimate < 0.1 * error_per_step ) { d_ksi = d_ksi * 2; };


bubble_data[1] = ksi-d_ksi / 2;


return ( sig_ini );

}
```

```
/*****************************************************************************
                    Routine to set up data array to store bubble profile
*****************************************************************************/

void bubble_profile ( double omega,                 double psi_plus,
                      double field_mass,            double sig_ini,
                      double bubble_ksi_max,        double sigma_array[],
                      double chi_array[],           double rho_array[] )


{

 double  sigma,                 ksi,                chi,
         rho,                   d_ksi,              ksi_interval,
         ksi_store_value,       sig_error,          chi_error,
         rho_error,             error_estimate,     chi_inc[3],
         sig_inc[3],            rho_inc[3],         increment[3];

 int counter = 1;


 ksi = 0;

 chi = 0;

 rho = 0;

 d_ksi = 0.001;

 sigma = sig_ini;

 ksi_interval = bubble_ksi_max / ( num_data_points - 1 );

 ksi_store_value = ksi_interval;

 sigma_array[0] = sig_ini;

 chi_array[0] = chi;

 rho_array[0] = rho;


 while( counter < num_data_points )
  {
   do {

      rk( ksi,          chi,          sigma,
          rho,          omega,        psi_plus,
          field_mass,   d_ksi,        increment);
```

```
sig_inc[0] = increment[0];

chi_inc[0] = increment[1];

rho_inc[0] = increment[2];


rk( ksi,            chi,            sigma,
    rho,            omega,          psi_plus,
    field_mass,     d_ksi / 2,      increment );

 sig_inc[1] = increment[0];

 chi_inc[1] = increment[1];

 rho_inc[1] = increment[2];


rk( ksi+d_ksi/2,            chi + chi_inc[1],       sigma + sig_inc[1],
    rho + rho_inc[1],       omega,                  psi_plus,
    field_mass,             d_ksi / 2,              increment );


sig_inc[2] = increment[0];

chi_inc[2] = increment[1];

rho_inc[2] = increment[2];


 if( sigma != 0 )

   sig_error = fabs( ( sig_inc[0]  -  sig_inc[1]  -  sig_inc[2] )  / sigma );

 else sig_error = 0;


if( chi != 0 )

      chi_error = fabs( ( chi_inc[0]  -  chi_inc[1]  -  chi_inc[2] )  / chi );

else chi_error = 0;

 if( rho != 0 )

   rho_error = fabs( ( rho_inc[0]  -  rho_inc[1]  -  rho_inc[2] )  / rho );

 else rho_error = 0;
```

```
    error_estimate = sqrt(  pow( sig_error , 2 ) + pow( chi_error , 2 ) + pow( rho_error , 2 ) );

   d_ksi = d_ksi / 2;

  } while( error_estimate >= error_per_step );


 d_ksi = d_ksi * 2;

 if ( (ksi+d_ksi) >= ksi_store_value )
       {

        if ( (ksi_store_value - ksi) > 0 )
          {

           d_ksi = ksi_store_value - ksi;

           rk( ksi,                chi,            sigma,
               rho,                omega,          psi_plus,
               field_mass,         d_ksi,          increment );

           sig_inc[0] = increment[0];

           chi_inc[0] = increment[1];

           rho_inc[0] = increment[2];
          };

    sigma = sigma + sig_inc[0];

    chi = chi + chi_inc[0];

    ksi = ksi + d_ksi;

    rho = rho + rho_inc[0];


    sigma_array[ counter ] = sigma;

    chi_array[ counter ] = chi;

    rho_array[ counter ] = rho;

    ksi_store_value = ksi + ksi_interval;

    counter = counter + 1;
     }

  else
    {
     sigma = sigma + sig_inc[0];
```

```
        chi = chi + chi_inc[0];

        rho = rho + rho_inc[0];

        ksi = ksi + d_ksi;
           };
  if ( error_estimate < 0.1 * error_per_step ) { d_ksi = d_ksi * 2; };


  };

  }

/*****************************************************************************
                        Routine to evaluate the O(4) euclidean action
*****************************************************************************/

double o4_euc_action ( double sigma_data[],          double chi_data[],
                       double rho_data[],            double ksi_max,
                       double omega,                 double psi_plus,
                       )

{

  double o4_action,
         ksi_interval,
         integral,
         integ_count;

  ksi_interval = ksi_max / ( num_data_points - 1);

  integral = 0.0;

  integral += o4_integrand ( 0,    sigma_data,    rho_data,    omega,    psi_plus );

  integral += o4_integrand ( (num_data_points-1),    sigma_data,    chi_data,    omega,    psi_plus );

  for( integ_count=1 ;     integ_count < (num_data_points-1) ;     integ_count += 2 )

    {
     integral += 4 * o4_integrand ( integ_count,    sigma_data,    rho_data,    omega,    psi_plus    );
    };


  for( integ_count=2 ;     integ_count < (num_data_points-1) ;     integ_count += 2 )

    {
     integral += 2 * o4_integrand ( integ_count,    sigma_data,    rho_data,    omega,    psi_plus );
    };
```

```
  o4_action =  -2 * pow( pi , 2 ) * ksi_interval * integral / 3;

  return ( o4_action );

}


/*****************************************************************************
        Routine to evaluate the integrand for the euclidean action
*****************************************************************************/

double o4_integrand( int integrand_count,
                     double sigma_data[],
                     double rho_data[],
                     double omega,
                     double psi_plus )

{
 double sigma,
        rho,
        integrand;

 rho = rho_data[ integrand_count ];

 sigma = sigma_data[ integrand_count ];

 integrand = pow( rho , 3 ) * pot( sigma,        omega,        psi_plus    );

 return ( integrand );

}
```